Aus der

Abteilung für Klinische Pharmakologie

Klinikum der Ludwig-Maximilians-Universität München

Interindividual variability and the interplay of innate and adaptive immunity in the yellow fever vaccination model

Dissertation

zum Erwerb des Doctor of Philosophy (Ph.D.)

an der Medizinischen Fakultät

der Ludwig-Maximilians-Universität München

vorgelegt von

Magdalena Aneta Zaucha

aus

Krakow / Polen

Jahr

2024

Erstes Gutachten: Prof. Dr. Simon Rothenfußer

Zweites Gutachten: Prof. Dr. Anne Krug

Drittes Gutachten: Prof. Dr. Karl-Heinz Herbinger

Viertes Gutachten: Prof. Dr. Johannes Hübner

Dekan: Prof. Dr. med. Thomas Gudermann

Tag der mündlichen Prüfung: 16.09.2024

Table of content

Disclaimer

1) The determination of study participants' neutralizing antibody titers against the yellow fever vaccine virus (as depicted in Figure 29) was conducted by Lisa Lehmann as part of her doctoral thesis. These results are also included in a published article titled: Prior flavivirus immunity skews the yellow fever vaccine response to cross-reactive antibodies with potential to enhance dengue virus infection. Nature Communications 15(1):1696 (2024), doi: 10.1038/s41467-024-45806-x.

2) The T cell parameters depicted in Figures 33-37 were measured by Antonio Santos del Peral as part of his PhD thesis. The cohort classification (Figure 30), along with T-cell level data is also included in an article titled Basal T-cell activation predicts yellow fever vaccine response independently of cytomegalovirus infection and sex-related immune variations (submitted).

3) The initial determination of RIG-I ligands during infection with the yellow fever virus was conducted by Paul Schwarzlmüller as part of his doctoral thesis.

4) This dissertation includes data that are part of Zaucha, Winheim et al. RLR-dependent type I IFN production regulates antigen dose and activation in YF17D-infected DCs (manuscript in preparation). The shared content includes Figure 8-10.

Abstract

Understanding the activation of the immune system in response to various perturbations such as infections, cancer, or autoimmune diseases necessitates a comprehensive examination of the diverse components of the immune system at different levels of granularity. One strategy, which enables a systematic analysis of immune activation is the systems immunology approach.

To mimic the perturbation of the immune system with a viral infection, we have used the live-attenuated yellow fever 17D (YF17D) vaccine, which provides a controlled platform, serving as a model to study viral infections in humans. In this model, the live-attenuated yellow fever vaccine virus activates innate and adaptive immune responses and allows us to dissect and explore mechanisms of antiviral immunity. Our understanding of the details of how antiviral immune responses are activated is still limited, as is the understanding of factors and mechanisms that underlie the interindividual differences in the responses to the same viral agent.

The presented work identifies, by *in vitro* experiments, the RIG-I-like helicases as the main pattern recognition receptors that trigger the innate immune response to the YF17D infection. Using a collection of bio-samples from a cohort of 250 volunteers taken just before (day 0) and on day 3, 7, 14, and 28 after vaccination with YF17D, the early transcriptional response to the vaccine was measured in isolated peripheral blood monocytes by RNA-seq on day 7 and compared to the expression on day 0. This dataset of the early transcriptional response together with additional innate response parameters in the form of a panel of cytokines measured in the plasma of vaccinees on days 3 and 7 were then correlated to a large set of parameters quantifying in detail the developing humoral and cellular adaptive immune response to the vaccine virus. Integration of these vaccine response data with data of a genome-wide SNP-chip analysis of the vaccinees, along with information on previous infections and vaccinations, the basal immune cell composition and activation prior to the vaccine shot allowed the identification of genetic factors using quantitative trait loci studies (QTL and response-eQTL) as well as non-genetic factors causing interindividual variability in the vaccine response.

These analyses showed that infection with the YF17D virus leads to significant alterations in immune cell composition, gene expression, and pro-inflammatory cytokine production. The transcriptomic study identified 4,604 up-regulated genes and 3,528 down-regulated genes in monocytes after YF17D vaccination comprising multiple pathways and functional gene modules. This study thereby emphasizes the central role of interferons in orchestrating the initial immune response and the intricate interplay between innate and adaptive immunity. Interestingly, these findings suggest a potential link between baseline gene expression patterns and the subsequent immunogenic

response elicited by the vaccine, allowing for the identification of individuals with higher or lower responsiveness based on their pre-existing gene expression profiles. The cytokine response profile on day 7 revealed significant variability, particularly in CCL22, CXCL11, CXCL13, RANTES, and PDGF-bb levels, which were found to be influenced by genetic factors. The study identified a promising trans-QTL candidate in an intergenic region and the FOSL2 locus, which influence CCL22 and CXCL11 levels respectively. Subsequent validation in an *in-vitro-loss* of function cell infection model could confirm a role for FOSL2 in the induction of interferon and interferon-induced cytokines after infection with YF17D. The eQTL study identified 36 gene loci in monocytes that influence the transcriptional response to the vaccine (response-eQTLs). Interestingly, besides new gene candidates that need to be validated the identified response-eQTLs include the gene coding for RIG-I, the pattern recognition, identified in this work as the main sensor for YF17D.

In summary, this study underscores the impact of YF17D vaccination on monocyte dynamics and their gene expression, shedding light on the intricate mechanisms underlying vaccine response variability, while also identifying potential biomarkers for assessing vaccine efficacy in individuals.

Graphical abstract

List of figures

List of tables

List of supplementary figures

List of supplementary tables

List of abbreviations

APC: Antigen Presenting Cell
BAFF: B-cell Activating Factor
BM: Bone Marrow
CCL: CC Chemokine Ligand
CLRs: C-type Lectin Receptors
CMV: Cytomegalovirus
cTfh: Circulating Follicular Helper T cells
CXCL: C-X-C Ligand
DCs: Dendritic Cells
DEG: Differentially Expressed Gene
DENV: Dengue Virus
dsRNA: Double-stranded RNA
EBNA2: Epstein-Barr Nuclear Antigen 2
EBV: Epstein Barr Virus
ELISA: Enzyme-linked Immunosorbent Assay
E protein: Envelope Protein
FluoRNT: Fluorescence Focus Reduction Neutralization Test
GC: Germinal Center
GM-DCs: Granulocyte-Macrophage Dendritic Cells
GM-Macs: Granulocyte-Macrophage Macrophages
GO: Gene Ontology
GSEA: Gene Set Enrichment Analysis
GTEx: Genome-Tissue Expression Project
GWAS: Genome-Wide Association Study
HLA: Human Leukocyte Antigen
HSV: Herpes Simplex Virus
Inflam. endotype: Inflammatory endotype
IFN: Interferon
IFNAR: Interferon Alpha/Beta Receptor
IFNGR: Interferon Gamma Receptor
IgG: Immunoglobulin G
IgM: Immunoglobulin M
IL: Interleukin
ISG: Interferon-Stimulated Gene
ISGF3: Interferon-Stimulated Gene Factor 3
ISRE: Interferon-Stimulated Response Element
JAK-STAT: Janus Kinase-Signal Transducer and Activator of

Transcription
LD: Linkage Disequilibrium
log-CPM: Log-Count Per Million
LPS: Lipopolysaccharide
MAVS: Mitochondrial Antiviral Signaling Protein
MDA5: Melanoma Differentiation-Associated Protein 5
MHC: Major Histocompatibility Complex
MMR: Measles, Mumps, Rubella
MOI: Multiplicity of Infection
NF-κB: Nuclear Factor κB
NK: Natural Killer
PAMP: Pathogen-Associated Molecular Pattern
PBMC: Peripheral Blood Mononuclear Cell
PRR: Pattern Recognition Receptor
QTL: Quantitative Trait Loci
RIG-I: Retinoic Acid-Induced Gene I
RLR: RIG-I-like Receptor
rRNA: Ribosomal Ribonucleic Acid
SNP: Single Nucleotide Polymorphism
TAP: ATP Binding Cassette Subfamily
TBE: Tick-Borne Encephalitis
T-CM: Central Memory T-cell
T-EM: Effector Memory T-cell
TF: Transcription Factor
Th: T-helper cells
TIR: Toll/Interleukin-1 Receptor
TIV: Trivalent Influenza Vaccine
TLR: Toll-Like Receptor
TNFRSF: Tumor Necrosis Factor Receptor Superfamily
TNFSF: Tumor Necrosis Factor Ligand Superfamily
TRIF: TIR-Domain Containing Adaptor-Inducing Interferon-β
TSS: Transcription Start Site
UTRs: Untranslated Regions
WNV: West Nile Virus
WGCNA: Weighted Gene Co-expression Network Analysis
YF17D: Yellow Fever 17D vaccine

1.   Introduction

1.1 The immune system

The immune response is a complex network that consists of two branches: innate and adaptive immunity. The innate immune response serves as the first line of defense against bacteria, viruses, and other microorganisms. It is a rapid and broadly effective system designed to provide immediate protection. The innate system is made up of both chemical and anatomic barriers such as the skin or mucous tissue and by host immunity that comprises different cellular elements but also soluble effector proteins such as cytokines and the complement system. In contrast, the adaptive immune response is characterized by its specificity and a slower development process. It primarily involves antigen-specific T and B cells, which can recognize and target specific pathogens. This branch of immunity takes time to develop as it necessitates the generation and clonal expansion of specialized immune cells, and the production of antibodies tailored to the encountered pathogen. Although the innate and adaptive immune systems have their own distinct characteristics, they are interconnected and work in synergy to provide comprehensive protection (Parkin and Cohen, 2001; Janeway and Medzhitov, 2002).

1.1.2 The innate immune response

The innate immune system comprises diverse cell types, including monocytes, dendritic cells (DC), macrophages, granulocytes (neutrophils, basophils, and eosinophils), and natural killer (NK) cells, all equipped with distinct germline-encoded pattern recognition receptors (PRRs) crucial for sensing PAMPs (pathogen-associated molecular patterns) and initiating the immune response. PRRs can be categorized based on their cellular localization into two classes: transmembrane-localized on cell surfaces or within the endosomal compartment sensing extracellular PAMPs, including Toll-like receptors (TLRs) and C-type lectin receptors (CLRs); and those in the cytoplasm, activated by cell infections, such as NOD-like receptors (NLRs), AIM2-like receptors (ALRs), and RIG-I-like receptors (RLRs) (Janeway and Medzhitov, 2002; Reikine *et al.*, 2014; Chan and Gack, 2016).

PRRs play a pivotal role in discriminating between self and non-self-derived molecules by recognizing conserved structures shared by various pathogens that are absent in host cells (Chan and Gack, 2016). Detection of viral PAMPs directly activates the effector cell

function. Activated macrophages, dendritic cells, and granulocytes such as neutrophils, degrade pathogens and other debris followed by their presentation in professional antigen-presenting cells (APCs) such as DCs and macrophages (Banchereau and Steinman, 1998).

APCs, in their immature state, continuously survey tissues for potential pathogens. Upon detecting a threat via PRRs, they initiate the secretion of interferons and cytokines, then migrate to secondary lymphoid organs where they mature, and present the pathogen-derived peptides through two types (I and II) of major histocompatibility complexes (MHC) on their surface (Mair and Liechti, 2021). Through their activation and secretion of inflammatory mediators such as cytokines and chemokines, they attract other myeloid cells to the site of infection such as monocytes, DCs, or lymphoid cytotoxic NK cells creating an inflammatory microenvironment that stimulates activation and differentiation of immune cells (Parkin and Cohen, 2001).

The APCs link innate and adaptive branches of immunity by the presentation of antigens that activate T and B cells within the adaptive immune system (Parkin and Cohen, 2001). When activated, APCs upregulate many accessory molecules e.g. CD80, CD86, CD40 that interact with receptors on T cells to enhance adhesion and signaling. The activation of cytotoxic CD8$^+$ T cells is mediated through MHC class I, presenting peptides derived from the cytosol. Additionally, exogenous antigens derived by phagocytosis are expressed by MHC class II, which stimulates CD4+ T-helper (Th) (Banchereau and Steinman, 1998; Mair and Liechti, 2021). Recognition of antigens by naïve lymphocytes leads to their clonal expansion and the generation of long-lived memory cells, contributing to immune protection. CD4$^+$ T cells, which are activated by DCs, modulate cytokine production, support CD8$^+$ T cell activation and proliferation and drive B cell differentiation and expansion. This activation triggers B cells to transform into antibody-secreting plasma cells and memory B cells, essential components of the adaptive immune response (Sherwood *et al.*, 2022).

1.1.3 Pattern Recognition Receptors

Sensing pathogens by innate immunity is necessary for invoking any mechanism of defense (Chan and Jin, 2022).

Toll-like receptors sense a broad range of ligands including DNA, ssRNA, and dsRNA, while the RLRs are specialized in recognizing viral double-stranded RNA (dsRNA) (Kato

et al., 2006). Both classes of innate immune receptors interact with signaling adaptors; specifically, TLRs transfer the signal to myeloid differentiation primary response protein 88 (MyD88) and TIR-domain containing adaptor (TRIF), while RIG-I-like receptors to the mitochondrial antiviral signaling protein (MAVS, also known as IPS1). Once activated, adaptors recruit further regulatory factors forming oligomeric assemblies that ultimately activate transcription factors and gene expression modules including immune cytokines, primarily type I interferon (IFN) (Reikine *et al.*, 2014).

1.1.4 RIG-I like receptors

Toll-like receptors (TLRs) are among the most extensively studied receptors; they belong to the transmembrane glycoprotein receptor family and exhibit structural similarities (Kumar *et al.*, 2011). Each TLR comprises an N-terminal domain that consists of leucine-rich repeats (LRRs), which recognize PAMPs, a C-terminal Toll/IL-1 receptor (TIR) domain responsible for downstream signaling, and a central transmembrane domain that anchors TLRs to either the plasma or endosomal membrane. In humans, ten TLRs have been described. TLR3, TLR7, TLR8, and TLR9 are expressed in the endoplasmic membrane and recognize nucleic acids derived from viruses and bacteria. In contrast, TLR1, TLR2, TLR4, TLR5, TLR6, and TLR10 are expressed on the cell surface (Takeuchi and Akira, 2010; Chow *et al.*, 2018) TLR7 and TLR8 signal through the MyD88 adaptor, transmitting signals to nuclear factor NF-κB and additionally activating interferon regulatory factors such as IRF7. TLR3 signals through TRIF, activating IRF3 and NF-κB (Chow *et al.*, 2018).

RLRs, being cytoplasmic receptors, play a pivotal role in directly sensing replicating viruses (Janeway and Medzhitov, 2002; Kawai and Akira, 2011). The RLR family has three members: RIG-I (also known as DDX58), MDA5 (melanoma differentiation-associated protein 5, known as IFIH1), and LGP2 (laboratory of genetics and physiology 2). Structurally, RLRs are similar. Each of the three RLRs contains a DExD/H RNA helicase domain that facilitates ATP hydrolysis and interacts with dsRNA, and a C-terminal domain (CTD) that aids in RNA ligand recognition and binding specificity. However, only RIG-I and MDA5 contain two N-terminal caspase activation and recruitment domains (CARDs) required for downstream signal transduction (Figure 1). (Yoneyama *et al.*, 2005; Kowalinski *et al.*, 2011; Bruns and Horvath, 2012). RIG-I and MDA5 act as typical PPRs recognizing cytoplasmic viral RNA and mediating the

interaction with downstream molecules, whereas the function of LGP2, apart from binding ability, has not been fully elucidated so far. It has been reported as a regulator of RLRs and coactivator of MDA5 (Rothenfusser *et al.*, 2005; Satoh *et al.*, 2010; Bruns *et al.*, 2014).

Although MDA5 shares the domain architecture with RIG-I, the two receptors sense different types of viruses. RIG-I is a sensor for negative and positive-stranded RNA viruses including the Vesicular Stomatitis Virus (VSV), the Newcastle Disease virus (NDV), the Sendai virus (SeV), the influenza virus, the Japanese Encephalitis virus (JEV) and the Hepatitis C virus (HCV). MDA5 has been reported to detect picornaviruses such as Encephalomyocarditis viruses (EMCV) or the Mengo virus. Studies have also shown that some viruses including flaviviruses (dengue virus (DENV) and the West Nile virus (WNV)) and reoviruses are sensed by both RIG-I and MDA5 (Kato *et al.*, 2005, 2006; Loo *et al.*, 2008; Loo and Gale, 2011).

The detection of specific viruses depends largely on the type of RNA ligands that are generated during the course of the infection. RIG-I shows a preference for short, dsRNAs with 5'- di- and tri-phosphate groups while ligands of MDA5 are long dsRNAs (Hornung *et al.*, 2006; Kato *et al.*, 2008; Schmidt *et al.*, 2009; Goubau *et al.*, 2014; Li *et al.*, 2022).

1.1.5 Interferons

Interferons have been therapeutically exploited not only for the treatment of viral infections but also in the management of autoimmune disorders and various types of cancer due to their immunoregulatory and antiproliferative properties (Platanias, 2005).

The major groups include type I IFNs, comprising IFN-α, IFN-β, IFN-ε, IFN-κ, and IFN-ω, type II IFN which solely consists of IFN-γ, and the more recently discovered type III IFNs including IFN-λ1, IFN-λ2, and IFN-λ3, also known as interleukins (IL)-29, IL-28A, and IL-28B, respectively. Secreted interferons bind to respective surface receptors on cells (IFNAR 1/2 for type I IFNs, IFNGR 1/2 for type II, and IFNLR1/IL10R2 for type III) and activate the JAK-STAT pathway (Schneider *et al.*, 2015).

The binding of secreted type I and type III IFN to their respective receptors, activates the JAK-STAT pathway, leading to the phosphorylation and nuclear translocation of interferon-stimulated gene factor 3 (ISGF3), consisting of signal transducer and activator of transcription 1 or 2 (STAT1 and STAT2) and IRF9. This complex migrates to the

nucleus where it binds to IFN-stimulated response elements (ISREs) and initiates the transcription of IFN-stimulated genes (ISGs) that encode a multitude of different restriction factors (Takeuchi and Akira, 2010; González-Navajas *et al.*, 2012). Secretion of IFNs, type I and type III, inhibits viral replication, and promotes monocyte/DCs differentiation and maturation as well as recruitment of immune cells to the site of infection (McNab *et al.*, 2015).

Type II IFN is not involved in forming the ISGF3 complex but, instead, it activates STAT1 homodimers that bind to gamma-activated sequence (GAS) elements in the promoters of IFN-γ-induced genes, thus, activating their transcription (Schneider *et al.*, 2015). IFN-γ is mainly produced by T and NK cells and it stimulates upregulation of MHC class I and II, enhancing antigen presentation and activating macrophages, However, it also can exhibit antiviral functions (Schoggins and Rice, 2011; González-Navajas *et al.*, 2012). Each type of IFN activates partially unique and overlapping ISGs (Schoggins and Rice, 2011).

1.1.6 RLR signaling

Binding of RNA ligands by RIG-I and MDA5 activates the downstream MAVS adaptor via CARD-CARD interactions which leads to the formation of the MAVS prion-like protein complex and initiates the activation of an antiviral cascade (Hou *et al.*, 2011). The signal is subsequently transmitted to the TANK-biding kinase 1 (TBK1)/ IκB kinase (IKK) ε as well as to the IKK complex containing IKKα,β, and IKKγ (NEMO), which activate transcription factors including interferon regulatory factors 3 and 7 (IRF3/IRF7) and the nuclear factor (NF-κB), respectively, which trigger the expression of interferons, antiviral cytokines and chemokines (Kawai *et al.*, 2005; Kumar *et al.*, 2011; Liu *et al.*, 2013, 2015; Chathuranga *et al.*, 2021).

The activation of the RLRs signaling pathway initiates the production of mainly type I but also type III interferons, which, through the Janus kinase signal transducer and activator of transcription (JAK-STAT) pathway, induce the expression of ISGs. Over 1000 ISGs have been described, each with different antiviral functions (Schoggins and Rice, 2011). Some of the best-known ISGs include myxovirus resistance protein (MX), the interferon-induced double-stranded RNA-activated protein kinase (PKR/EIF2AK2), IFIT (interferon-induced proteins with tetratricopeptide repeats), 2'-5'-oligoadenylate synthetase (OAS), the tripartite motif-containing (TRIM) and the apolipoprotein B mRNA editing enzyme,

catalytic polypeptide-like (APOBEC) family (McNab *et al.*, 2015). These ISGs play pivotal roles in restricting various stages of the viral replication cycle. For instance, IFITM (interferon-induced transmembrane proteins) inhibits viral uncoating, viral replication is suppressed by RNASEL (ribonuclease L), ADAR (adenosine deaminases acting on RNA), and APOBEC3, while IFIT impedes viral protein synthesis. Additionally, BST2 (bone marrow stromal antigen 2), also known as tetherin, prevents viral release from the host cell (Goubau *et al.*, 2013). Pattern recognition receptors, including RIG-I and MDA5, are also classified as ISGs; their stimulation, creates a positive feedback loop that amplifies the RLRs' response and stimulates adaptive immunity (Goubau *et al.*, 2013; Chiang *et al.*, 2014).

1.2 The yellow fever virus

1.2.1 Characterization of the yellow fever virus

Since its discovery in the late 18th century, Yellow Fever has been implicated in causing millions of deaths. The YF17D vaccine strain, developed in 1937 by Max Theiler, has proven highly effective in preventing infections and has been administered widely ever since (Pulendran, 2009). As there is no specific treatment available, vaccination remains the sole mitigation strategy until today.

The Yellow fever virus belongs to the *Flaviviridae* family, which is a diverse group of viruses, that comprises four genera: *Flavivirus*, *Pestivirus, Pegivirus,* and *Hepacivirus.* Within the *Flavivirus* genus, there are over 70 different viruses including the yellow fever virus (YFV), dengue virus (DENV), Japanese encephalitis virus (JEV), West Nile virus (WNV), tick-borne encephalitis virus (TBEV), and the Zika virus (Figure 1). They share similarities in morphology and genome organization, yet differ significantly in biological aspects such as host diversity, pathogenicity, and transmission methods (Gould and Solomon, 2008; Heinz and Stiasny, 2012; Kleinert *et al.*, 2019). Flaviviruses constitute a serious threat to global health since their infections can lead to different diseases such as hemorrhagic fever (YFV and DENV) or encephalitis (JEV, WNV, and ZIKV). *Flaviviruses* are arthropod-borne and primarily transmitted by mosquitos and ticks, their geographical distribution varies depending on specific vectors and the presence of natural habitats for their hosts. The yellow fever virus primarily occurs in the tropical regions of Africa and South America. It follows a transmission cycle that typically involves

non-human primates and mosquitoes although humans can also act as viremic hosts. The infection with YFV can lead to clinical phenotypes ranging from asymptomatic and mild to severe and death (Monath, 2001; Gould and Solomon, 2008; Kleinert *et al.*, 2019). The incubation period lasts 3-6 days after infection by a mosquito bite. The viral concentration in the blood ranges between 10^5 to 10^6 infectious particles/mL. In most of the symptomatic cases, the infection is self-limiting and causes unspecific symptoms including fever, chills, dizziness, headache, and lower back pain, which makes the disease difficult to diagnose. During this phase, patients are usually viremic. However, in around 15%-25% of patients, the disease progresses to the fatal phase, which is characterized by vomiting, epigastric pain, renal failure, liver damage, and hemorrhagic fever (Monath, 2001). The final stage of fatal YF disease in humans is characterized by a cytokine storm, circulatory shock, and multi-organ failure. The lethality of the disease is associated with the viremia levels in the blood as well as with genetic or intrinsic factors modulating host immunity. It has been reported that pro and anti-inflammatory cytokines produced by the infected cells as well as cytotoxic T cells are associated with the immunopathology of the YF infection (Monath, 2001; Kleinert *et al.*, 2019).
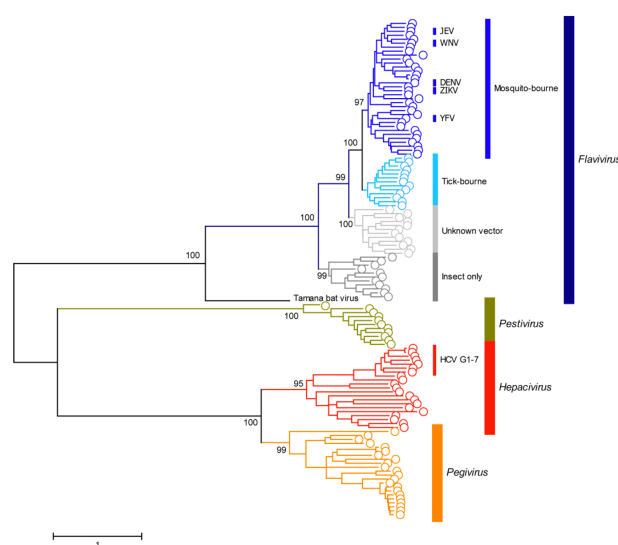
Figure 1. The Phylogenetic tree of the Flaviviridae family.

The tree depicts evolutionary relationships across the Flaviviridae (taken from Kleinert *et al.*, 2019).

1.2.2 Molecular characterization

Molecularly, the YFV is a small virus whose genome is a single positive-sense RNA strand, 10,800 bases in length, including the 5' and 3' UTRs. The viral genome is translated into a single polyprotein precursor, which is cleaved into three structural proteins: capsid (C), membrane (M, expressed as prM the M precursor), and envelope (E), as well as seven nonstructural proteins (NS1, NS2A, NS2B, NS3, NS4A, NS4B, and NS5) (Figure 2). The C protein is responsible for encapsulating the viral genome within a nucleocapsid, which is consecutively surrounded by a host-derived lipid envelope into which the E and M glycoproteins are inserted. The E protein mediates viral entry into the host cell. The prM protein acts as a chaperon that facilitates the folding of the E protein (Lindenbach *et al.*, 2007). The remaining nonstructural proteins are all involved in replication acting as polymerases, proteases, helicases, and transcription factors. The 5' and 3' untranslated regions (UTRs) are non-coding sequences, which flank the coding region. The 5'UTR of *Flaviviruses* is a short fragment (95-132 bases in length) whereas the 3'UTR is usually longer (444-524 bases in length). Both fragments form secondary structures, which are involved in regulatory functions, RNA stabilization, and modulating of replication (Proutski *et al.*, 1997; Bryant *et al.*, 2005; Oliveira and Peron, 2019).
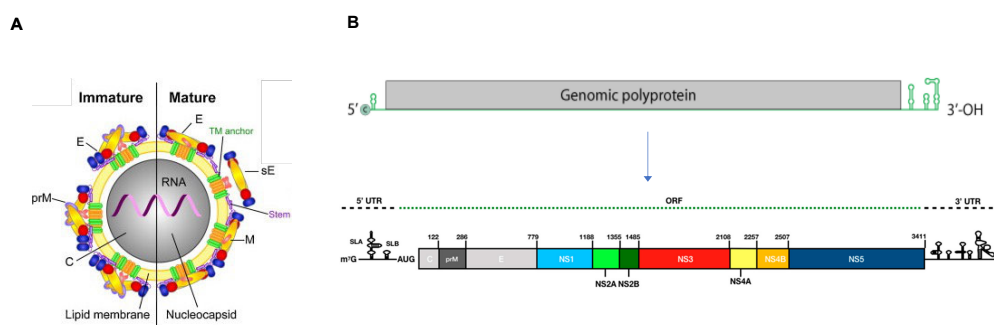
Figure 2.The yellow fever genome organization.

A) Model of the flavivirus particle. Left: immature virus, right: mature virus. Mature virions contain two virus-encoded membrane proteins (M and E), while immature virions contain the membrane protein precursor (Heinz and Stiasny, 2012). B) Genome structure and schema of the translation. The polyprotein is processed and cleaved into structural and nonstructural proteins (taken form Kleinert *et al.*, 2019).

1.2.3 Life cycle

The replicative cycle of the YF virus involves the disassembly of viral particles, replication of the viral genome, synthesis of viral proteins by the host translational machinery, and the re-assembly of viral particles. The YFV enters the host cell by endocytosis, which involves the binding of the viral E protein to a still not characterized host cell receptor. The acidic pH of the endosome environment facilitates the E protein-mediated fusion of the viral and endosomal membranes. This results in the release of the viral genome and capsid protein into the cytosol. The positive-strand RNA is translated into a single polyprotein, which is processed co- and post-translationally to yield the individual virus-associated proteins. Viral replication takes place on the surface of the endoplasmic reticulum (Mukhopadhyay *et al.*, 2005; Lindenbach *et al.*, 2007). Finally, the viral particle assembly takes place in the endoplasmic reticulum, initially forming immature viruses that contain the precursor of the M (prM) protein, the newly synthesized RNA, and structural proteins and bud into the lumen of the ER. The immature virions are transported through the *trans*-Golgi network (TGN) where the prM protein is proteolytically cleaved into its mature form. This is followed by the exocytic release of mature virions (Figure 3) (Heinz and Stiasny, 2012).
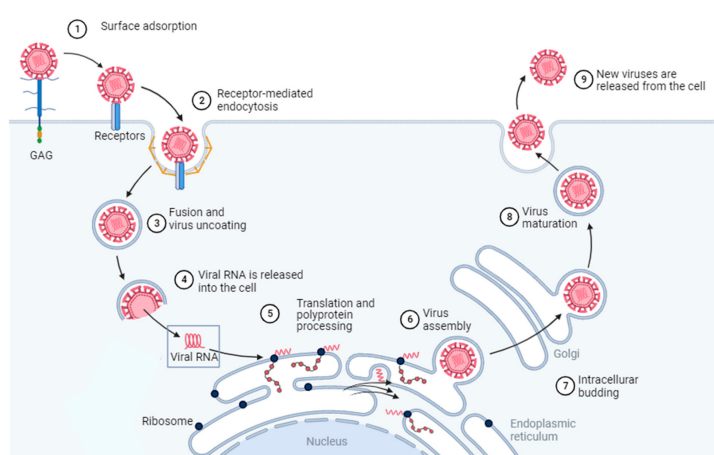
Figure 3. The flavivirus life cycle.

The attachment of the viral envelope protein E to the host receptor; fusion of the virus membrane with host endosomal membrane; release of viral RNA, translation of the viral RNA to the polyprotein and cleavage to produce the structural and nonstructural proteins; replication; virus assembly occurs in the endoplasmic reticulum after budding of the newly synthesized virions to the endoplasmic reticulum; transport of immature virions to the Golgi apparatus; cleavage of the prM; exocytosis of mature virions. (taken from Nazarenko *et al.*, 2023).

1.2.4 Characterization of the YF17D model

Live-attenuated vaccines tend to trigger stronger immune responses compared to non-live vaccines containing inactivated pathogens or their fragments. While non-live vaccines may contain PAMPs, their ability to activate the immune system is often weaker than that of live vaccines (Plotkin, 2014).

The yellow fever vaccine stands out as one of the most potent immunizations ever developed, eliciting robust innate and adaptive immune responses. Known for its efficacy and safety, it serves as an excellent model for studying antiviral immunity in YF infection-naïve individuals (Theiler and Smith, 1937; Poland *et al.*, 1981; Pulendran, 2009; Pulendran *et al.*, 2013).

The YF17D vaccine strain is based on a live-attenuated version of the wild-type Asibi strain (isolated from Mr. Asibi who was infected with the virus in 1927), obtained by over 200 serial passages through monkey, mouse, and chicken embryonic tissue cultures resulting in mutations in structural and non-structural genes (Heinz and Stiasny, 2012; Pulendran *et al.*, 2013). Despite its attenuation, the strain retains the capacity to replicate and induce an immune response (Monath and Vasconcelos, 2015).

Differing by only 68 nucleotides from the wild-type Asibi strain, YF17D presents 32 missense mutations out of the total 10,800 nucleotides in the full genome. The E protein, critical in the initial phase of infection, viral entry, and the main target of neutralizing antibodies, has 11 nucleotide and 8 amino acid differences and is the most heavily mutated region of the genome. Some of these mutations are expected to alter virus tropism, affecting YF17D virulence (Pulendran, 2009).

The vaccine is very well tolerated. Mild symptoms are caused by the secretion of pro-inflammatory cytokines and adverse effects are very rare (Monath, 2001).

Post-vaccination, viremia is transient and low, and virus replication peaks at days 5–7 and subsequently declines. The production of IgM-neutralizing antibodies is induced at day 7 -10 post-vaccination and peaks at 2 weeks persisting for at least 18 months before their levels start decreasing. IgG-neutralizing antibodies are elicited more slowly but can stay active for up to 40 years, generating a life-long immune protection. It was initially believed that neutralizing antibodies, developed by more than 90% of vaccine recipients, primarily accounted for immune protection, however, it is suspected that the interplay between humoral (antibody-based) immunity and cellular components plays a pivotal role in generating a robust immune response (Poland *et al.*, 1981; Monath, 2001; Pulendran, 2009).

1.2.5 The immune response to YF17D

It has been hypothesized that the activation of an antibody response may not be sufficient to provide effective immune protection necessitating the activation of innate components and adaptive immune cells.

Studies demonstrate that YF17D elicits innate immunity, involving the activation of various elements such as the complement system, inflammasomes, and interferons. These innate responses seem to be pivotal in driving the activation of high-quality adaptive immunity and the production of antigen-specific antibodies. (Gaucher *et al.*, 2008; Monath and Vasconcelos, 2015).

Research has revealed that the YF17D vaccine engages the innate immune system by stimulating distinct DCs subsets through TLRs 2, 7, 8, and 9 (Querec *et al.*, 2006) as well as through the involvement of RIG-I-like receptors (Querec *et al.*, 2006; Bruni *et al.*, 2015). This stimulation leads to DCs maturation, which contributes to establishing a pronounced adaptive immune response (Bookchin and Schumacher, 2000; Barba-Spaeth *et al.*, 2005a).

Activation of PRRs leads to the release of type I IFN and cytokines that further activate various immune cells including T cells contributing to antibody response (Querec *et al.*, 2006; Gaucher *et al.*, 2008; Pulendran *et al.*, 2013). Studies have shown that YF17D replication results in the robust activation of type I but also II and III interferons. Plasmacytoid DCs (pDCs) contribute to type I and type III IFN levels (Querec *et al.*, 2006; Sinigaglia *et al.*, 2018). Additionally, CD8+ T cells and NK cells are involved in IFNγ, type II production (Neves *et al.*, 2013; Lam *et al.*, 2018).

Despite a very low replication rate, YF17D appears to facilitate presentation to T cells effectively. Multiple studies indicate early activation of polyfunctional effector CD4^{+} T cells and cytotoxic CD8^{+} T cells in response to YF17D, leading to the development of a long-lasting memory T cell population (Kohler *et al.*, 2012).

The vaccine induces a balanced Th1 and Th2 CD4^{+} T cell response (Querec *et al.*, 2006; Gaucher *et al.*, 2008; Kohler *et al.*, 2012) with Th1 cells, in particular, shown to positively correlate with the magnitude of the YF-specific antibody response. This aids B cell development and the subsequent production of high-quality neutralizing antibodies (Kohler *et al.*, 2012). Additionally, in the production of long-lasting neutralizing antibodies, CD4^{+} follicular T-helper cells (Tfh) have been shown to be involved. These cells aid B cells within germinal centers (GCs), influencing isotype-switching affinity

maturation, and the ultimate differentiation into effective antibody-secreting cells. Specifically, circulating Tfh1 cells have been shown to be associated with generating protective neutralizing antibodies (Huber *et al.*, 2020). Antigen processing by DCs also activates CD8$^+$ T cells. Their activation and proliferation peak around two weeks post-immunization, limiting the spread of the infection, and the CD8 T cell response continues as long-lived memory cells (Barba-Spaeth *et al.*, 2005b; Miller *et al.*, 2008; Akondy *et al.*, 2009, 2015).

The YF17D vaccine triggers both innate and adaptive immunity, yet the specific populations of antigen-presenting cells (APCs) and the signaling pathways of pattern recognition receptors (PRRs) that are activated remain incompletely understood. This leaves unanswered questions about how the innate immune response influences the adaptive immune system following YF17D immunization.

1.3 Systems biology

Systems biology is a holistic, simultaneous analysis of biological systems. In the context of immunology, this approach is specifically termed as systems immunology. It involves a comprehensive examination of the immune system, aiming to understand its complexity and interactions across various biological components through large-scale quantification (Brodin and Davis, 2017).

1.3.1 Systems immunology

The complex interaction between innate and adaptive immunity results in an effective immune response. Systems immunology tries to comprehensively analyze the immune system by studying interactions between different entities – cell abundances and their respective gene and protein levels and analyzing how they change in response to diseases or other perturbations using high-throughput multi-omics technologies like genomics, proteomics, and transcriptomics. Integrating information from different data modalities helps to better understand the complexity of the immune system and how it functions as a network (Bonaguro *et al.*, 2022).

Using vaccines as models of infections provides a safe and controlled method for perturbing the immune system, allowing for a precise analysis of changes within the

cellular and molecular networks in the human immune system over time (Brodin and Davis, 2017). Due to the necessity of extracting a large amount of information from limited material, systems immunology leverages the wealth of information easily obtainable from non-invasively extracted blood samples allowing for the simultaneous extraction of diverse molecular measurements from numerous individuals. Blood samples contain a diverse array of circulating immune cells that dynamically change during the course of infection. Information extracted from these samples, along with other bodily fluids, reveals the sensitivity of an individual's immune system and the variation across individuals, in responses to perturbations across the population. Such insights aid the analysis of interactions among immune system components and may even allow predicting the immune responses to immunological challenges (Davis *et al.*, 2017).

1.3.2 Interindividual variability of the immune response

Research has demonstrated significant variability in the human immune system among individuals. This variability arises from factors such as sex, age, genetic polymorphisms, previous exposure to infections, vaccinations and diseases, and epigenetic modifications. However, a comprehensive exploration of these aspects remains largely unexplored (Brodin and Davis, 2017).

Uncovering the contributions of both heritable and non-heritable factors to interindividual variability is essential for understanding the complexity of immune responses and thereby, individuals' predispositions or susceptibilities to different pathogens. Recent research highlights the significance of baseline determinants, such as genetic, intrinsic, and environmental factors, in shaping the immune response (Piasecka *et al.*, 2018; Poon *et al.*, 2021). The application of systems biology to measure the immune state before and after the infection allows us to generate large datasets and build integrative models to investigate and characterize the immune response across individuals (Davis *et al.*, 2017).
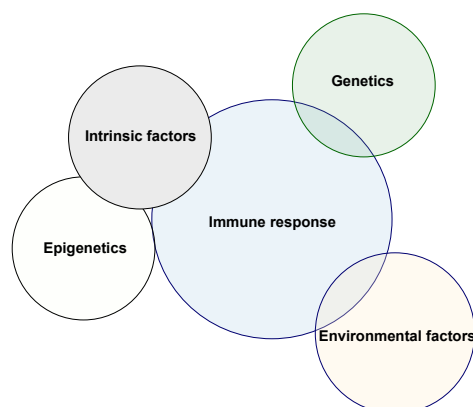
Figure 4.Influences on the immune response.

The immune response is shaped by a range of factors, encompassing both genetic and non-genetic host determinants.

Non-heritable intrinsic factors, like age, sex, and overall health status such as previous infections, influence the immune response (Figure 4). This can be quantified by an array of factors including cytokine levels, cell population abundances or serum proteins (Forlin *et al.*, 2023). Age-related changes in immune parameters significantly impact immune responses, particularly in older adults. Studies indicate a decrease in cell numbers and receptor diversity in T and B cells with age, resulting in lower antibody responses to vaccinations like diphtheria, tick-borne encephalitis (TBE), or tetanus in the elderly (Brodin and Davis, 2017; Zimmermann and Curtis, 2019; Poon *et al.*, 2021).

Similarly, sex-related differences affect immune responses to vaccines. Transcriptional analyses reveal higher expression of pro-inflammatory genes in PBMCs extracted from females post-infection, as compared to males (Klein and Flanagan, 2016). Variability in antibody responses between sexes has been also observed. Previous studies suggested that females exhibit a higher antibody response to dengue, smallpox, or inactivated influenza vaccines (TIV), while males tend to have higher levels of antibodies against diphtheria or tetanus vaccines, although these findings have not been consistently replicated across studies (Zimmermann and Curtis, 2019). Data on the antibody response to the YF17D vaccine vary across studies. Transcriptomics data revealed 660 differentially expressed genes (DEG) in females related mainly to innate immune responses compared to only 67 DEG in males (Klein *et al.*, 2010).

Additionally, prior infections have been reported to contribute to the variability of the immune response, especially that of chronic or latent infections including wide-spread

cytomegalovirus (CMV), Epstein Barr virus (EBV), or the herpes simplex virus (HSV). These infections can induce prolonged immune reactions and have been demonstrated to modulate host immunity extensively. The cytomegalovirus (CMV) has been described as a potent immune response modulator. Its infection is known to increase the number of effector memory T cells. Approximately, 10% of the T cell repertoire is estimated to be CMV-specific (Brodin *et al.*, 2015; Patin *et al.*, 2018). Moreover, it has been reported that prior CMV exposure can enhance antibody levels to influenza vaccines in young individuals. Conversely, the Epstein-Barr virus (EBV) appears to have the opposite effect. Exposure to EBV reduces antibody responses to routine infant vaccines (Tsang *et al.*, 2020).

In addition, heritable genetic variations play a substantial role in the diverse immune reactions observed among individuals. Genetic polymorphisms within the genes responsible for the immune response and regulation of inflammation including PRRs, human leukocyte antigen (HLA) genes of MHC complex, or cytokine genes have been identified as influential factors that affect responses to infectious diseases across the population (Linnik and Egli, 2016). Several studies have linked single nucleotide polymorphisms (SNPs) to differences in immune responses following vaccination. For instance, quantitative trait loci (QTL) studies have pinpointed SNPs within CD46 (20 significant SNPs) and IFI44L (9 significant SNPs) genes that influence interindividual variability in neutralizing antibody levels in response to the measles vaccine (Haralambieva *et al.*, 2018). Furthermore, a SNP (rs669260) in the RIG-I gene has been associated with elevated antibody titers against measles and rubella antigens in individuals vaccinated with the MMR (Measles, Mumps, Rubella) vaccine (Ovsyannikova *et al.*, 2015).

1.3.3 Quantitative trait loci (QTLs)

It is anticipated that a significant portion of the variability in immune responses to infections and vaccines can be attributed to common genetic variants, such as SNPs, present within hosts. Associating these variants with specific traits aims to provide a deeper understanding of heritable factors contributing to interindividual variability (Aguet *et al.*, 2023).

SNPs are the most common DNA variation across populations occurring both in coding and non-coding genomic regions (Figure 5). They can impact RNA, protein levels, and

their function (Flynn and Lappalainen, 2022). SNPs in protein-coding regions may cause missense variants that change the amino acid sequence of the transcript and affect its structure and stability, nonsense resulting in a stop codon effectively yielding an incomplete, often dysfunctional protein transcript or synonymous with no effect on protein primary structure (Linnik and Egli, 2016). In non-coding regions, SNPs may have regulatory functions, affecting transcription rates, and transcript levels, mRNA splicing, or binding sites for transcription factors (Majewski and Pastinen, 2011).
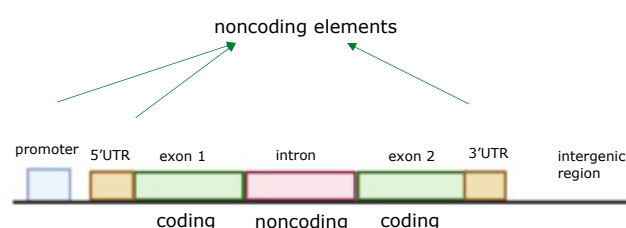
Figure 5.The overview of the genomic localization of SNPs.

The SNPs that affect a certain trait, or the immune response can be identified by their statistical association with common effects, typically measured as quantitative traits (e.g., antibody levels or gene-specific RNA abundance). This methodology, known as quantitative trait locus mapping (QTLs), or specifically as eQTLs when assessing gene expression, reveals the SNPs' role in influencing these traits.

QTLs can be categorized into two main types: cis-QTLs, and trans-QTLs. Cis-QTLs are situated near the affected gene, typically within 1Mb of the transcription start site (TSS) and exert their effects locally. These variants often have a substantial effect size, enabling their detection with a relatively modest sample size. They can alter transcription binding sites and regulatory elements, impacting gene expression regulation. However, they explain only a modest proportion of trait heritability. Trans-QTLs, on the other hand, reside in different genomic locations, typically over 5Mb away from the TSS or even on separate chromosomes; they are challenging to detect despite being numerous. These variants usually have smaller effects, demanding larger sample sizes for detection. Furthermore, they require more extensive correcting for multiple tests due to each SNP potentially affecting multiple genes. Trans-QTLs are particularly intriguing when they exhibit associations with changes in the expression of multiple genes that are likely to be associated with disease pathogenesis, offering insights into potential co-regulation of

multiple genes that are members of specific biological pathways (Figure 6) (Gilad *et al.*, 2008; Westra and Franke, 2014; Flynn and Lappalainen, 2022).

Genetic mapping including GWAS (genome-wide association studies), and QTL analysis have successfully identified numerous loci associated with phenotypes. However, like any scientific methodology, it comes with its own set of limitations. Many eQTL have been identified outside of the coding region, (over 80%) in the intergenic region or in regulatory elements, which makes it difficult to understand how they exert their effects. Additionally, while the statistical association has been successful in identifying polymorphisms responsible for Mendelian disorders characterized by single-gene inheritance patterns, many common diseases including hypertension, diabetes, cancer, or infections are multigenic traits affected by thousands of genetic variants, each making a small contribution to the phenotype (Witte *et al.*, 1996). Given that many eQTLs especially trans-eQTLs, tend to have small effect sizes, the association between gene variants and expression isn't robust enough to detect them in studies with limited sample sizes. Nevertheless, these effects can have a meaningful downstream impact (Gilad *et al.*, 2008; Cano-Gamez and Trynka, 2020). In addition to that, genetic associations are challenging to interpret, and it is difficult to pinpoint causal variants due to the linkage disequilibrium (LD). LD refers to the tendency of neighboring genetic variants to be inherited together, and thus to be correlated, due to their physical proximity on the chromosome. As a result, when studying associations between these variants and traits of interest, it is difficult to differentiate their individual contributions to the observed phenotypes and to identify which variants are truly causal (Flynn and Lappalainen, 2022). Moreover, variations in gene expression levels across diverse cell types and tissues significantly impact eQTL analyses. Current studies have indicated that variants associated with traits exhibit cell-type-specific effects. The Genotype-Tissue Expression Project (GTEx) investigated cis and trans QTLs across numerous tissues, estimating that approximately over 40% exhibit tissue-specific patterns (Flynn and Lappalainen, 2022). Furthermore, eQTLs can vary within the same cell under different environmental conditions, adding another layer of complexity to their regulatory mechanisms (Westra and Franke, 2014; Flynn and Lappalainen, 2022).
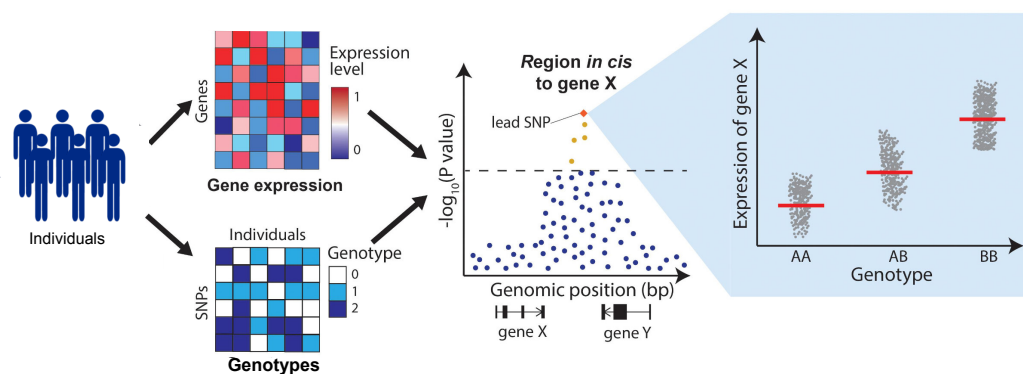
Figure 6.Schematic depiction of eQTL analysis.

For eQTL mapping, gene expression from a high number of individuals is tested for associations with genotypes. SNPs located close to the affected genes, within 1Mb from the transcription start site (TSS) are referred to as cis-QTLs whereas trans-QTL are found further away, often exceeding 1Mb or even residing on different chromosomes (taken from Cano-Gamez and Trynka, 2020).

1.3.4 Systems immunology in infections

The systems immunology approach has been successfully applied to study the immune response to different vaccines and viruses including influenza, yellow fever, and SARS-Cov-2. These studies have been able to uncover gene signatures and key immune components that align with the immune response, offering valuable insights into their interrelationships (Gaucher *et al.*, 2008; Nakaya *et al.*, 2011; Tsang *et al.*, 2014).

The analysis of the YF17D vaccine's transcriptional response has brought to light a wide spectrum of genes expressed post-vaccination. Notable among these are transcription factors like IRF7, STAT1, and ETS2, along with IFN-stimulated genes such as OAS1-3, IFI27, IFI30, MX1, and various viral sensing receptors like MDA5, RIG-I, TLR7, or LGP. Additionally, the vaccination stimulates DCs/macrophages-associated markers such as CD86, genes encoding the inflammasome and complement pathways, the TNFRSF13B gene associated with B cell activation or Transporter 1/2, ATP binding cassette subfamily B member (TAP1 and TAP2), which are engaged in antigen processing and presentation. This robust innate response tends to peak approximately seven days post-vaccination (Gaucher *et al.*, 2008; Querec *et al.*, 2009). Hou et al. confirmed that the innate and antiviral pathways induced at day 7 were associated with the expression of transcription factors (e.g. STAT1, JUN, FOS, NFκBIA) and observed distinct expression

patterns at the early 4h timepoint, characterized by the downregulation of cytokines and innate pathways as compared to 5 and 7 days post-vaccination, highlighting differences in gene regulation over time (Hou *et al.*, 2017).

The work by Querec et al. applied a systems immunology approach and identified early post-vaccination gene signatures correlating with later immune responses. The study identified several genes associated with T cell responses. However, only two genes were verified in two independent test sets; EIF2AK4 involved in stress response and the sugar transporter SLC2A6, demonstrated a correlation with the subsequent magnitude of the CD8+ T cells' response whereas the TNFRSF17 gene involved in B cell development correlated with the induction of neutralizing antibodies.

Several studies have explored universal signatures. Kotliarov et al. demonstrated that baseline gene signatures, including C15orf57, LONP2, PAPSS2, EPHB1, ADAM12, SMC1A, RETN, ENPP1, CD101, and C2orf63, can predict the antibody response in influenza-vaccinated individuals. Moreover, these signatures were also predictive of antibody responses to yellow fever. Additionally, their levels correlated with disease activity in lupus patients (Kotliarov *et al.*, 2020). Fourari et al. investigated responses across 13 vaccines, including YF17D, identifying three inflammatory endotypes (high, medium, low). The high inflammatory profile displayed elevated interferon signaling, pro-inflammatory genes, and myeloid immune cell signatures before vaccination (including DCs and monocytes).This primed immunity was characterized by higher CD4+ helper cell levels, improved antigen presentation, stimulated B cell differentiation, and antibody production (Fourati *et al.*, 2022). Using the same dataset, Hagan et al. have studied universal signatures associated with antibody response post-vaccination. The study showed that vaccine responses are not homogenous and different vaccines induce distinct immune response patterns. For some vaccines like Ebola or HIV, innate signatures peaked on day 1, for malaria on day 3, whereas yellow fever upregulated innate pathways later, on day 7 post-vaccination. Additionally, YF17D showed transient B and T cell signatures on day 1. Given the heterogeneity in responses, the study revealed a correlation between the early activation of the plasma cell module and the antibody response across different vaccinations (Hagan *et al.*, 2022).

eQTLs have significantly advanced our understanding of how genetic variations impact gene expression and immune response to infections and vaccinations. Franco et al. demonstrated the feasibility of an eQTL analysis in a study of immune responses to vaccination against influenza. The study integrated genotype, gene expression, and

antibody titer data to uncover genetic variation affecting the antibody response. It led to the identification of 20 genes including TAP2, ribosomal protein L14 (RPL14), HECT, and RLD domain containing E3 ubiquitin protein ligase 2 (HERC2), revealing that most of the affected genes are not directly associated with the immune system, but with intracellular antigen transport and membrane trafficking (Franco *et al.*, 2013). Several studies have explored response eQTLs, revealing changes in response to infection or stimulation, indicating context-specificity. Kim-Hellmuth et al. investigated eQTLs in the monocyte population, revealing cis effects of SNPs in NEU4, CCL14, and IRF5 genes post-LPS stimulation, with effects on TLR4 signaling. The study also highlighted the enrichment of eQTLs associated with lysosomal and trafficking pathways, particularly identifying cisQTL in lysozyme, which was suggested as a monocyte-specific master regulator of expression (Kim *et al.*, 2014). Additionally, other studies have described activating and suppressing response eQTLs, with transient or prolonged effects, by mapping eQTLs linked to responses from LPS and IFN-γ treatments. These studies demonstrated that cis-eQTLs were detectable only in activated monocytes, and additionally, revealed a temporal trans-effect of variants (Fairfax and Knight, 2014; Fairfax *et al.*, 2014; Kim *et al.*, 2014; Kim-Hellmuth *et al.*, 2017).

2.   Objectives

The project aims to use the yellow fever vaccine YF17D to investigate mechanisms of antiviral immunity and how innate immune characteristics influence the strength of adaptive immunity. Additionally, it seeks to identify genetic and non-genetic host factors that impact interindividual differences in responses to viruses and aims to detect biomarkers for stratifying patients based on their immune responses.

Aim 1: Investigate the activation of nucleic acid sensing pathways in response to YF-17D.

Aim 2: Analyze global transcriptomic changes to uncover broader patterns in the vaccine response as well as the transcriptomic profiles of individuals before and after vaccination with YF17D using RNA-seq.

Aim 3: Explore the association of single nucleotide polymorphisms (SNPs) at a genome-wide level, by conducting QTL and eQTL mapping. Identify interindividual variability in

vaccine response and discover cis- and trans-acting QTLs by analyzing the effects of SNPs on immune traits including neutralization, cytokine or immune cell levels, and induced gene expression post-vaccination.

3. Material and Methods

3.1 Materials

3.1.1 Technical Equipment

Equipment		Company
Analytical balance	CPA1003S	Sartorius Laboratory, Germany
autoMACS® Pro Separator		Miltenyi Biotec, Germany
Bioanalyzer	2100	Agilent, USA
	4200 TapeStation	
Cell culture incubator	BD 6220	Heraeus, Germany
Cell culture laminar flow	HeraSAFE 2025	Thermo Scientific, USA
Centrifuges	3L-R Multifuge	Heraeus, Germany
	5424/5315R	Eppendorf, Germany
	Rotina 420R	Hettich GmbH, Germany
	Optima MAX-XP	Beckman Coulter GmbH, Germany
Confocal microscope	Leica SP2 AOBS	Leica Microsystems, Germany
ELISA reader	Tristar 3	Berthold Technologies, Germany
FACS	Canto II	BD Biosciences, USA
	Cytoflex	Beckman Coulter GmbH, Germany
	Fortessa	BD Biosciences, USA
Fine scale	MC1 Analytic AC 210 S	Sartorius, German
Gel electrophoresis system		Peqlab, Germany
GloMax®	Explorer	Promega, USA
Heating block	Thermomixer 5436	Eppendorf, Germany
Imaging System	ChemiDoc™	Bio-Rad, Germany
LightCycler®	480 Instrument II	Roche, Switzerland
Magnetic rack	DynaMag-96	Thermo Scientific, USA
Microscope	Axiovert25	Zeiss, Germany
NanoDrop®	2000c	Thermo Scientific, Germany
pH-Meter	inoLab pH720	WTW GmbH, Germany
Thermocycler	T3	Biometra, Germany
Trans Blot Cell		Bio-Rad, Germany
Vortex mixer	Genie 2	Scientific Industries, Germany
Water bath	1012	GFL, Germany

3.1.2 Materials

Material	Company
Cell culture dishes	Greiner, Germany
Cell culture flasks (T25 to T175)	Costar Corning, USA
Cell culture plates (6- to 96 well)	Becton Dickinson, USA
Cell scraper	Sarstedt, Germany
Cryo tubes 2 mL	Grainer Bio-One, Austria
ELISA microplates (96-well)	Costar Corning, USA
Eppendorf tubes (0,5 ml, 1,5 ml, 2,0 mL)	Eppendorf, Germany
Eppendorf LoBind® Tubes (1,5mL)	Eppendorf, Germany
Eppendorf LoBind® plates (96-well)	Eppendorf, Germany
FACS tubes	BD Biosciences, USA
Falcons (15mL, 50mL)	Sarstedt, Germany
LS Columns	Miltenyi Biotec, Germany
Serological pipettes	Costar Corning, USA
Syringes	Becton Dickinson, USA

3.1.3 Kits

Kit	Company
Agilent RNA 6000 Pico Kit	Agilent, USA
CD 14+ Microbeads	Miltenyi Biotec, Germany
DC protein assay	Bio-Rad, Germany
ELISA Human DuoSet IFN-beta	R&D Systems, USA
ELISA substrate Reagent A/B	BD Pharmingen, USA
GeneJET Plasmid Miniprep kit	Thermo Scientific, USA
Human IP-10 ELISA set	BD Biosciences, USA
High Sensitivity RNA ScreenTape	Agilent, USA
High Sensitivity D5000 ScreenTape	Agilent, USA
High Sensitivity DNA Kit	Agilent, USA
IFN-beta DuoSet ELISA kit	R&D systems, USA
ILLUMINA Tag DNA Enzyme & Buffer Small Kit	Illumina, UK
Kapa HiFi HotStart ReadyMix 2X	Roche, Switzerland
NEBNext Ultra II Directional RNA Library Prep Kit	New England Biolabs, USA
NEBNext Poly(A) mRNA Magnetic Isolation Module	New England Biolabs, USA
NEBNext rRNA Depletion Kit	New England Biolabs, USA
NucleoSpin RNA virus	Macherey-Nagel, Germany
PeqGOLD kit (total RNA)	Peqlab, Germany
RevertAid First-Strand Synthesis System for RT-PCR	Thermo Fisher Scientific, USA
RNAeasy Plus Micro kit	Qiagen, Germany
RNasin® Plus Ribonuclease Inhibitor	Promega, USA

Pro Human Cytokine Assay	Bio-Rad, Germany
Pro Chemokine Assay	Bio-Rad, Germany
Pro Human Inflammation Assay	Bio-Rad, Germany
SuperSignal West Femto Sensitivity Substrate	Thermo Fisher Scientific, USA
SuperScript™ II (reverse transcriptase 200 U/µL, 5X buffer)	Thermo Fisher Scientific, USA
QuantiFluor® dsDNA System	Promega, USA

3.1.4 Chemicals and Reagents

Reagents	Company
5'-polyphosphatase	Biosearch Technologies, UK
Agencourt AMPure XP Beads	Beckman Coulter GmbH,Germany
Albumin Fraction V (BSA)	Sigma-Aldrich, Germany
Ammoniumpersulfate (APS)	Sigma-Aldrich, Germany
Ampicillin	Sigma-Aldrich, Germany
autoMACS Running Buffer	Miltenyi Biotec, Germany
autoMACS Washing Solution	Miltenyi Biotec, Germany
Betaine	Sigma-Aldrich, Germany
Blasticidin 100 mg	InvivoGen, USA
Bromophenol blue	Roth, Germnay
Calcium chloride	Sigma-Aldrich, Germany
Dimethyl sulfoxide (DMSO)	Sigma-Aldrich, Germany
DNase I	Roche, Germnay
dNTP-Mix, 10mM each	Thermo Fisher Scientific, Germany
dNTP -Mix, 10mM	Promega, USA
ERCC RNA Spikie-in Mix	Thermo Fisher Scientific, USA
Ethanol 96-100 %	Sigma-Aldrich, Germany
Ethylenediaminetetraacetic acid (EDTA)	Sigma-Aldrich, Germany
FACSFlow/FACSClean	BD Biosciences, USA
Fixable viability Dye (FVD) eFlour 780	Thermo Fisher Scientific, USA
Glycerol	Roth, Germany
Glycin	Roth, Germany
Heparin sodium (25,000 I.U./5 ml)	Ratiopharm, Germnay
HEPES	Sigma-Aldrich, Germany
Hydrogen peroxide (H_2O_2)	Merck, Germany
Human Serum	Sigma-Aldrich, Germany
Isopropanol	Applichem, Germnay
Lipofectamine RNAiMAX	Thermo Fisher Scientific, USA
Magnesium chloride solution 1M	Sigma-Aldrich, Germany
β-Mercaptoethanol	Sigma-Aldrich, Germany
Methanol	Merck, Germany
Milk powder	Roth, Germany
Paraformaldehyde (PFA)	Merck, Germany
Polyethylene glycol 8000	Roth, Germany
Potassium chloride	Sigma-Aldrich, Germany
Puromycin 100mg	InvivoGen, USA
RNase III	Thermo Fisher Scientific, USA

Rotiphoresis Gel 30 (37,5:1)	Roth, Karslruhe, Germany
Sodium azide (NaN$_3$)	Sigma-Aldrich, Germany
TE buffer low EDTA	VWR Chemicals, Germany
Sodium dodecyl sulfate (SDS)	Roth, Germnay
Sodium hydroxide (NaOH)	Roth, Germnay
TE buffer low EDTA	VWR Chemicals, Germany
Tetramethylethylendiamine (TEMED)	Roth, Germnay
TransIT-X2	Marius Bio, USA
Trichlorethanol	Sigma-Aldrich, Germany
Tris hydroxymethylaminomethan (Tris)	Roth, Karlsruhe, Germany
TRIS hydrochloride (Tris-HCl)	Roth, Germany
TRIzol reagent	Invivogen, USA
TruStain fcX	Biolegend, Germany
Tween-20	Roth, Germany
Trypan blue	Sigma-Aldrich, Germany
UltraPure™ DEPC-Treated Water	Thermo Fisher Scientific, USA

3.1.5 Solutions and cell culture media

Solution	Company
Dulbecco´s Modified Eagle Medium (DMEM) high glucose	Sigma-Aldrich, Germany
Fetal bovine serum (FBS)	Gibco Products, USA
L-glutamine (200 mM)	Sigma-Aldrich, Germany
MEM-NEAA (non-essential amino acids)	Life technologies, Germany
Opti-MEM	Gibco Products, USA
Penicillin/Streptomycin (1000U/ml/100 x)	Sigma-Aldrich, Germany
Phosphate-buffered saline (PBS)	Sigma-Aldrich, Germany
Recombinant GM-CSF murine	PeproTech, Germany
RPMI 1640	Sigma-Aldrich, Germany
Sodium pyruvate	Sigma-Aldrich, Germany
Trypsin-EDTA (10 x)	Lonza, Switzerland

DMEM culture medium
1% L-glutamine
100U/ml Pen-Strep
10% FCS
In DMEM

DC differentiation medium
1% L-glutamine
10% FCS
1% Penicillin/Streptomycin
1 % sodium pyruvate
1% MEM-NEAA
in RPMI 1640

3.1.6 Buffers and Solutions

FACS and sorting buffers

FACS buffer	2 mM EDTA, 2 % FBS, 0.1 % NaN_3
Fixation buffer	4% PFA
MACS buffer	0.2% FBS, 2 mM EDTA in PBS

SDS-PAGE and Western Blot

Stacking buffer (4x)	0.5 M Tris (pH 6.8), 0.1% SDS, 0.01% bromophenol blue
Separation buffer (4x)	1.5 M Tris (pH 8.8), 0.1% SDS
Running buffer	25 mM Tris, 200 mM glycine, 0.1% SDS
TBS-T	50 mM Tris (pH 7.6), 150 mM NaCl, 0.1%Tween 20
Transfer buffer	25 mM Tris, 200 mM glycine, 20% methanol

Virus purification buffer

TNE buffer	20 mM Tris-HCl pH 8, 150 mM NaCl, 2 mM EDTA

3.1.7 Sequencing primers and oligonucleotides

	Concentration	5'-3' sequence
Oligo-dT$_{30}$VN	100 μM	AAG CAG TGG TAT CAA CGC AGA GTA CTT TTT TTT TTT TTT TTT TTT TTT TTT TTT TVN
TSO	100 μM	AAGCAGTGGTATCAACGCAGAGTGAATrGrG+G
IS PCR	100 μM	AAGCAGTGGTATCAACGCAGAGT
i7		
N701		CAA GCA GAA GAC GGC ATA CGA GAT TCG CCT TAG TCT CGT GGG CTC GG
N702		CAA GCA GAA GAC GGC ATA CGA GAT CTA GTA CGG TCT CGT GGG CTC GG
N703		CAA GCA GAA GAC GGC ATA CGA GAT TTC TGC CTG TCT CGT GGG CTC GG
N704		CAA GCA GAA GAC GGC ATA CGA GAT GCT CAG GAG TCT CGT GGG CTC GG
N705		CAA GCA GAA GAC GGC ATA CGA GAT AGG AGT CCG TCT CGT GGG CTC GG
N706		CAA GCA GAA GAC GGC ATA CGA GAT CAT GCC TAG TCT CGT GGG CTC GG
N707		CAA GCA GAA GAC GGC ATA CGA GAT GTA GAG AGG TCT CGT GGG CTC GG
N708		CAA GCA GAA GAC GGC ATA CGA GAT CCT CTC TGG TCT CGT GGG CTC GG
N709		CAA GCA GAA GAC GGC ATA CGA GAT AGC GTA GCG TCT CGT GGG CTC GG
N710	100 μM	CAA GCA GAA GAC GGC ATA CGA GAT CAG CCT CGG TCT CGT GGG CTC GG
N711		CAA GCA GAA GAC GGC ATA CGA GAT TGC CTC TTG TCT CGT GGG CTC GG
N712		CAA GCA GAA GAC GGC ATA CGA GAT TCC TCT ACG TCT CGT GGG CTC GG
N714		CAA GCA GAA GAC GGC ATA CGA GAT TCA TGA GCG TCT CGT GGG CTC GG
N715		CAA GCA GAA GAC GGC ATA CGA GAT CCT GAG ATG TCT CGT GGG CTC GG
N716		CAA GCA GAA GAC GGC ATA CGA GAT TAG CGA GTG TCT CGT GGG CTC GG
N718		CAA GCA GAA GAC GGC ATA CGA GAT GTA GCT CCG TCT CGT GGG CTC GG
N719		CAA GCA GAA GAC GGC ATA CGA GAT TAC TAC GCG TCT CGT GGG CTC GG
N720		CAA GCA GAA GAC GGC ATA CGA GAT AGG CTC CGG TCT CGT GGG CTC GG
N721		CAA GCA GAA GAC GGC ATA CGA GAT GCA GCG TAG TCT CGT GGG CTC GG

N722		CAA GCA GAA GAC GGC ATA CGA GAT CTG CGC ATG TCT CGT GGG CTC GG
N723		CAA GCA GAA GAC GGC ATA CGA GAT GAG CGC TAG TCT CGT GGG CTC GG
N724		CAA GCA GAA GAC GGC ATA CGA GAT CGC TCA GTG TCT CGT GGG CTC GG
N726		CAA GCA GAA GAC GGC ATA CGA GAT GTC TTA GGG TCT CGT GGG CTC GG
N727		CAA GCA GAA GAC GGC ATA CGA GAT ACT GAT CGG TCT CGT GGG CTC GG
N278		CAA GCA GAA GAC GGC ATA CGA GAT TAG CTG CAG TCT CGT GGG CTC GG
N729		CAA GCA GAA GAC GGC ATA CGA GAT GAC GTC GAG TCT CGT GGG CTC GG
i5		
S501		AAT GAT ACG GCG ACC ACC GAG ATC TAC ACT AGA TCG CTC GTC GGC AGC GTC
S502		AAT GAT ACG GCG ACC ACC GAG ATC TAC ACC TCT CTA TTC GTC GGC AGC GTC
S503		AAT GAT ACG GCG ACC ACC GAG ATC TAC ACT ATC CTC TTC GTC GGC AGC GTC
S504		AAT GAT ACG GCG ACC ACC GAG ATC TAC ACA GAG TAG ATC GTC GGC AGC GTC
S505		AAT GAT ACG GCG ACC ACC GAG ATC TAC ACG TAA GGA GTC GTC GGC AGC GTC
S506		AAT GAT ACG GCG ACC ACC GAG ATC TAC ACA CTG CAT ATC GTC GGC AGC GTC
S507		AAT GAT ACG GCG ACC ACC GAG ATC TAC ACA AGG AGT ATC GTC GGC AGC GTC
S508	100 μM	AAT GAT ACG GCG ACC ACC GAG ATC TAC ACC TAA GCC TTC GTC GGC AGC GTC
S510		AAT GAT ACG GCG ACC ACC GAG ATC TAC ACC GTC TAA TTC GTC GGC AGC GTC
S511		AAT GAT ACG GCG ACC ACC GAG ATC TAC ACT CTC TCC GTC GTC GGC AGC GTC
S513		AAT GAT ACG GCG ACC ACC GAG ATC TAC ACT CGA CTA GTC GTC GGC AGC GTC
S515		AAT GAT ACG GCG ACC ACC GAG ATC TAC ACT TCT AGC TTC GTC GGC AGC GTC
S516		AAT GAT ACG GCG ACC ACC GAG ATC TAC ACC CTA GAG TTC GTC GGC AGC GTC
S517		AAT GAT ACG GCG ACC ACC GAG ATC TAC ACG CGT AAG ATC GTC GGC AGC GTC
S518		AAT GAT ACG GCG ACC ACC GAG ATC TAC ACC TAT TAA GTC GTC GGC AGC GTC

3.1.8 qPCR Primers

	5'-3' sequence
huINFb	F: CGACACTGTTCGTGTTGTCA
	R: GAGGCACAACAGGAGAGCAA
huHRPT	F: TGACCTTGATTTATTTTGCATACC
	R: CGAGCAAGACGTTCAGTCCT
muCXCL10	F: GCTGCCGTCATTTTCTGC
	R: TCTCACTGGCCCGTCATC
muHRPT	F: GGAGCGGTAGCACCTCCT
	R: CTGGTTCATCATCGCTAATCAC

3.1.9 FACS antibodies

Specificity	**Fluorophore**	**Company**
CD11b anti-mouse	BV785	BioLegend
CD11c anti-mouse	PB	BioLegend
MHCII anti-mouse	PE	BioLegend

F4/80 anti-mouse	APC	BioLegend
CD14 anti-human	PE	BioLegend
CD3 anti-human	FITC	BioLegend
CD89 anti-human	AF700	BioLegend
CD88 anti-human	APC	BioLegend

3.1.10 Softwares

Software	Company	Website
Affinity Designer	Serif (Europe) Ltd., UK	*https://www.graphpad.com/*
ComplexHeatmap v 2.2.0		*https://bioconductor.org/packages/release/bioc/html/ComplexHeatmap.html*
CrossMap v. 0.2.6		*https://pythonhosted.org/CrossMap/*
clusterProfiler 3.14.3		*https://bioconductor.org/packages/release/bioc/html/clusterProfiler.html*
edgeR v.3.28.1		*https://bioconductor.org/packages/release/bioc/html/edgeR.html*
FastQTL		*https://github.com/francois-a/fastqtl*
FlowJo v.9.9.5	Tree Star, USA	*https://www.flowjo.com/*
Graphpad Prism v.10	Graphpad Software, USA	*https://www.graphpad.com/*
GSVA 1.34.0		*https://github.com/rcastelo/GSVA*
Limma .3.42.2		*https://bioconductor.org/packages/release/bioc/html/limma.html*
PLINK 1.9		*https://www.cog-genomics.org/plink/*
SNPTEST v.2.5.6		*https://www.chg.ox.ac.uk/~gav/snptest/*
R v.3.6.3/v.4.3		*https://www.r-project.org/*
WGCNA v. **v.** 1.72-1		*http://horvath.genetics.ucla.edu/html/CoexpressionNetwork/Rpackages/WGCNA/*

3.2 Methods

3.2.1 Cell biological methods

3.2.1.1 Cell culture

All cell lines were grown in DMEM (10% FCS, 1% L-glutamine, 100U/ml Pen-Strep) under standard conditions (37°C, 5% CO_2, >90% humidity). Vero cells and BHK-21 cells were derived from ATCC. The human melanoma cell line 1205Lu was kindly provided by Robert Besch (University Hospital, LMU Munich, Germany) and validated by STR-typing. The used 1205Lu knockout cells were generated by CRISPR-Cas 9 gene editing as described in Boehmer et al. (Boehmer *et al.*, 2021). Additionally, sgRNA: TCAGCTCCCGGCGTCGGTTC for FOSL2 KO and the vector construct were ordered at VectorBuilder (USA).

3.2.1.2 Virus strains

To perform measurements of the functional assays (such as neutralizing antibody assays), we produced and purified the yellow fever virus: YF17D derived from a Stamaril® vaccine and the modified YF17D with fluorescent reporter gene Venus (YF17D-Venus). The YF17D-Venus plasmid was a kind gift from Charles M. Rice and Margaret MacDonald (The Rockefeller University, New York, USA).

3.2.1.3 Virus purification

The virus was purified using the previously established protocol (Scheck *et al.*, 2022). BHK-21 cells or Vero B4 cells were infected with YF-17D (MOI 0.1) at a confluency of 70%. Cell culture supernatants were collected and pooled post-infection after a 60% cytopathic effect was observed (after 2-3 days for YF-17D and 3-4 days for YF-17D Venus). The supernatant was clarified to remove cellular debris by centrifugation at 2200 × g at 4° C for 15 min. Polyethylene glycol (PEG 8000) was gradually added to the clarified supernatant on ice until 7% (w/v) concentration was achieved and subsequently rotated at 4°C at low speed for at least 3 h. The supernatant containing the PEG was next pelleted at 3800 × g at 4°C for 80 min and resuspended in cold TNE buffer (20 mM Tris-HCl pH 8, 150 mM NaCl, 2 mM EDTA). After resuspension in 2.5 mL TNE buffer the virus solution was layered on top of a double sucrose cushion of 1mL, 30% sucrose in TNE buffer on top and 2 mL, 60% sucrose on the bottom of a Beckaman Coulter ultracentrifuge tube (5 mL). Ultracentrifugation was performed at 160000 × g at 4°C for 2 h in an MLS 50 rotor (Beckman Coulter). Successful fractionation results in a clear virus band which can be collected and diluted in cold TNE buffer. The purified virus was stored at -80°C until use. The number of infectious units in the viral fraction was determined by plaque assay.

3.2.1.4 Infection of 1205Lu cell lines

The Venus-YF17D virus, diluted to the desired multiplicity of infection (MOI) in Opti-MEM, was used to infect 1205Lu cells. The cells were then incubated for 24 or 48 hours. Following the incubation period, the medium was collected, and the cells were subsequently lysed.

3.2.1.5 Enzymatic treatment and transfection of RNA

Wild-type 1205Lu cells were infected with the YF17D virus at MOI of 3 PFU/mL and plated in a 6-well plate at a density of $2x10^5$ cells per well in 2 mL of DMEM culture medium. After 24, 48 or 72 hours total RNAs were isolated using TRIzol reagent (Invitrogen) according to the manufacturer's guidelines. The extracted RNAs underwent treatment with various RNA-modifying enzymes before re-transfection into 1205Lu cells. Specifically, 1 µg of RNA was incubated with RNase III (Thermo Scientific) or 5'-polyphosphatase (Biosearch Technologies) for 30 minutes at 37°C, using the respective buffers as directed by the manufacturer's protocol. Subsequently, 100 ng of RNA either treated or untreated with enzyme was re-transfected into 1205Lu cells seeded in a 96-well plate (2,5 $x10^3$ cells) using 0.3 µL of Lipofectamine RNAiMAX (Thermo Scientific) following the manufacturer's instructions. The concentration of CXCL10 in the cell culture medium was quantified via ELISA after 24 hours, following the manufacturer's protocol.

3.2.1.6 Generation and infection of bone marrow-derived macrophages and DCs

Femurs and tibiae of C57BL/J6 mice lacking MyD88, TRIF/MyD88, TRIF/MyD88/MAVS, TRIF/MyD88/STING, and TRIF/MyD88/STING/MAVS were kindly provided by the group of Ulrich Kalinke (TWINCORE, Hannover, Germany). The isolated bone marrow (BM) cells from the femurs and tibia of C57BL/J6 mice were cultured in 10 cm dishes. To generate GM-CSF-derived dendritic cells (GM-DCs) and macrophages (GM-Macs), BM cells were seeded at a density of 2x10^5 cells/ml in 10 ml of RPMI-1640 differentiation medium supplemented with 20 ng/ml recombinant murine GM-CSF, 10% FCS, 1% L-glutamine, 1% Pen-Strep, 1% NEAAs, and 1% Na-Pyruvate. The cells were then cultured at 37°C in a humidified atmosphere with 5% CO_2 for 7 days. During this period, the differentiation medium was filled to 20 ml and exchanged every 2 days for macrophages or every 3 days for dendritic cells, with the addition of fresh GM-CSF. The success of the differentiation process was confirmed using flow cytometry.

3.2.1.7 Infection of bone marrow-derived macrophages and DCs

Following differentiation, GM-CSF DCs and Macs were seeded for FACS analysis in a 12-well plate at a density of 5x10^5 cells/well and for qPCR in a 96-well plate at a density of 5x10^4 cells.

All cells were infected with YF17D Venus at an MOI of 1 or 5 PFU/ml. After 24 h, cell lysates were prepared, and CXCL10 levels were quantified by qPCR. Subsequently, virus replication was assessed by monitoring Venus's expression levels using flow cytometry after 48 h. For that GM-Macs and GM-DCs cells were collected and transferred onto a 96-well plate. They were then washed in a FACS buffer containing 0.5% BSA and 2 mM EDTA, followed by a 10-minute incubation in an FcR-blocking reagent TruStain fcX (Biolegend) at room temperature. Surface marker expression on GM-Macs and GM-DCs was analyzed using a panel of antibodies including CD11b (BV785), CD11c (PB), MHCII (PE), F4/80 (APC), and a live-dead stain (APC-Cy7). Staining was performed in a FACS buffer containing the fluorescently labeled antibodies mentioned above, and the cells were incubated at room temperature for 15 minutes. After staining, the cells were washed and fixed in 4% PFA at room temperature for 20 minutes. Samples were then analyzed using a FACS Fortessa (BD Bioscience) flow cytometer, and the data were processed using FlowJo software v 9.9.5.

3.2.2 Human samples

The cohort comprised 250 healthy Caucasian volunteers who required the yellow fever virus vaccine (STAMARIL®; Sanofi Pasteur, Lyon, France) for travel purposes. Recruitment occurred between 2015 and 2019 at the Division of Infectious Diseases and Tropical Medicine, as well as the Department of Clinical Pharmacology, LMU in Munich, Germany.

Research ethics committees granted approval for the volunteer recruitment and vaccination protocols used this study (IRB #86-16). The clinical study was registered retrospectively in the ISRCTN registry (ISRCTN17974967).

Bio-samples (serum and plasma) were taken before the vaccination (day 0) and then successively on days 3, 7,14, and 28 days after the vaccination and stored at -80°C or in liquid nitrogen. PBMC samples were isolated using Ficoll-Paque PLUS (GE Healthcare) gradient centrifugation and cryopreserved in bovine serum with 10% DMSO in liquid nitrogen.

3.2.3 Immunological methods

3.2.3.1 Enzyme-linked immunosorbent assay (ELISA)

Cytokine levels in the cell culture supernatant were determined using the commercial IFN-beta DuoSet ELISA kit (R&D systems) or Human IP-10 ELISA Set (BD) according to the manufacturer's protocol.

3.2.3.2 Multiplex measurement of cytokine levels

Plasma samples were centrifuged at 10000g for 10 min. Prior to cytokine analysis, the Bio-Rad human cytokine Bio-plex immunoassay was carried out according to the manufacturer's instructions using three different panels (pro Human Cytokine Assay, pro Human Chemokine Assay, pro Human Inflammation Assay). To generate the standard curve, serial dilutions of standards were performed in a standard diluent. The assays were run using plasma samples for each timepoint. A 50 μl volume of each sample (diluted 1:3 in assay buffer) and standards were added to a 96-well plate (provided with the kit) containing 50 μl of antibody-coated fluorescent beads. Biotinylated secondary and streptavidin-PE antibodies were added to the plate with alternate incubation and washing steps. After the last wash step, 125 μl of the assay buffer was added to the wells, the plate was incubated and read on the Bio-plex array reader (Bio-Plex Luminex-200) station using a 5-PL regression curve, giving the standard curve. Data were subsequently analyzed using the Bio-plex Manager software.

The raw data measured in pg/ml were log2-transformed and next corrected for batch (corresponding to assay days) effects. This was done by taking the difference between the total mean of each cytokine and the mean of each batch as follows,

$$x_j^{i'} = x_j^i + (\overline{\mu} - \mu^i)$$

where μ is the mean, i is the batch index and j is the patient index. Thus, each data point belonging to each batch was corrected to yield batches with the same means.

3.2.3.3 Neutralizing antibody titer measured by Fluorescence Reduction Neutralization Test (FluoRNT assay)

The following protocol was described previously (Scheck *et al.*, 2022). Vero cells were seeded in a flat-bottom 96-well plate (2.5×10^4 cells /well) and cultured in 100 μl of DMEM (10% FCS, 1% L-glutamine, 1% Pen-Strep). The cells were incubated overnight at 37°C.

On the following day, each serum was centrifuged at 10000g for 10 min, diluted 1:5 in DMEM and incubated for 30 min at 56°C. The serum was diluted serially in DMEM containing 0,02% BSA. For each serum, the starting dilution was 1/10 with nine 3-fold dilutions up to the final dilution of 1/196,830. The serum was mixed with a concentration of the YF-17D Venus virus, which infects 50% of the cells. The virus-serum mixture was incubated at 37°C for 1 h and transferred onto the Vero cell plate and incubated for another 24h at 37°C. Next, the cells were stained with the Fixable Viability Dye at 4°C for 20 min and fixed in a fixation buffer for 20 min at RT. The cells were resuspended in PBS and analyzed using flow cytometry.

The neutralizing titer (NT) was determined from the serum dilution (days 14 and 28) that gave an 80% reduction of the YF17D Venus fluorescence positive cells in the FACS readout (NT80) compared to the serum control without an antibody (serum from day 0). For these calculations, the serum dilutions were log10-transformed: the standard curve was generated using a 4-PL regression curve. The data were plotted using Prism 10 (GraphPad).

3.2.4 Molecular methods

3.2.4.1 Reverse transcription PCR (RT-PCR) and quantitative real-time PCR (qPCR) analysis

Cellular RNA was extracted from cell lysates using the total RNA PeqGOLD kit (Peqlab). Subsequently, the RNA was reverse transcribed into cDNA utilizing oligo-dT or random hexamers with the RevertAid First-Strand Synthesis System for RT-PCR (Thermo Fisher Scientific) according to Table 3.2A. The master mix was incubated for 1 h at 42°C, followed by a 10 min inactivation step at 70°C.

Table 3.2A RT-PCR master mix

Component	Stock concentration	1x reaction
RNA	Up to 1000ng	11 μl
Oligo-dT/random hexamers	10 μM	2 μl
Ribolock	20 U/μl	0.5 μl
dNTP	10 mM	2 μl
RevertAid	200 U/μl	0.5 μl
5x Reaction buffer		4 μl
H$_2$O		9 μl

The qPCR Master mix was prepared as described in the table 3.2B. Gene-specific primers for human or murine targets were designed using the universal probe library

center (Roche). The qPCR was performed on the Roche Light Cycler 480-II/96. The samples were incubated in a thermal cycler as described in Table 3.2C.

The $\triangle$CT method was used for gene expression analysis. Data were normalized relative to the expression of the HPRT reference and then $\triangle\triangle$CT was used to calculate the fold-changes relative to uninfected control.

Table 3.2B qPCR master mix

Component	Stock concentration	1x reaction
cDNA		3 μl
Fwd Primer	10 μM	0.2 μl
Rev Primer	10 μM	0.2 μl
Probe		0.1 μl
qPCR buffer (2x)		5 μl
H$_2$O		up to 10 μl

Table 3.2C qPCR program

Step	Temperature (ºC)	Time	Cycles
Pre-incubation	95	10 min	1 cycle
Denaturation	95	10 sec	40 cycles
Elongation	60	30 sec	
Cooling	40	∞	

3.2.4.2 RNA-seq library generation using the Smart-seq2 protocol

The monocyte population was isolated from frozen PBMCs using CD14^{+} MACS beads and autoMACS (Miltenyi), a high-speed magnetic sorting device. The cells were sorted into MACS buffer and after isolation were immediately transferred into an RNAse-free, LoBind 1,5 mL tube (Eppendorf) containing the RLT lysis buffer (RNAeasy Plus Micro kit, Qiagen). Cells were lysed and stored frozen at –80°C. The RNA isolation was executed using the RNAeasy Plus Micro kit according to the manufacturer's protocol. Total RNA sample quality was evaluated using the High Sensitivity RNA ScreenTape and Bioanalyzer (TapeStation, Agilent). The 3.7 μl of the isolated RNA was transferred onto a RNAse-free, LoBind 96-well plate (Eppendorf). The next steps were performed following the modified Smart-Seq2 protocol (Picelli *et al.*, 2014), using primers listed in Table 3.1.7. For the reverse transcription reaction, 0.1 μl of Oligo-dT$_{30}$VN primer (100 μM),1 μl of dNTP mix (10 mM,Promega) and 0.2 μl of 1:125 000 ERRC spike-in RNA were added to the isolated RNA, then centrifuged and placed on ice. The samples were incubated for 3 min at 72 °C and transferred back on ice. The reverse transcription mix

was prepared according to Table 3.2D and 5 μl of it was added to the samples. The samples were incubated in a thermal cycler (Table 3.2E). The cDNA was pre-amplified (Table 3.2F and 3.2G). The pre-amplified cDNA was purified with 21 μl AMPure XP DNA beads diluted with 15 μl water per sample (Beckman Coulter). The concentration of each sample was quantified with the QuantiFluor dsDNA system (Promega). Next, tagmentation and PCR enrichment of adaptor-ligated DNA were performed. The Tagmentaion mix (1,5 μl) was added (Table 3.2H) to the purified cDNA (diluted to 1 ng/μl final concentration) and incubated for 10 min at 55°C and then placed on ice. Next, 11,2 μl of KAPA HiFi HotStart Ready Mix (Roche) and 4,4 μl of i5 and i7 adaptors primers (5 μM) were added and amplified according to Table 3.2I. Afterwards, the PCR product was purified using 13,5 μl AMPure XP beads/per sample. The cDNA library quality was checked with Bioanalyzer using the High Sensitivity D5000 ScreenTape (Agilent). In the end, the libraries derived from patients were pooled and analyzed with an Illumina NovaSeq6000 sequencer.

Table 3.2D Reverse transcription mix

Component	Volume μl/reaction	Final concentration in 10 μl
Superscript II Reverse transcriptase 200 U/μl	0,25	50 U
RNAse Inhibitor	0,25	10 U
Superscript II First strand buffer	2	1x
DTT 100 mM	0,5	5 mM
Betaine 5 M	1,84	0,92 M
MgCl2 1 M	0,06	6 mM
TSO Primer 100 μM	0,1	1 μM
Total volume	5	

Table 3.2E PCR program for reverse transcription reaction

Cycle	Temperature (°C)	Time (min)	Step
1	42	90	RT and template switching
10	50	2	Unfolding of RNA secondary
	42	2	structure
			Continuation of RT
12	70	15	Enzyme inactivation
13	4	Hold	Safe storage

Table 3.2F cDNA pre-amplification mix

Component	Volume μl/reaction	Final concentration in 10 μl
KAPA HIFI HotStart Ready Mix 2x	12,5	1x
IS PCR Primer 10 μM	0,25	0,1 μM
Nuclease free water	2,25	
Total volume	15	

Table 3.2G PCR program for cDNA pre-amplification

Cycle	Temperature (°C)	Time (min)	Step
1	98	3	Denaturation
13	98	2	Denaturation
	67	2	Annealing
	72	6	Extension
20	72	5	Extension
21	4	Hold	Safe storage

Table 3.2H Tagmentation mix

Component	Volume μl/reaction	Final concentration in 10 μl
Tagmentaion DNA buffer (2x)	1,25	1x
TDE1	0,25	–
Nuclease free water	-	–
Total volume	1,50	

Table 3.2I PCR-program for tagmentation

Cycle	Temperature (°C)	Time (min)	Step
1	98	3	Denaturation
2-19	98	2	Denaturation
	67	2	Annealing
	72	6	Extension
20	72	5	Extension
21	4	Hold	Safe storage

3.2.5 Data analysis

3.2.5.1 RNA-seq data processing and differential gene expression analysis

For the entire cohort, RNA-seq reads were processed using the publicly available nf-core RNA-seq pipeline with standard options available at https://github.com/nf-core/rnaseq. For the QC step, gene counts obtained after STAR alignment and Salmon quantification were transformed into log counts per million (log-CPM) and normalized to account for library size using the calcNormFactors and TMM functions (Robinson and Oshlack, 2010) in the R package edgeR v.3.28.1 (Robinson *et al.*, 2009). Low-expressed genes were filtered out for each sample using the filterByExpr function in edgeR (with a minimum count threshold of 5) after the normalization step. Differential expression analysis between day 0 (before vaccination) and day 7 (after vaccination) was performed using the limma-voom function (Law *et al.*, 2014) that transforms RNA-seq read counts to log-CPM and applies TMM normalization. A linear mixed regression model was fitted using the limma lmFit function from the R package limma v.3.42.2 (Ritchie *et al.*, 2015) with the fixed effects being the timepoint (day 0 vs. day 7) and the batch. Differentially expressed genes were evaluated using empirical Bayes moderated t-statistics and corrected for multiple testing (BH-FDR p-value < 0.05).

3.2.5.2 Genotype data processing

DNA samples from 250 individuals underwent genotyping using the Illumina Infinium Global Screening Array-24 v.3.0 SNP chip. Genotype calling was carried out with GenomeStudio Version 2.0 using default parameters and mapped to GRCh37 using online tools (http://www.well.ox.ac.uk/~wrayner/ strand/index.html). Quality control procedures were applied to both samples and genotyped variants using PLINK 1.9 and R. Samples with a call rate < 0.98, minor allele frequency (MAF) ≥ 0.01 or MAF < 0.01 and relatedness (PI_HAT ≤ 0.2) were excluded, resulting in the removal of 7 samples. Additionally, 5 individuals with non-European ethnicity were identified by comparing genotypes with those from the 1000 Genomes dataset. These 5 samples were included after correction for population structure using PC analysis. Subsequently, SNP quality control was performed, leading to the exclusion of 23,000 SNPs (call rate < 0.98 and Hardy-Weinberg equilibrium (HWE) p < 0.0001) resulting in the final dataset containing of 243 individuals and 634,265 SNPs .To enhance genotype calling breadth, imputation was conducted using the Haplotype Reference Consortium panel (HRC version 1.1) and

the Michigan Imputation Server (Das *et al.*, 2018) with Eagle2 (v2.3) phasing. SNPs with an INFO score of R ≥ 0.9 post-imputation or MAF > 0.05 were selected for further QTL mapping using the SNPTEST program v.2.5.6 using sex, age, and age^2, 20 PCs (for ethnical correction), along with seasonality and TBE positivity as covariates.

3.2.5.3 eQTL mapping

For cis-eQTL mapping, the variant coordinates were converted from GRCh37 to GRCh38 using CrossMap software v. 0.2.6 (Ongen *et al.*, 2016). For eQTL analyses, we focused on common variants (MAF >= 0.05) that are biallelic. Variants were excluded if the call rate was <99%. All filtering steps were performed using bcftools v. 1.1. To ensure the normal distribution of gene expression data, a rank-based inverse normal transformation of the log-CPM gene counts was applied. To identify hidden factors and batch effects associated with the cohort, Probabilistic Estimation of Expression Residuals (PEER) method (Stegle *et al.*, 2012) was used. For cis-eQTL analysis, along with the 20 principal components (PCs) employed for ethnicity correction, sex, age, and age^2 together with 30 PEER factors were included as covariates. Mapping was conducted for SNPs located within 1Mb of the transcription start site (TSS) using the FastQTL software (Ongen *et al.*, 2016), following the GTEx pipeline (Aguet *et al.*, 2017, 2023). Permutation p-values for each association were obtained using the --permute 100 10000 option. As described in Steinberg et al.(2020,2021) genes with significant eQTLs ('eGenes') were defined at the 5% Storey–Tibshirani FDR using the q-values generated from the empirical p-values. For each eGene, significant eQTLs were defined as variants with nominal p-value below the nominal p value threshold for that gene generated in FastQTL (Steinberg *et al.*, 2020, 2021).

To identify eQTLs associated with the response to infection (res-eQTLs), the multivariate adaptive shrinkage (mashr) software (Urbut *et al.*, 2019) was employed. Effect sizes were calculated from nominal p-values following previously established GTex:workflows:https://github.com/stephenslab/gtexresults/blob/master/workflows/fast qtl_to_mash.ipynb). Significant res-QTLs were defined as those with a local false sign rate (LFSR) < 0.05 in day 7 post-vaccination and not on day 0 (pre-vaccination).

3.2.5.4 Pathway Analysis

For the pathway enrichment analysis in the detected DEGs, Gene Ontology (GO) analysis was conducted with the enrichGO function for biological processes terms, while the Reactome pathway enrichment was performed using the enricher function. Overrepresented and underrepresented pathways were identified separately for the up- and down-regulated DE genes.

Gene set enrichment analysis (GSEA) (Subramanian *et al.*, 2005) was carried out using the MSigDB Hallmarks collection and the fgsea function.

All pathway enrichment analyses were performed using the clusterProfiler R package v. 3.14.3 (Wu *et al.*, 2021) with minimum and maximum gene set sizes of 10 and 300, respectively Benjamini Hochberg's FDR correction for multiple testing was applied (q-value threshold of <0.02).

3.2.5.5 Transcription factor activity

Transcription factor activity was inferred using the R package decoupleR (Badia-I-Mompel *et al.*, 2022) based on the CollecTRI a TF-gene interaction database (Müller-Dott *et al.*, 2023) with TF scores taken as t-values calculated from the multivariate linear model applied to DEGs (FDR<0.05).

3.2.5.6 Gene set variation analysis (GSVA)

To evaluate transcriptional profiles across individuals, gene set module scores were calculated from normalized gene expression data at day 0 and day 7 using the gene set variation analysis (GSVA) R package v. 1.34.0 (Hänzelmann *et al.*, 2013) and the MSigDB Hallmarks collection.

3.2.5.7 Weighted gene co-expression analysis (WGCNA)

To identify co-expressed genes associated with the adaptive immune response, the weighted gene co-expression analysis (WGCNA) R package v. 1.72-1 was used (Langfelder and Horvath, 2008). Normalized gene expression data from day 0 and day 7 were employed to construct a signed co-expression network, with a soft power of 3 and a mergeCutHeight of 0.25. Modules were identified from the gene dendrogram using

the cutreeDynamic function, with a minimum cluster size of 30. Pearson correlation analysis was conducted to assess the association of modules with traits, including CD4$^+$/CD8$^+$ T cell frequencies and neutralization levels.

3.2.5.8 Hierarchical clustering

All heatmaps were generated using the ComplexHeatmap package v 2.2.0 in R.(Gu, 2022) Hierarchical clustering using Euclidean distance with the linkage method as indicated in the respective figure's caption was used to cluster samples. The optimal number of clusters was determined by the NbClust function (index = all). The visualization was performed by factoextra R packages.

3.2.6 Statistical analysis

Data are displayed as the mean and standard deviation (SD) or medians (center lines) and first and third quartiles, as indicated in the respective figure legend. To assess the statistical significance of the differences between two groups, Wilcoxon Rank Sum test or t-tests were performed; for more than two groups, one-way analysis of variance (ANOVA) with Dunnett's test (for independent samples) or ANOVA for non-independent samples, followed by post-hoc paired t-tests between selected samples with Bonferroni correction for multiple hypothesis tests was performed. For differences between more than two groups with non-normally distributed samples, the Kruskal-Wallis H test, followed by the Mann–Whitney–Wilcoxon's post-hoc U test with Benjamini-Hochberg's correction for multiple tests was used. All statistical tests were performed using the GraphPad Prism 10 software, or R and adjusted P values < 0.05 were considered as significant. Significance levels are indicated as *, **, *** for < 0.05, < 0.01, and < 0.001, respectively.

4. Results

4.1 Interferon-signaling induced in response to YF17D via the RLR-pathway restricts viral replication

To get insight into receptors and pathways sensing YF17D, a study using murine human cells and cell lines *in vitro* was performed. We derived macrophages and dendritic cells from mouse bone marrow cells lacking one or multiple signaling adaptors using GM-CSF (GM-Macs and DCs) and infected them with 1 MOI of YF17D variant encoding the Venus fluorescent protein (Figure 7) (Zaucha, Winheim *et al.* manuscript in preparation), see disclaimer page 7.
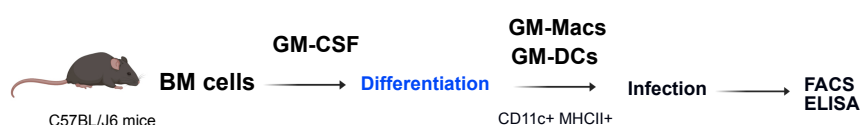
Figure 7.Schematic depiction of murine BM cell differentiation into macrophages.

After differentiation, the cells were infected with YF17D Venus, and the infection rate was assessed by flow cytometry and cytokine secretion by ELISA.

Flow cytometric quantification of Venus-positive CD11c$^+$ MHCII$^+$ cells within the GM-CSF BM culture enabled the simultaneous analysis of two subpopulations: Macrophages (GM-Macs) expressing intermediate levels of MHCII and DCs (GM-DCs) expressing high levels of MHCII (Supplementary Figure 1).

Overall, the YF17D infection rate in GM-Macs was higher than in GM-DCs which suggest that macrophages are more susceptible to viral infection with YF17D than DCs. These data revealed a significant rise in the proportion of Venus+ infected cells in IFNAR KO GM-Macs and GM-DCs (p-value < 0.0001). Furthermore, MAVS KO GM-Macs and GM-DCs (p-value 0.0285) displayed increased frequencies of infected cells, while cells lacking MyD88 alone, TRIF and MyD88 or TRIF, MyD88, and STING displayed no difference in comparison to the wild-type (WT) control. Combining knockout of TRIF/MyD88 or TRIF/MyD88/STING with MAVS did not yield a further increase in infection rates compared to MAVS-deficient cells (Figure 8A). The clearly increased YF17D infection rate in cells deficient in MAVS, the common adapter of the sensing receptors RIG-I and MDA5, compared to cells deficient in MDA5 alone suggests an

important role for RIG-I as a restriction factor for YF17D. The RIG KO mouse does not breed well on the Bl6 background and was therefore not included in the presented experiment. Analysis of the interferon-induced CXCL10 gene after infection with YF17D in the same cells displayed a pattern inverse but compatible with the flow cytometry results, demonstrating a decrease in CXCL10 mRNA levels in MAVS KO and IFNAR KO GM-DCs/Macs mixture as shown in Figure 8B.
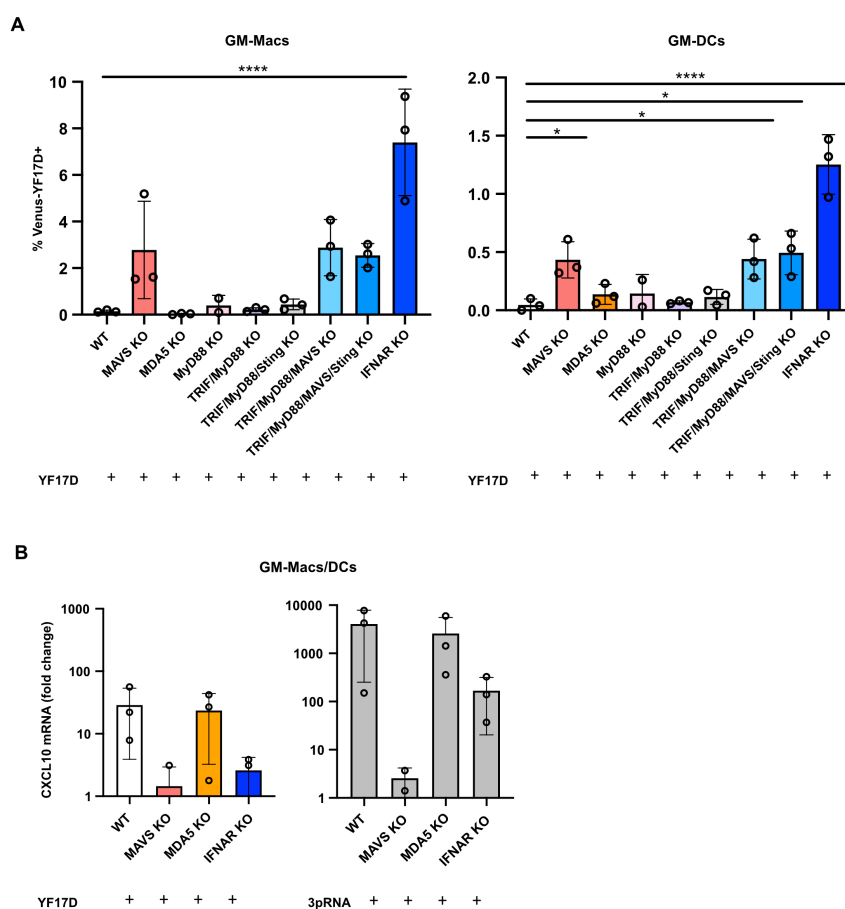
Figure 8.Interferon-signaling is induced in murine cells in response to YF17D via MAVS and restricts viral replication.

A) GM-Macs and GM-DCs from each genotype cultured with 20ng/ml GM-CSF were infected with Venus YF17D at an MOI 1. Flow cytometry was used to measure the percentage of Venus-positive cells 48 hours post-infection (hpi). One-way ANOVA test with Dunnett's test was used to compare WT cells with the indicated knockout phenotype, n = 3, except for MyD88 B). The mRNA levels of CXCL10 were quantified using qRT-PCR 24 hpi. The data were normalized to the relative expression of the HPRT reference gene and presented as fold changes relative to uninfected cells. One-way ANOVA test with Dunnett's test was used to compare WT cells with the indicated knockout phenotype, n = 3. Error bars indicate means and standard deviations (*, **, ***and **** represent adjusted p-values ≤0.05, ≤0.01, ≤0.001 and ≤0.0001 respectively).

Additionally, to confirm the previous findings in human cells, the CRISPR/Cas9 gene editing technology was used to create knockout cell clones in the 1205Lu human melanoma cell line (responsive to RIG-I, MDA5, and TLR3 but not TLR7/8 ligands). The FACS results show that the percentage of infected cells increased significantly in 1205Lu cells lacking MAVS (p-value <0.0001) or RIG-I, (p-value 0.0016) but not in cells lacking MDA5 or TRIF (Figure 9A and B). Double knockouts of MDA5/RIG-I, TRIF/MAVS, or TRIF/RIG-I exhibited an increased infection rate, however similar to single knockout cell lines lacking MAVS, RIG-I, or IFNAR. This indicates that in 1205Lu cells, YF17D replication is restricted by type I IFN and MAVS signaling, where RIG-I appears to play a dominant role. The viral replication in MAVS and RIG-I knockout cell lines correlated with a remarkable decrease in YF17D-induced IFN-β mRNA expression. The most significant reduction in IFN-β expression in response to YF17D occurred in MAVS and RIG-I/MDA5 double knockout cells, comparable to the reduction observed after stimulation with 5'-triphosphate RNA, used as a positive control. After YF17D infection, IFN-β mRNA expression was also reduced in RIG-I single knockout cells, although not to the same degree as in MAVS knockout or MDA5/RIG-I double knockout cells (Figure 9C). Concentrations of IFN-β in the supernatants were undetectable in YF17D-infected MAVS knockout and MDA5/RIG-I double knockout cells. However, residual IFN-β production was observed in RIG-I knockout and MDA5 single knockout cells, indicating that MDA5 also contributes to the overall IFN-β response in 1205Lu cells (Figure 9D).
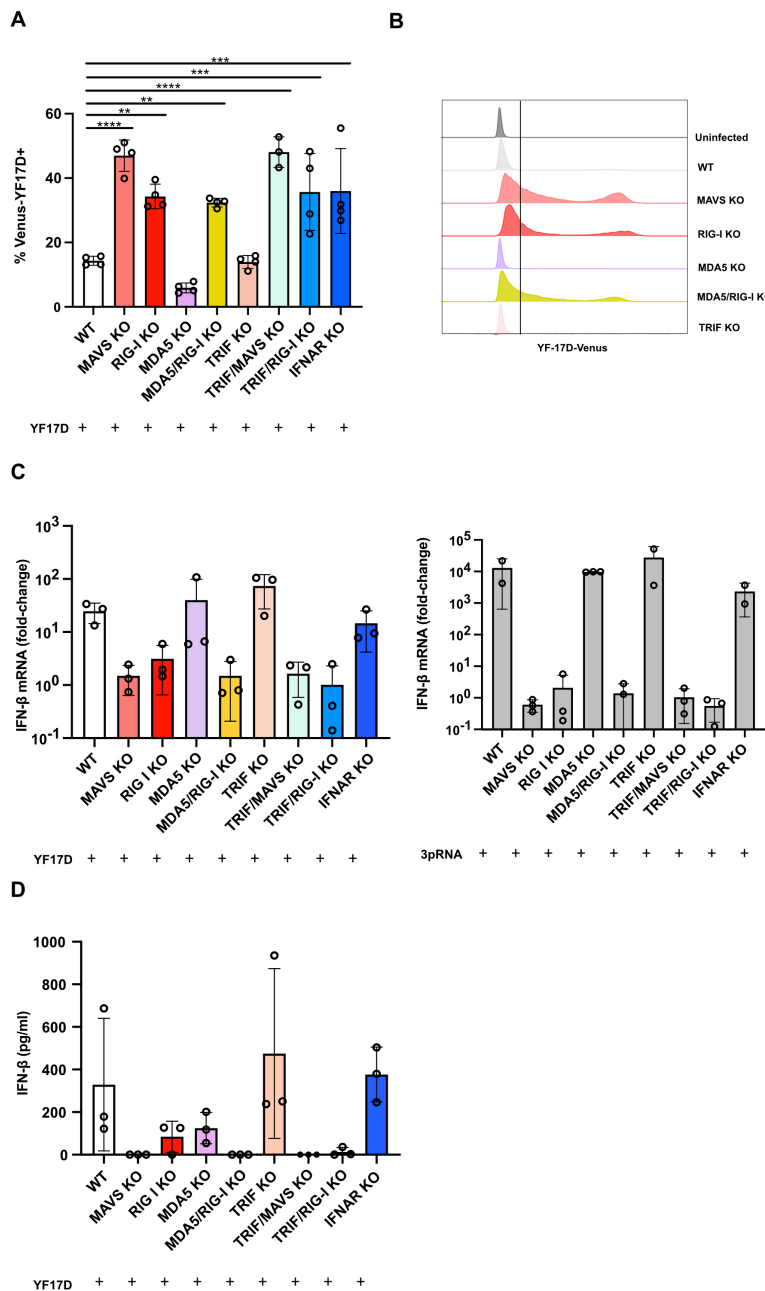
Figure 9. The RLR pathway is activated in 1205Lu melanoma cells in response to YF17D.

Wild-type (WT) and CRISPR-knockout (KO) 1205Lu cells deficient for the indicated proteins were infected with Venus-YF17D at an MOI of 5. A) Flow cytometry analysis was used to measure the percentage of Venus-YF17D+ cells 48 hpi. One-way ANOVA test with Dunnett's correction was used to determine the significance of differences between WT and the indicated KO phenotypes, n = 4). B) Representative overlay plots of 1205Lu cells from panel A. C) RNA extraction was performed after 24 hours, and IFN-β mRNA levels were quantified by qRT-PCR. Data were normalized to the relative expression of the HPRT reference gene and expressed as fold change relative to uninfected cells. One-way ANOVA followed by Dunnett's correction, was used to determine the significance of differences between WT and the indicated KO phenotypes, n = 3). D) IFN-β production in the culture supernatant was measured by ELISA at 48 hpi. Kruskal-Wallis test with Mann–Whitney–Wilcoxon's post-hoc with Benjamini-Hochberg's correction was used to determine the significance of differences between wt and the indicated KO phenotypes, n = 3. Error bars represent means and standard

deviations (*, **, ***and **** represent adjusted p-values ≤0.05, ≤0.01, ≤0.001 and ≤0.0001 respectively).

Since RLRs have been identified as the primary receptors sensing YF17D, we aimed to identify the specific viral RNA species recognized by RLRs after infection with YF17D. RLRs have been described to sense dsRNA. First, to observe any potential formation of dsRNA, the 1205Lu cell line was infected with YF17D at a ratio of 1 MOI. The cells were stained with a dsRNA-specific antibody at intervals of 24-, 48-, and 72-hours post-infection (hpi) and examined by confocal microscopy. Within the initial 24 hours, we observed the emergence of dsRNA in the cytoplasm, which notably increased at 48 and 72 h. This accumulation of dsRNA-positive cells strongly suggested the creation of viral dsRNA intermediates (data generated by Paul Schwarzlmüller, unpublished).

Further, the structural aspects crucial for the RLR-mediated response to YF17D infection were investigated. Total RNA from wild-type 1205Lu cells infected with YF17D was isolated 48 hpi and treated with RNA-modifying enzymes before re-transfection into 1205Lu cells. Treatment with the RiboShredder and RNase III enzymes, which degrade total RNA and dsRNA respectively, led to a loss of immunostimulatory activity as measured by CXCL10 release. Interestingly, the RNase R enzyme, targeting single-stranded RNA, did not significantly impact CXCL10 induction compared to the control (w/o enzyme). Testing the importance of 5' phosphate residues for RLR activation, we used a 5'-polyphosphatase enzyme to remove tri- and di-phosphate groups from the RNA's 5' end. This treatment significantly decreased CXCL10 induction compared to untreated RNA (control) from infected cells, indicating that immunostimulatory RNA extracted from YF-infected cells is double-stranded and harbors 5' tri- or di-phosphate groups (data generated by Paul Schwarzlmüller, unpublished).

Since 5'-phosphate dsRNA serves as the primary RIG-I ligand, we further explored the significance of the 5'-phosphate and the double-strand structure in the immunostimulatory effect of RNA isolated from YF17D-infected 1205Lu cells at early (24 h) and late (72 h) timepoints. CXCL10 induction significantly decreased after RNase III digestion of dsRNA at both timepoints post-infection compared to untreated RNA from the same timepoints. Treatment with 5'-polyphosphatase also reduced CXCL10 induction of RNA from infected cells at both timepoints, with the most substantial reduction observed 24 hpi (Figure 10A). This suggests an early dominance of RIG-I ligand formation within 24 h of YF17D infection, with a less stringent requirement for a 5'-phosphate end at later stages that could suggest the formation of MDA5 ligands at later timepoints.

To assess the contributions of RIG-I and MDA5 towards the recognition of YF17D viral ligands, cells lacking RIG-I, MDA5 receptors, or those with double knockouts were transfected with RNA extracted from WT-infected cells at 24 and 48 hpi. The downregulation of CXCL10 levels was observed again 24 hpi in RIG-I KO cells. However, no reduction of CXCL10 induction was observed in cells lacking MDA5 after 48 h as compared to WT. In contrast, the double knockouts showed complete inhibition of CXCL10 secretion (Figure 10B).
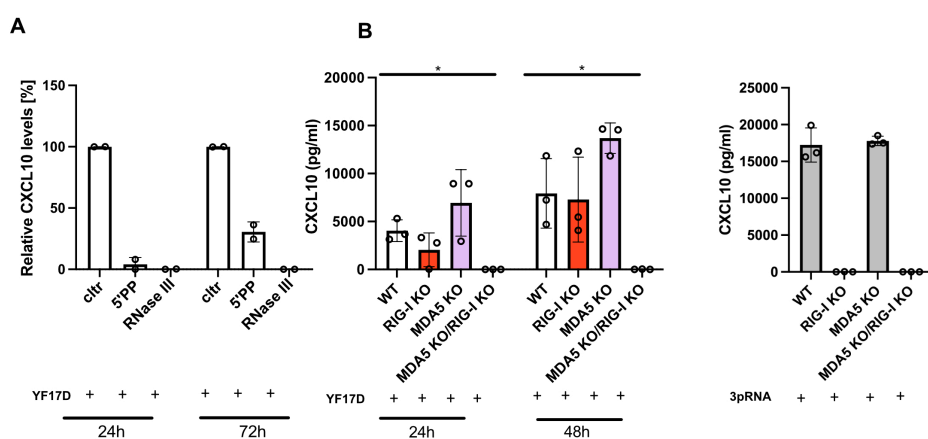
Figure 10.Kinetics of RIG-I and MDA5 dependent YF17D sensing.

A) RNA isolated at the indicated timepoints from YF-infected wild-type 1205Lu cells were re-transfected after enzymatic treatment into 1205Lu melanoma cells. CXCL10 levels were measured in the culture supernatant after 24 hours by ELISA. Results are shown as relative concentrations to the untreated controls from each experiment (w/o enzyme), n=2. B) RNA isolated from YF17D infected cells (wild-type 1205Lu) at the indicated timepoints were re-transfected into CRISPR-knockout (KO) 1205Lu cells. CXCL10 production was measured in the supernatant after 24 hours by ELISA. Results of stimulation with the known RIG-I ligand 3pRNA, used as a positive control are shown in the right panel in B. One-Way ANOVA test with Dunnett's correction was used to determine the significance of differences between WT and the indicated KO phenotype,n=3.Error bars represent means and standard deviations (*, **, ***and **** represent adjusted p-values ≤0.05, ≤0.01, ≤0.001 and ≤0.0001 respectively).

4.2 Characterization of the cohort

To study the response to viral infections in humans, a cohort consisting of 250 healthy Caucasian volunteers has been recruited. Individuals were vaccinated subcutaneously with the yellow fever virus vaccine (YF17D; Stamaril) and their blood samples were collected on day 0 just before the vaccination and on days 3,7,14, and 28 post-vaccination (pv) (Figure 11).
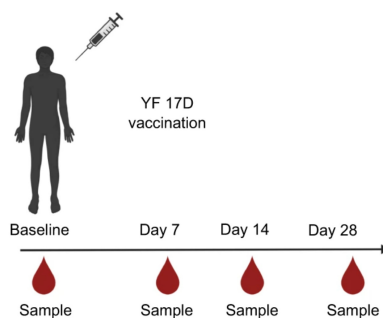
Figure 11.Overview of sample collection.

The samples (serum, plasma, PBMCs) were collected before vaccination (day 0) and after vaccination (days 3, 7,17,28) (Santos-Peral *et al.*, 2024).

Out of 250 study participants, 169 were females, and 81 were males. All individuals at the time of vaccination were young and healthy, with a median age of 24 years old and a median body mass index (BMI) of 22.27. TBE vaccination is recommended in the region where the study was conducted; thus, 166 participants (66.4%) were vaccinated against TBE, 70 (42,16%) were TBE naive, and the status of 14 individuals was unknown (Table 1). The tick-born encephalitis virus (TBEV) and the yellow fever virus are distantly related and share cross-reactive epitopes. The effect of pre-vaccination with the inactivated TBE vaccine on the antibody response to YF17D in our cohort is described in Santos et al (2024).

	All	**TBE positive**	**TBE negative**
Total	250	166	70
Sex			
Female	169	112	49
Male	81	54	21
Age (median)	24	24	24,5
Age(range)	19-47	19-46	20-38
BMI (median)	22,27	22,31	22,11

Table 1.The overview of cohort characteristics.

The table shows the number of participants with regard to age, sex, and BMI, stratified into TBE-positive and TBE-negative individual.

The vaccination and consecutive 28-day sample collection cycle was started at 21 specific timepoints between 2015 and 2019, referred to as collection batches (1510-1907), shown in Table 2.

Collection	Number of individulas
Years	
2015	32
2016	69
2017	83
2018	52
2019	14
Batch	
1510	16
1511	16
1604	10
1606	15
1607	16
1610	12
1611	16
1702	14
1703	12
1705	12
1706	14
1710	16
1711	15
1801	11
1802	9
1806	6
1807	10
1810	10
1811	6
1901	8
1907	6
Season	
Winter (Dec-Feb)	43
Spring (Mar-May)	32
Summer (Jun-Aug)	67
Autumn (Sep-Nov)	107

Table 2.Characteristics of cohort recruitment.

The table shows the year and month/season of vaccination and sampling along with the distribution of the vaccinees within these collection batches.

4.3 Characteristics of the early immune response to YF17D

4.3.1 Plasma cytokines response to vaccination with YF17D

For cytokine measurements in the plasma (K-EDTA) of vaccinees using the Bio-plex platform, an initial pilot study was performed This study involved analyzing 49 different cytokines on days 0, 3, 7, 14, and 28 from 22 individuals. Among these readings, 21 cytokines fell within the detectable range including Eotaxin (CCL11), IL-1ra, IL-18, IP-10 (CXCL10), MCP-1 (CCL2), MIF, MIG (CXCL9), PDGF-bb, RANTES (CCL5), TNF-α, MIP-1a (CCL3), MIP-1b, IL-9, BCA-1 (CXCL13), I-TAC (CXCL11), MDC (CCL22), APRIL (TNFSF13), BAFF (TNFSF13B), sIL-6ra, and Osteopontin. In the pilot study, measurements were also conducted for type I (IFN-α2, IFN-β), type II (IFN-γ), and type III (IL-29/IFN-λ1, IL-28A/IFN-λ2) interferons. However, all interferons were found to be below the limit of detection. The measured cytokines levels usually peaked on day 7, decreasing thereafter on days 14 and 28 back to the level of day 0 (Figure 12).
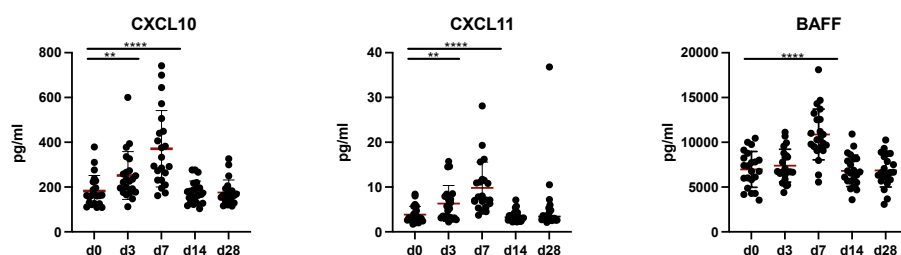
Figure 12.Cytokine levels in the plasma of individuals included in pilot study vaccinated with YF17D.

The plasma-samples were analyzed in the pilot-study for the presence of cytokines using the Bioplex assay system. The samples were measured at baseline and on days 3, 7,14, and 28 post-vaccination. The x-axis represents concentration and the y-axis represents collection days of cytokines. Statistical significance for differences between the data points on day 3, and 7,14 and 28 after vaccination and day 0 was analyzed using ANOVA for repeated measures followed by the paired-t-test post hoc with Benjamini-Hochberg's correction, n=22. Error bars represent means and standard deviations (*, **, ***and **** represent adjusted p-values ≤0.05, ≤0.01, ≤0.001 and ≤0.0001 respectively).

Based on the pilot study, 21 cytokines were selected for further analysis, and the plasma samples from days 0, 3, and 7 of the remaining 228 vaccinees were divided into 5 batches and analyzed on 5 different assay days (see Table 3).

Batch	1 (pilot study)	2	3	4	5	6
Assay day	d1	d2	d3	d4	d5	d6
Number of vacinnees	22	46	44	46	46	46

Table 3.Cytokine response to the YF vaccination.

The plasma-samples collected at the timepoints specified in the study design were analyzed for the presence of cytokines using the Bio-plex assay system (n=250). Cytokine levels were measured on days 0, 3, and 7 as well as 14 and 28 in the pilot study. The table specifies the number of samples measured on each assay day.

Eighteen cytokines fell within the measurable range. Of these, 15 showed significant induction or reduction after the vaccination, including Eotaxin, IL-1ra, IL-18, CXCL10, CXCL11, CXCL13, MCP-1, MIG, PDGF-bb, RANTES, TNF-α, MIP-1a, CCL22, APRIL, and BAFF. Most exhibited their highest values on day 7 post-vaccination. Osteopontin and the anti-inflammatory cytokine sIL6-ra were found to be downregulated (Figure 13).
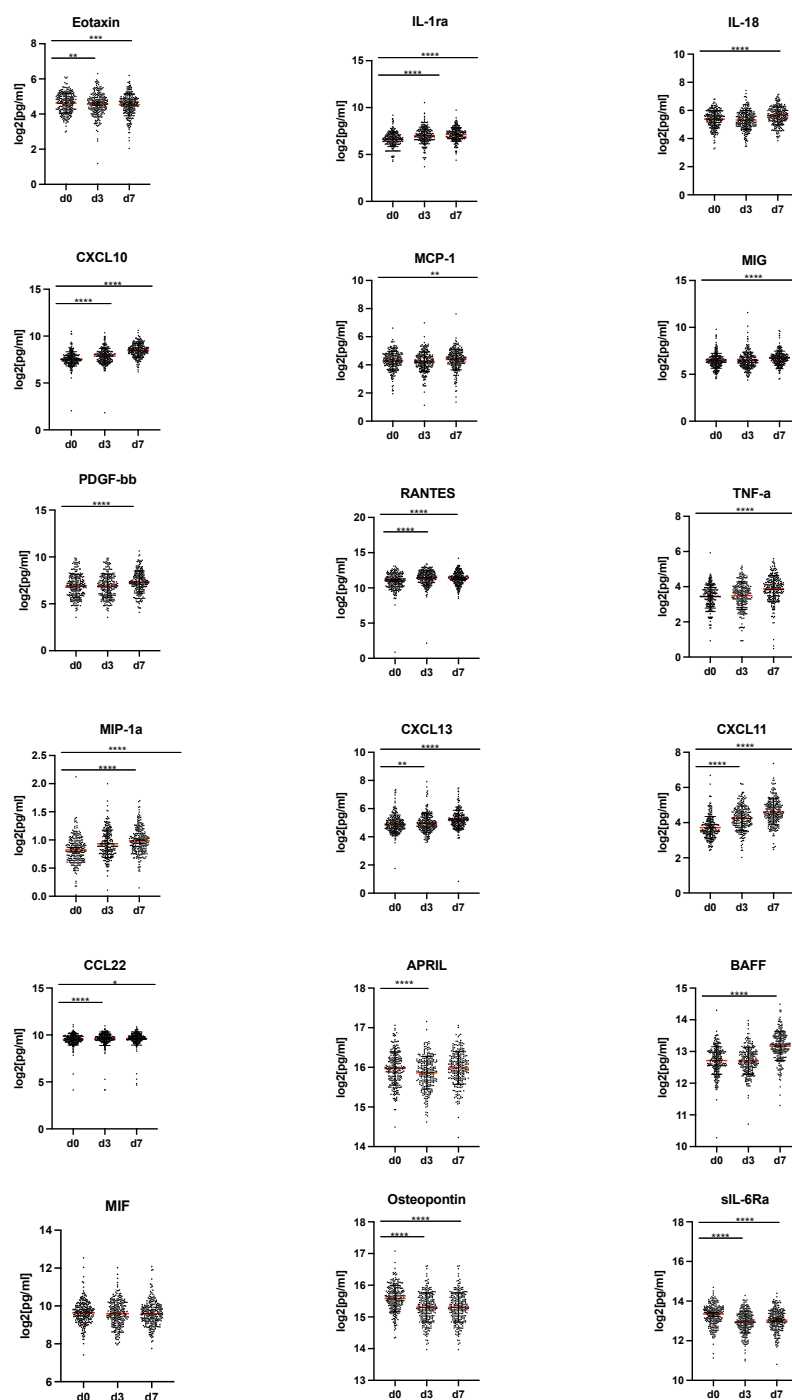
Figure 13. Time-resolved cytokine levels in the plasma of individuals vaccinated with YF17D.

The plasma samples collected at the timepoints specified in the study design were analyzed for the presence of cytokines using the bioplex assay system. The samples were measured at baseline and on day 3 and day 7 post-vaccination. The x-axis represents concentration and the y-axis represents collection days of cytokines. Data were log-transformed and corrected for batch effects. Statistical significance for differences between the data points on days 3 and 7 after vaccination and day 0 was analyzed using ANOVA for repeated measures followed by the paired-t-test post hoc with Benjamini-Hochberg's correction, n=250. Error bars represent means and standard deviations (*, **, ***and **** represent adjusted p-values ≤0.05, ≤0.01, ≤0.001 and ≤0.0001 respectively).

4.3.2 Transcriptome changes induced in peripheral blood monocytes on day 7 after vaccination with YF17D

RNA sequencing (RNA-seq) analysis, based on next-generation sequencing, is the standard method for analyzing the cellular transcriptome. The primary goal of RNA-seq is gene expression profiling, aimed at identifying differentially expressed genes and pathways between study conditions. It simultaneously measures thousands of genes, providing insight into the cell's regulatory network (Sheng *et al.*, 2017).

To select the appropriate, most relevant cell population in peripheral blood, for our planned transcriptomic and eQTL study, a pilot study in collaboration with Prof. Dr. Anne Krug and Elena Winheim (LMU, Munich) was performed. This study showed that YF17D within PBMCs can infect monocytes as well as several subpopulations of dendritic cells – even though at low frequencies. RNA-seq performed in diverse cell types—B cells, monocytes, and DCs—at different timepoints: baseline and at 3-, 7-, 14-, and 28-days post-vaccination in three individuals showed that vaccination with YF17D induced transcriptomic changes in all selected cell populations but monocytes showed the highest number of differentially regulated genes with a peak on day 7 post-vaccination (Winheim, 2022, Dissertation). Based on these results we have decided to use isolated monocytes of days 0 and 7 of the whole cohort and to perform RNA seq on these samples to identify the transcriptomic changes induced by YF17D and to analyze the variability within this response in a cohort.

4.3.2.1 Quality control of RNA-seq for the whole cohort

To perform RNA-seq analysis, an optimized pipeline was developed based on the Smart-Seq2 protocol (Picelli, 2017) (Figure 14A). At least 100,000 monocytes were isolated using the autoMACS separation method from frozen PBMCs (Figure 14B), which resulted in high RNA quality (RIN above 7) (Figure 14C). The libraries were then created using the polyA mRNA enrichment method, and cDNA was pre-amplified with 13 cycles to ensure an adequate amount of material (Figure 14D).

Figure 14.Overview of optimized experimental steps for bulk Smart-seq2 library construction.

A) The optimized pipeline involved isolating monocytes using CD14+ MACS beads from frozen PBMCs on both day 0 and day 7 with the autoMACS separator. The isolated RNA underwent mRNA enrichment using the polyA selection method, followed by cDNA amplification with 13 cycles. Tagmentation was performed using Tn5 transposase as previously described (Picelli et al., 2013) B) Representative FACS plot of the monocyte population isolated using CD14+ MACS beads with the autoMACS automated isolation system C) Representative plot of RNA quality, measured by Bioanalyzer. The RIN number represents the quality of RNA where 1 indicates low-quality, degraded RNA, while 10 corresponds to high-quality RNA. Each peak depicts a subunit of RNA C) Representative plot of the final cDNA library measured by Bioanalyzer after undergoing pre-amplification, and tagmentation steps.

Pair-end Illumina RNA-seq was conducted for 244 individuals, at two timepoints: day 0 and day 7, aiming for 10 million reads per sample sequencing depth. Post-sequencing, out of 488 samples (both timepoints), 67 were identified to have fewer than 3 million reads or fewer. To increase the number of reads, we re-sequenced these specific individuals and performed raw reads quality control checks and mapping for both datasets separately.

To assess the quality of the Illumina raw reads, FastQC was performed. The mean quality score was overall high for the primary sequencing (seq 1) except for one sample. Subsequently, upon mapping reads to the human genome using STAR alignment, an additional 6 samples exhibited low alignment scores (<60%), and 13 a low number of sequencing reads (sequencing depth lower than 1 million reads). Consequently, a total of 20 samples were excluded (Supplementary Figure 2A). After re-sequencing (seq2) of 67 samples, two samples had a low mean quality, 4 had low alignment scores, 4 had a low number of sequencing reads and one additional sample had a high percentage of

DNA contaminations, in total 12 samples were excluded from the data set (Supplementary Figure 2B).

After the QC, mapping, and counting of raw reads, both sequencing results were merged yielding a dataset comprising 475 samples from both timepoints: day 0 and day 7. For differential gene expression (DEG) analysis, the raw counts underwent transformation and normalization to account for variations in the total number of reads, sequencing depth, and other biases. The limma software transforms raw counts, which are not normally distributed into counts per million (CPM) or log-CPM, accounting for library size differences across samples (Smyth *et al.*, 2018).

Figure 15A shows the bimodal distribution of log-CPM, where a left peak indicates genes with no expression (zero-value genes) and a right peak represents expressed genes. Post-transformation, genes with no expression in the dataset were filtered out, by retaining only genes with a minimum count of 5 or more (cutoff log-CPM > 0.5) (Figure 15B). From an initial pool of 61,541 genes, 13,517 genes were identified as expressed after filtering out the low-count genes.

After removing lowly expressed genes, normalization was conducted using edgeR's trimmed mean of M values (TMM) method, which corrects for composition biases between libraries (Figure 15C) (Robinson and Oshlack, 2010). The density plot post-normalization revealed a few samples with numerous zero-value genes (Figure 15D). To address variations and outliers, dimensionality reduction techniques were employed. Specifically, principal component analysis (PCA) was applied to the normalized counts to detect any technical variability between datasets or samples (Figure 15E). The PCA plot did not exhibit significant technical issues between the two sequencing datasets. However, an additional 8 outliers were identified, primarily samples with low read numbers and many unmeasured genes. Consequently, these 8 samples were excluded from further analysis yielding a final data set containing 467 samples from day 0 and day 7.

Counts transformation and normalization
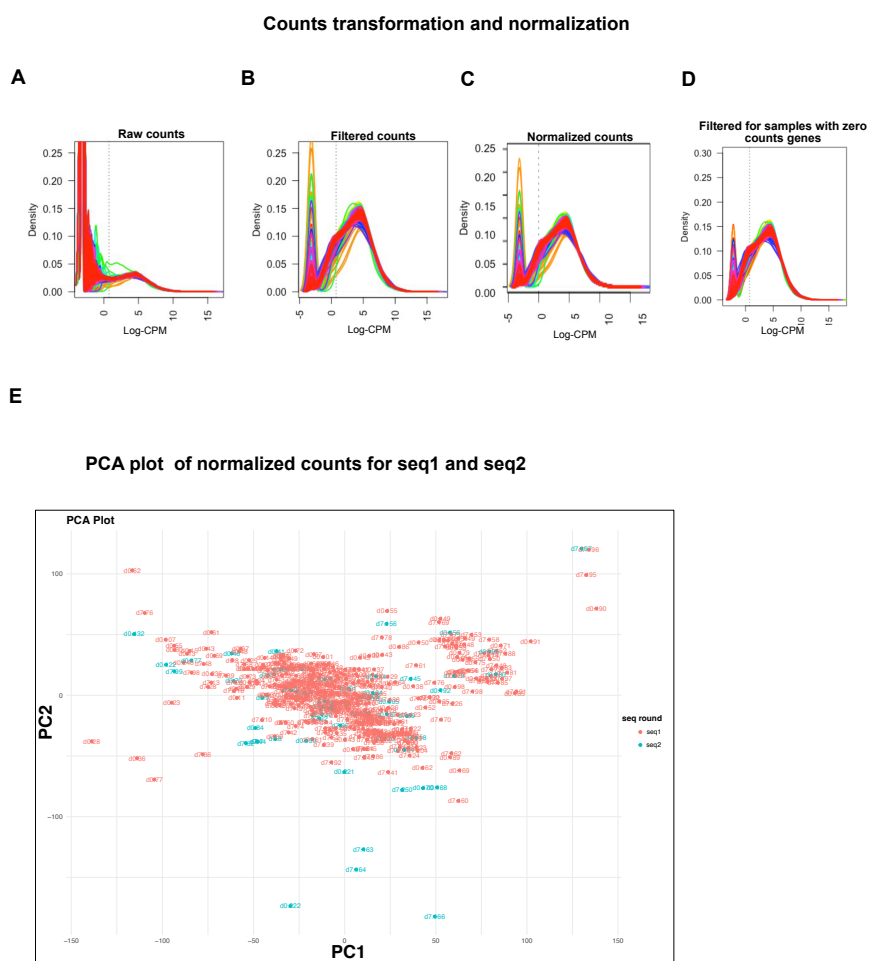
Figure 15.Overview of counts pre-processing.

A) The distribution of raw counts (not normally distributed); B) The counts' distribution after log-CPM transformation and filtering of genes with count <5 (cutoff log-CPM > 0.5); C) Counts normalized counts using the TMM method D) Removal of outliers with zero counts genes. Each line, colored in different colors, represents a sample. E) The PCA plot of normalized counts across two sequencing runs in red-seq1 and 2 in cyan-seq 2. Each dot represents a sample (n=475 before exclusion of outliers).

After removing lowly expressed genes and outliers, the analysis of differential gene expression analysis was conducted (Figure 16).

Figure 16.Schematic overview of the used DGE analysis steps.

After the QC of raw reads, reads were aligned against the human reference genome using STAR alignment, and the counts were normalized using TMM, DEGs were identified using the limma-voom method (Law *et al.*, 2014).

4.3.2.2 Differential gene expression in peripheral blood monocytes in response to YF17D vaccination

The comparison between gene expression on day 0 and day 7 was conducted using the limma-voom method (Law *et al.*, 2014; Ritchie *et al.*, 2015). This approach involves transforming counts into log-CPM and normalization using the TMM method, as described earlier. Subsequently, a linear mixed regression model was fitted to the transformed log-CPM counts, accounting for factors such as batch and other relevant covariates (see below). In the design matrix, the timepoint was used as the contrast.

To mitigate potential batch effects and identify influential covariates within the sequencing data, dimensionality reduction through PCA was employed. The PCA indicated that factors such as TBE immunity, sex, age, BMI, CMV status, and seasons (when the samples were collected) did not exert a discernable influence on gene expression. However, it identified batch/year of sample collection-related effects as having significantly impacted gene expression levels. Moreover, the timepoint-based PCA demonstrated the formation of a distinct cluster post-vaccination (timepoint2 - light blue), indicating a separate gene expression pattern (Figure 17).
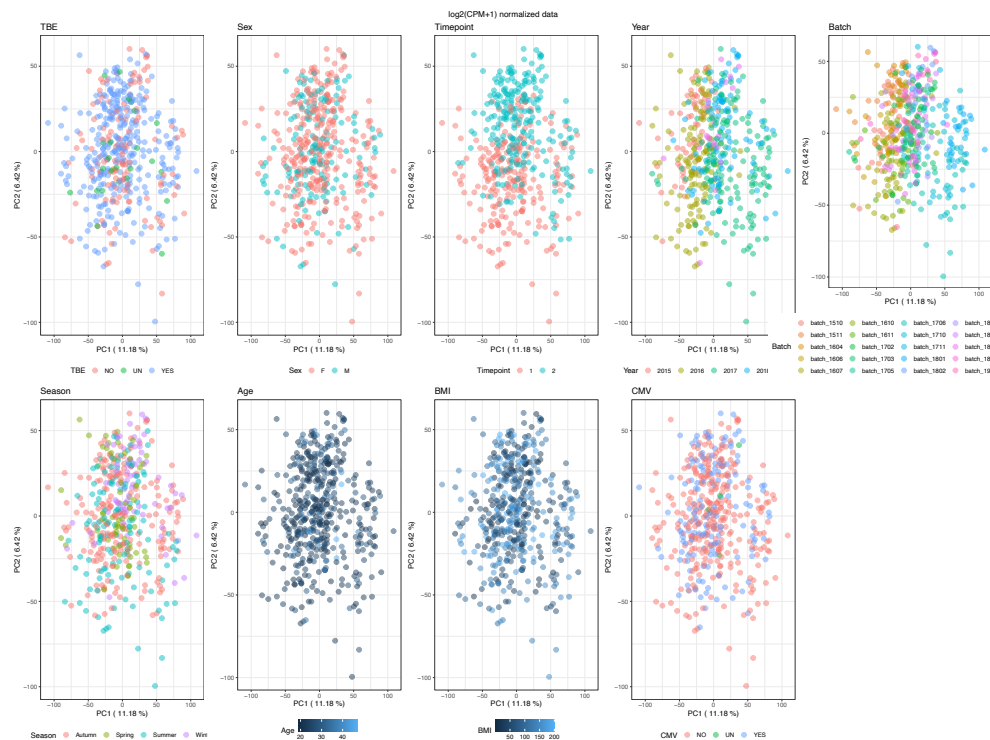
Figure 17.PCA analysis to identify potential covariates.

The analysis was conducted on normalized counts to identify potential batch effects or other factors influencing transcriptomic data. The plots visually represent cohort variability considering factors such

as TBE vaccination, sex, age, BMI, CMV infection, timepoint, collection year, and batch. Each dot represents a sample colored according to the tested factors (n=467).

The results of the global DE analysis were corrected for multiple testing by adjusting the raw p-value using the Benjamini and Hochberg false-discovery rate (BH-FDR) method with a cutoff of 0.05.

The yellow fever vaccination induced a broad and substantial transcriptional change in the monocyte population. A total of 8,132 genes were differentially expressed compared to pre-vaccination levels, as shown in the Volcano plot (Figure 18A). The analysis revealed 4,604 upregulated genes and 3,528 downregulated genes.

A heatmap was constructed for the top 100 DE genes, ranked by adjusted p-value, and reordered by hierarchical clustering (Figure 18B). This analysis highlighted a significantly upregulated expression of interferon-stimulated and antiviral gene expression. Notably, the top 15 significant DE genes included IFI44L interferon-induced protein 44-like (IFI44L), sialic acid binding Ig-like lectin 1(SIGLEC1), XIAP associated factor 1(XAF1), 2'-5'-oligoadenylate synthetase 2 (OAS2), epithelial stromal interaction 1 (EPSTI1), USP18 ubiquitin-specific peptidase 18 (USP18), MX dynamin-like GTPase 2 (MX2/viperin), lymphocyte antigen 6 family member E (LY6E), interferon-induced protein 44 (IFI44), eukaryotic translation initiation factor 2 alpha kinase (EIF2AK2/PKR), MX dynamin-like GTPase 1 (MX1), IFIT3 interferon-induced protein with tetratricopeptide repeats 3 (IFIT3), SPATS2L spermatogenesis-associated serine-rich 2-like (SPATS2L), and interferon alpha-inducible protein 6 (IFI6). The most downregulated genes were long non-coding RNA-DANCR (differentiation antagonizing non-protein coding RNA), ITGAE (integrin subunit alpha E), EIF4B (eukaryotic translation initiation factor 4B), and EIF3L (eukaryotic translation initiation factor 3 subunit L).
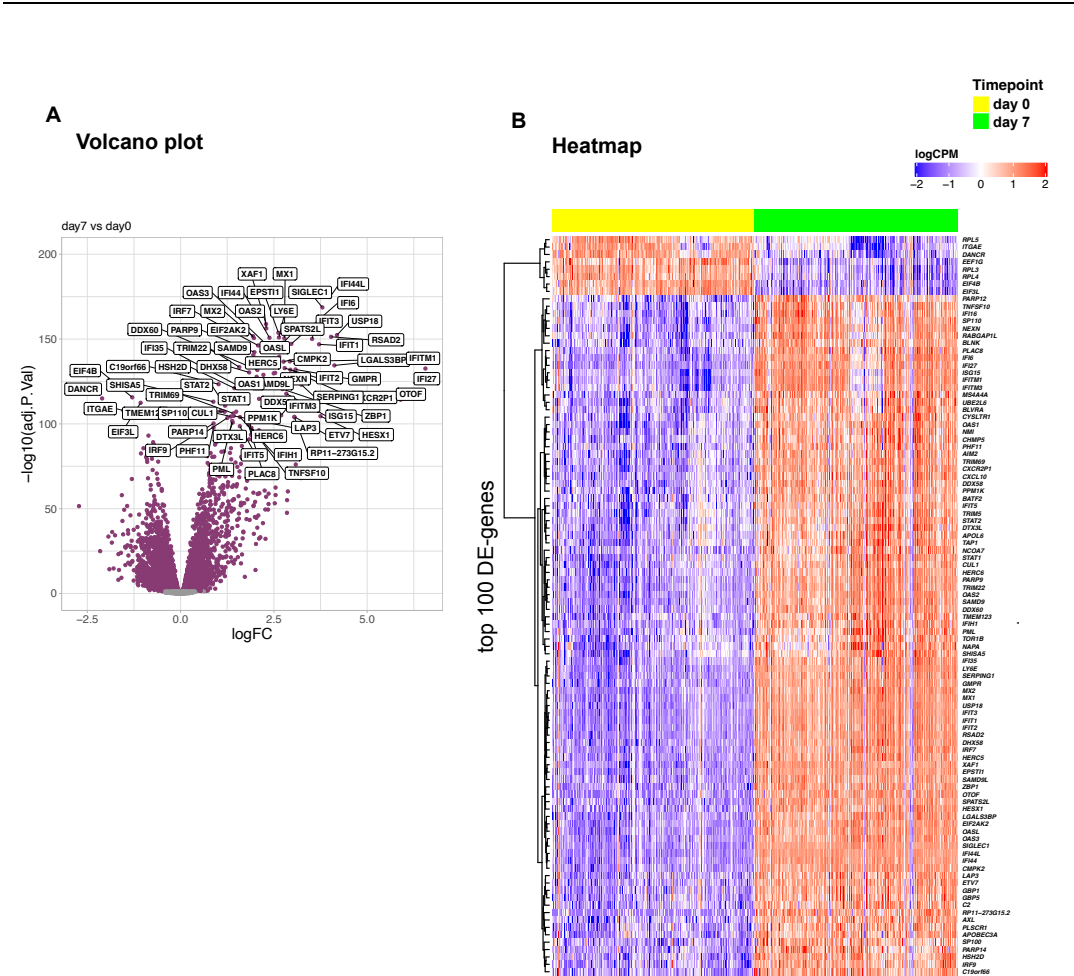
Figure 18.Differentially expressed gens after YF vaccination.

A) The volcano plot showing DE genes (x axis= log-fold change, y axis= -log10 adjusted p-value). The genes are colored if they pass the thresholds for FDR p<0.05. The most upregulated genes are on the right (log-fold change >0), the most downregulated genes are towards the left (log-fold change <0), and the most statistically significant genes are displayed towards the top of the pane,n=467l. B) A heatmap constructed only for paired samples (measured on day 0 and day, n-446) of the top 100 DEG ranked by adjusted p-value and clustered by similar expression using the ComplexHeatmap (Gu, 2022) and Ward.D2 linkage method (Murtagh, 1984).

4.3.2.3 Overview of pathway enrichment in monocytes after YF17d vaccination

To gain insight into the pathways undergoing modulation post-vaccination, we conducted a pathway enrichment analysis. Enrichment analysis commonly involves two methods: Over-Representation Analysis (ORA), reliant on a pre-filtered gene list of genes deemed as differentially expressed up to a predefined threshold (e.g. FDR adjusted p-value), and Gene Set Enrichment Analysis (GSEA), which considers the full list of genes based on their ranks and does not require a prefiltering (Reimand *et al.*, 2019). For our analysis,

we utilized the clusterProfiler package (Wu *et al.*, 2021). For the ORA approach, we have used a list of 8,132 differentially expressed genes to perform Gene Ontology (GO) terms and Reactome pathways enrichment analysis. The GO enrichment analysis revealed 95 activated and 42 repressed pathways. The top activated pathways were related to the defense response, Type I and IFN-gamma responses, antigen presentation via MHC class I, and TAP-dependent processes, along with cellular responses to IFN-gamma, and negative regulation of viral genome replication (Figure 19A).

Following vaccination, downregulation was observed in the SRP-dependent co-translational protein processes, targeting proteins to membranes, proteins targeting and localizing at the endoplasmic reticulum (ER) signaling, and those involved in the initiation of translation, viral gene expression, and transcription. The downregulated pathways involved primarily ribosomal genes from the RPL and RPS (ribosomal proteins) family (Figure 19B).

GO: Up-regulated

A

GO: Down-regulated

B
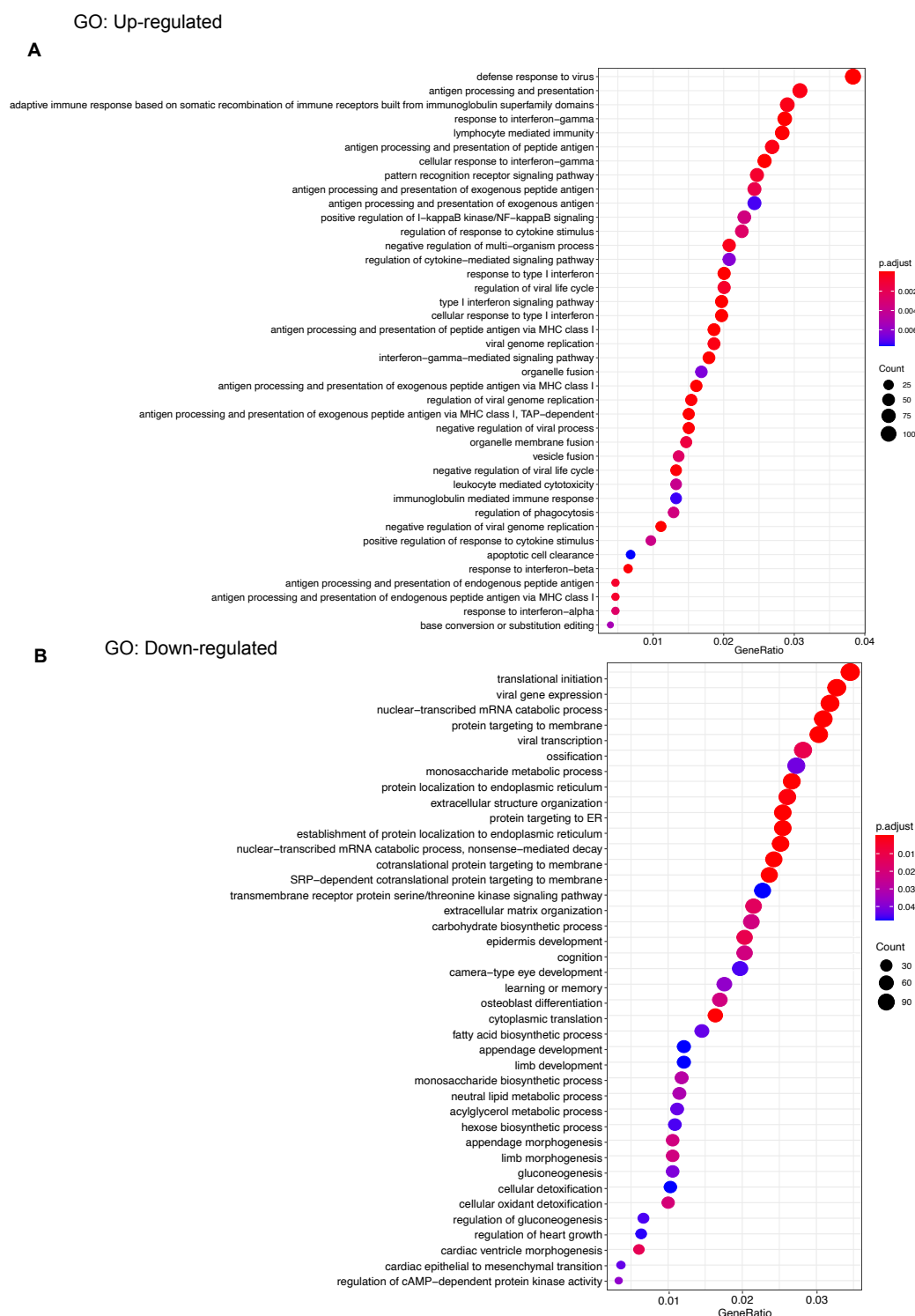
Figure 19.Gene Ontology enrichment pathway analysis of genes expressed in peripheral blood monocytes on day 7 after vaccination with YF17D.

The analysis was conducted using the clusterProfiler package. The dot plots illustrate the most significant GO terms. A) Represents the up-regulated GO terms (FDR adj. p-value < 0.05, logFC > 0), and B) the down-regulated GO terms (FDR adj. p-value < 0.05, logFC < 0). The x-axis represents the Gene Ratio; the number of DEGs compared to the background set of genes, the y-axis corresponds to specific pathways or terms. The most significant results are ranked in terms of

adjusted p-values (where red depicts the lowest p-value) and gene count. The count indicates the number of genes involved in each pathway.

The pathway and gene connectivity assessment identified four primary nodes among the first eight upregulated pathways with the lowest adjusted p-values using the cnetplot function from the clusterProfiler. These nodes include Cluster 1 (C1), defense response to viruses; Cluster 2 (C2), comprising several type II IFN pathways, Cluster 3 (C3), which involves antigen processing and presentation via MHC class I and Cluster 4 (C4), which includes type I IFN signaling (Figure 20). The defense response to viruses forms the largest cluster, with 107 genes, composed of C1 and C5-C7, which are shared across other modules. Cluster 1 contains IFN-stimulated and antiviral genes like IFI44L, EIF2AK2, IFIT5, APOBEC3C, or HERC5 (involved in ISGylation), as well as viral recognition genes such as DDX58/RIG-I, IFIH1/MDA5, TLR7, TLR8, chemokines (CXCL10, and CXCL9). Cluster 2 consists of receptors: TLR2/4, JAK2 and IFNGR2 - elements of IFN-γ signaling, and chemokines like CCL2/MCP-1 and CCL8/MCP-2. Cluster 3 focuses on antigen processing and presentation, involving genes like transporters associated with antigen processing genes (TAP1/2), and proteasome genes including proteasome 20S subunit alpha (PSMA2/3/4/5/6), proteasome 26S subunit (PSMC2/3/4/6), proteasome activator subunit (PSME1/2/3) as well as CD36 and NEMO/IKBKG. Cluster 4, a type I IFN-related cluster includes MYD88, USP18, XAF1, inhibitor of nuclear factor kappa B kinase subunit epsilon (IKBKE).

Cluster 5 includes elements involved in the antiviral response and type I IFN signaling, consisting of genes like MX1/2, IFIT1/2/3, radical s-adenosyl methionine domain containing 2 (RSAD2), ISG15/20 ubiquitin like modifier (ISG15/20), IFI6/27, transcription factor-STAT2, TBK1, and RNASEL. Cluster 6 contains genes involved in the defense and antigen presentation including TRIM5/22/25/38/34, GBP1/2, while Cluster 9 contains genes from antigen presentation and type II IFN signaling such as IFI30 and B2M (Beta-2-microglobulin), a component of MHC class I.

Central clusters include Cluster 7 and 8. Cluster 7 consists of ISG: OAS1/2/3, OASL, IFITM1/2/3, and transcription factors such as IRF1/2/3/5/7/9, STAT1, BST2/tetherin, all involved in virus recognition and antigen presentation and shared among defense response to viruses, type I IFN, and IFN-gamma pathways. Cluster 8 involves the expression of MHC-class I genes (HLA-A/B/C/E/F) pivotal in antigen presentation and it is positioned between the type I IFN, IFN-gamma, and antigen presentation pathways. Additionally, the analysis also detected pathways linked to adaptive immunity including positive regulation of B cell-mediated immunity and T cell-mediated cytotoxicity.

Figure 20.The gene interaction network constructed using the GO terms of differentially expressed genes in monocytes after YF17 vaccination.

The plot displays gene interactions, where nodes represent genes within specific gene sets, referred to as clusters. Each distinct color within the larger circles represents the main nodes, while smaller circles indicate connections between clusters. The graph presents the first eight upregulated pathways with the lowest adjusted p-value (FDR p<0.05). The count indicates the number of genes involved in each pathway.

Performing the over-representation analysis using the Reactome pathway database in addition to Gene Ontology terms reveals consistent upregulation of seven immune signaling cascades, including type I IFN, IFN-gamma, immunoregulatory reactions between lymphoid and a non-lymphoid cells and antigen processing and cross-presentation (Figure 21A), alongside with 22 downregulated pathways mainly involved in the translation process (Figure 21B).

A Reactome: Up-regulated

B Reactome: Down-regulated

Figure 21. Pathway enrichment analysis of genes expressed in peripheral blood monocytes on day 7 after vaccination with YF17D using the Reactome gene interaction database.

The analysis was conducted using the clusterProfiler package. The dot plots illustrate the most significant Reactome pathways. A) Represents the up-regulated Reactome pathways (FDR adj. p-value < 0.05, logFC > 0), and B) the down-regulated Reactome pathways (FDR adj. p-value < 0.05, logFC < 0). The x-axis represents the Gene Ratio, the number of DEGs compared to the background set of genes, the y-axis corresponds to specific pathways or terms. The most significant results are

ranked in terms of adjusted p-values (where red depicts the lowest p-value) and gene count. The count indicates the number of genes involved in each pathway.

Within the Reactome gene interaction network, significant clusters were identified including Cluster 1, which is the largest, with 297 genes, comprising different IFN pathways (interferon alpha and beta, interferon gamma and interferon signaling); Cluster 2 involved in immunoregulatory interactions between lymphoid and non-lymphoid cells; Cluster 3, which is related to antigen processing and cross-presentation, and Cluster 4, which is associated with the mitotic G2 and M phases and the endosomal vacuolar pathway (Figure 22). Cluster 1 consists of IFN receptors including IFNAR2, IFNGR2, JAK2, STAT1, many ISGs and transcription factors, while the Cluster 2 module includes various receptor proteins, such as CLEC2B (a C-type Lectin Receptor), CD40/TNFSF5 a co-stimulatory molecule from the TNF-receptor family, and the Siglec protein family including SIGLEC-1(CD169), SIGLEC-2(CD22), SIGLEC-5, SIGLEC-7, SIGLEC-9, SIGLEC-10, SIGLEC-11, or the CD300 family. These receptors play pivotal roles in immune responses, mediating cell-cell interactions, and regulating immune cell activation. Cluster 5 serves as a central hub positioned between Cluster 1, 2, and 3. It encompasses HLA genes, crucial components necessary for effective antigen presentation.

Figure 22.The transcriptional network of DEGs in monocytes after vaccination with YF17D constructed using the Reactome database.

The plot displays gene overlap, where nodes represent genes within specific gene sets, referred to as clusters. Each distinct color within the larger circles represents main nodes, while smaller circles indicate connections between modules. The graph presents all upregulated pathways with the lowest adjusted p-value (FDR p<0.05).

Additionally, pathway enrichment analysis was conducted using the GSEA method on genes pre-ranked by adjusted p-values. Enriched gene sets were identified through the Molecular Signatures Database (MsigDB), using the Hallmarks gene set collection. The activated pathways involved interferon alpha and gamma signaling, complement pathways, and inflammatory signaling whereas downregulated pathways included angiogenesis and epithelial-mesenchyma transition (Figure 23).

Figure 23.GSEA enrichment pathway analysis in monocytes after vaccination with YF17D.

The analysis was conducted using the clusterProfiler package and the MSigDB and Hallmarks collection. The dot plots illustrate activated or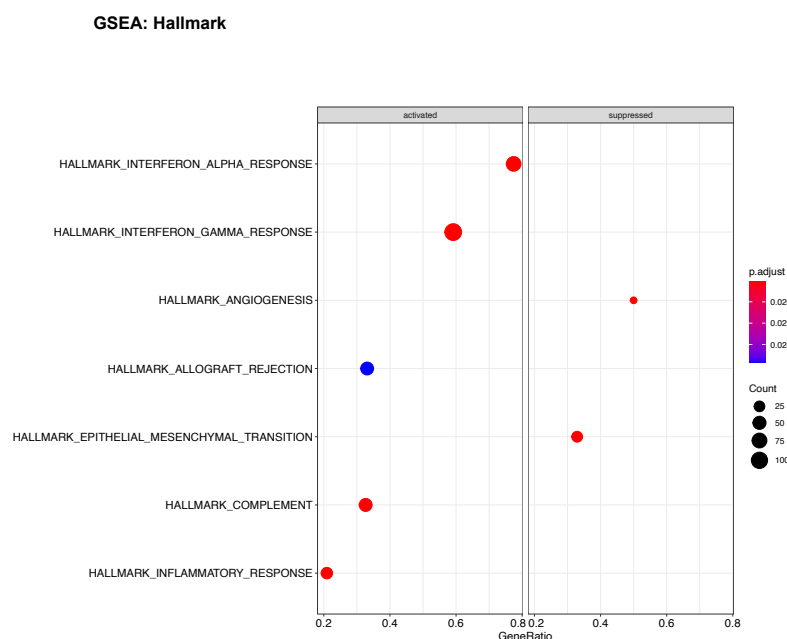 suppressed pathways. The most significant results are ranked in terms of adjusted p-values (where red depicts the lowest p-value) and gene count. The count indicates the number of genes involved in each pathway.

To infer transcription factor activity from gene expression data, the decoupleR tool (Badia-I-Mompel *et al.*, 2022) was used along with the Collection of Transcription Regulation Interactions (CollecTRI) database, a curated collection of TF-gene target interactions. Transcription factor activity scoring was conducted through a multivariate linear model on DEGs (FDR<0.05). The resulting t-values from this model served as TF scores. A positive t-value indicates that the TF is active within the analyzed conditions, implicating its role in regulating gene expression. Conversely, a negative t-value suggests TF inactivity within the studied context. The transcriptional profiling revealed the downregulation of the NF-kappa-B inhibitor, suggesting activation of NF-κB transcription factors and thus the activation of a robust antiviral and innate immune response through NF-κB as well as IRF cascades. Notably, the strongest activation was observed for STAT1, STAT2, IRF1, and IRF9 (Figure 24).
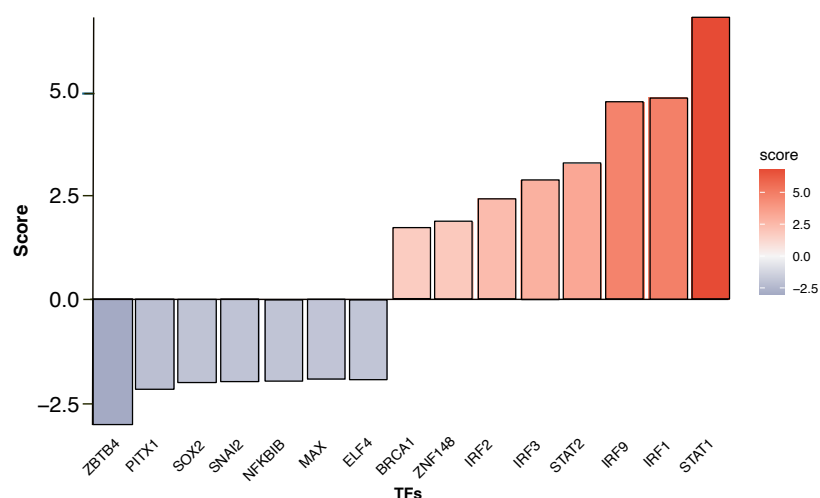
Figure 24. Transcription factors activity in monocytes after vaccination with YF17D derived from the analysis of DEG using the decoupleR tool along with the Collection of Transcription Regulation Interactions (CollecTRI) database.

The activity was inferred using the CollecTRI database. Blue indicates inactive TFs whereas red indicates active TFs.

4.4 Factors influencing variability in the early immune response to the YF17D vaccine

4.4.1 Variability in the cytokine response

Different intrinsic and non-genetic factors can influence cytokine levels. Assessing cytokine variability across individuals involved clustering them using the hierarchical clustering method.

On both days, 3 and 7 after the vaccination, plasma cytokines exhibit two distinct clusters of expression: a smaller cluster consisting of 5 cytokines—CCL22, CXCL11, CXCL13, RANTES, PDGFbb—exhibits high interindividual variability and the larger cluster comprises IL1ra, MIG, CXCL10, TNF-α, MIP1a, MCP1, Eotaxin, BAFF, APRIL, sIL6Ra, Osteopontin, IL18, and MIF (Figure 25A and B). This second cluster demonstrates three profiles of cytokine responses across individuals: high (C2), moderate (C1), or low (C3). (By day 7, most individuals show elevated cytokine levels). Furthermore, both sex and

season have been shown to have an effect on cytokine levels. An inspection of potential covariates including sex, age, seasonality, and BMI revealed an enrichment of females in cluster 3 (low) on day 7 (χ^2 p value = 2.46e-04). In addition to sex, individuals whose samples were collected in summer show higher cytokine responses indicating a possible role of seasonality in cytokine levels (Figure 25C).
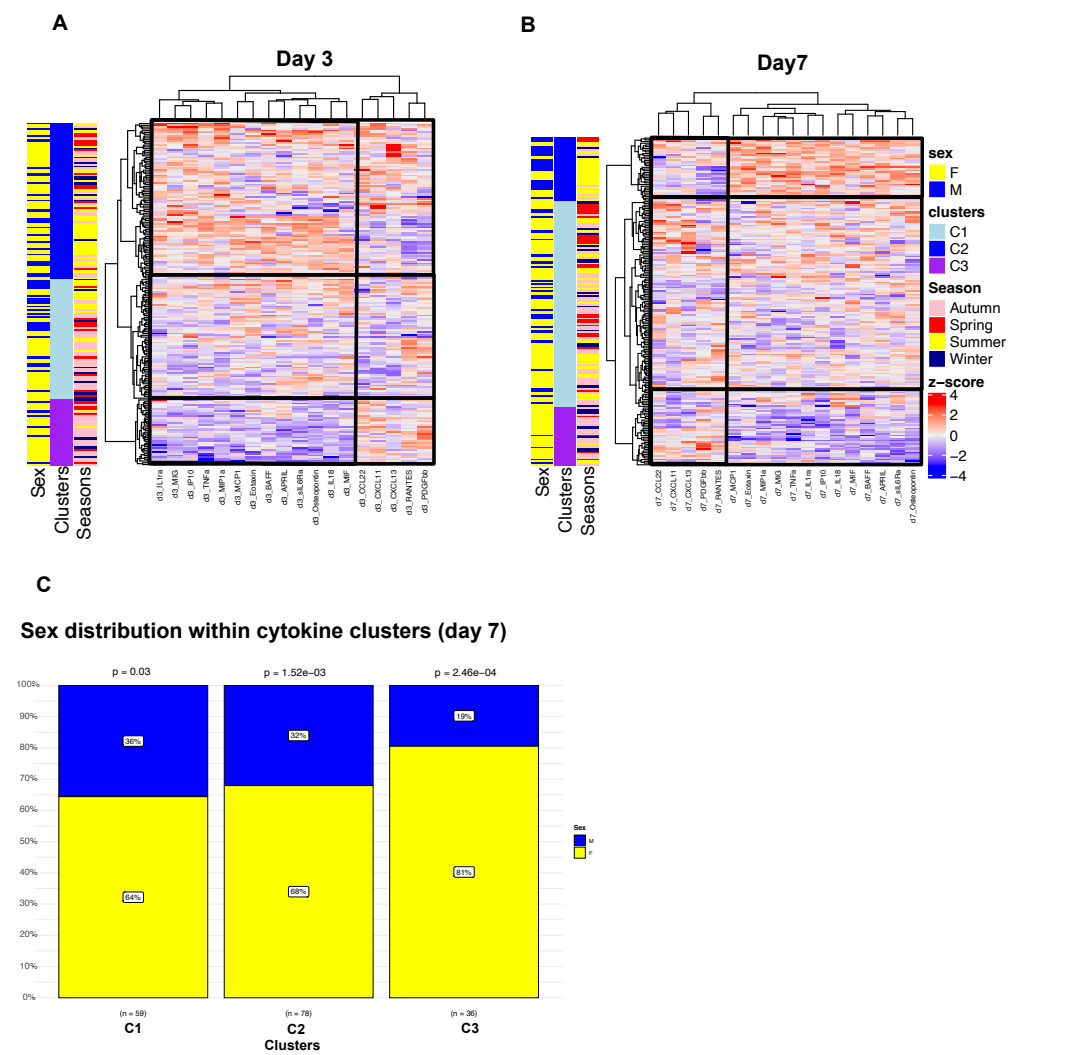
Figure 25. Cytokine levels post-vaccination.

The heatmap displays cytokine levels post-vaccination. A) on day 3 and B) on day 7, where blue indicates a decrease and red indicates an increase in cytokine concentrations compared to levels before the vaccination. Unsupervised hierarchical clustering was performed using Ward's method (Ward.D2) and visualized with the ComplexHeatmap package in R. C) The distribution of females and males across cytokine clusters on day 7. Statistical significance was evaluated using a Chi-square test to determine if the variables (the sex and clusters) were non-randomly associated (n = 223).

A correlation analysis revealed that cytokines are co-expressed, and that age and BMI had no influence on the cytokine levels (Figure 26).
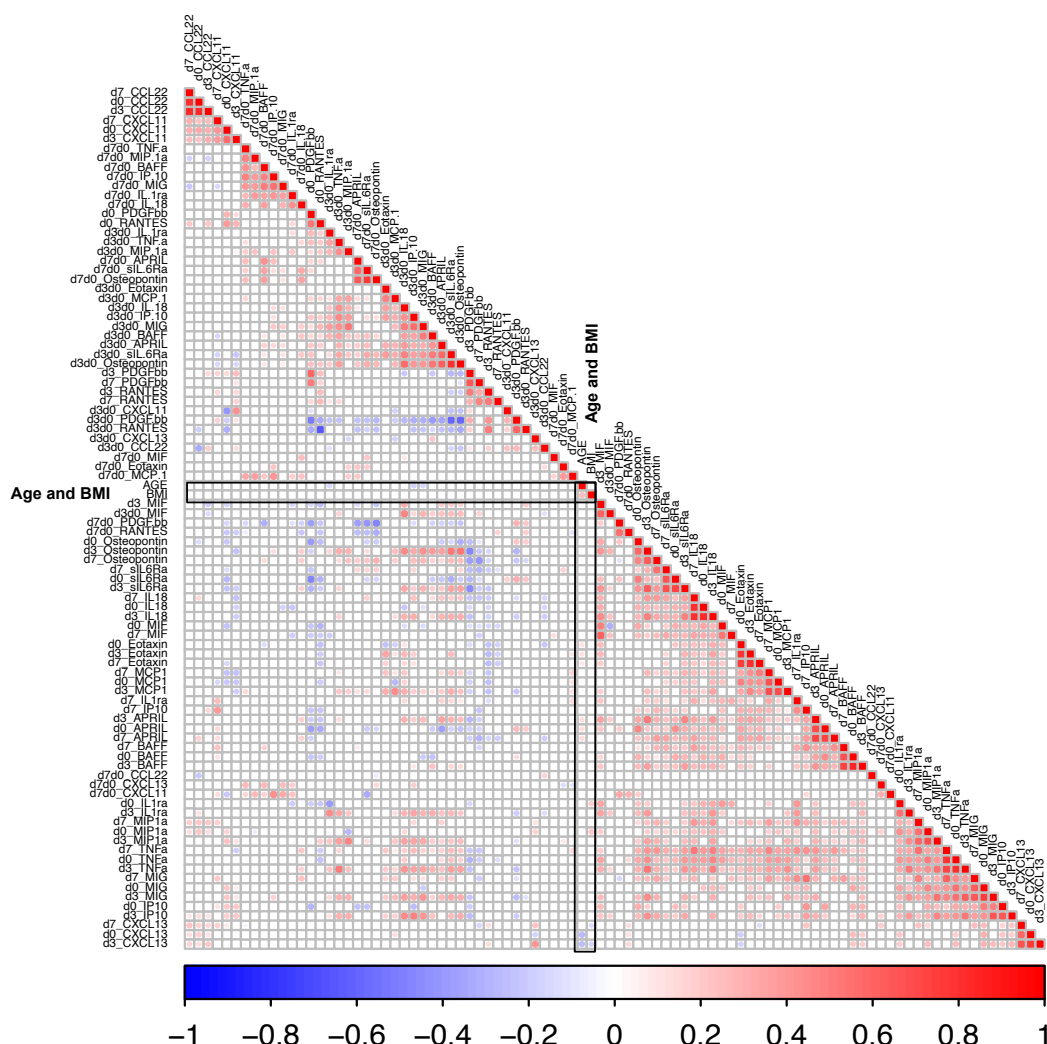
Figure 26.Clustering and correlation of cytokine levels.

The cytokines were correlated across day 0, day 3, and day 7, as well as the changes from baseline (delta d3d0 and d7d0). The correlation analysis was conducted using Spearman's correlation method. Red indicates a positive correlation, while blue indicates a negative correlation. The black lines represent the correlation of sex and BMI with the indicated cytokines. The correlation matrix was ordered using a hierarchical clustering function. Circle colors are equivalent to Spearman rho and indicate a significant p-value.

Significantly higher cytokine concentrations of APRIL, Eotaxin, TNF-α, MIF, MIP1a, and MCP1 were detected in males while females exhibited elevated levels of CXCL13 and RANTES at baseline and on day 7 (Figure 27A). The results show that the production of many cytokines shows annual seasonality. These cytokines, including APRIL, BAFF,

CCL22, CXCL11, Eotaxin, IL-18, IL1ra, CXCL10, MCP1, MIF, MIG, MIP1a, RANTES and, TNF-α, exhibit elevated expression primarily in spring and in summer (Figure 27B).
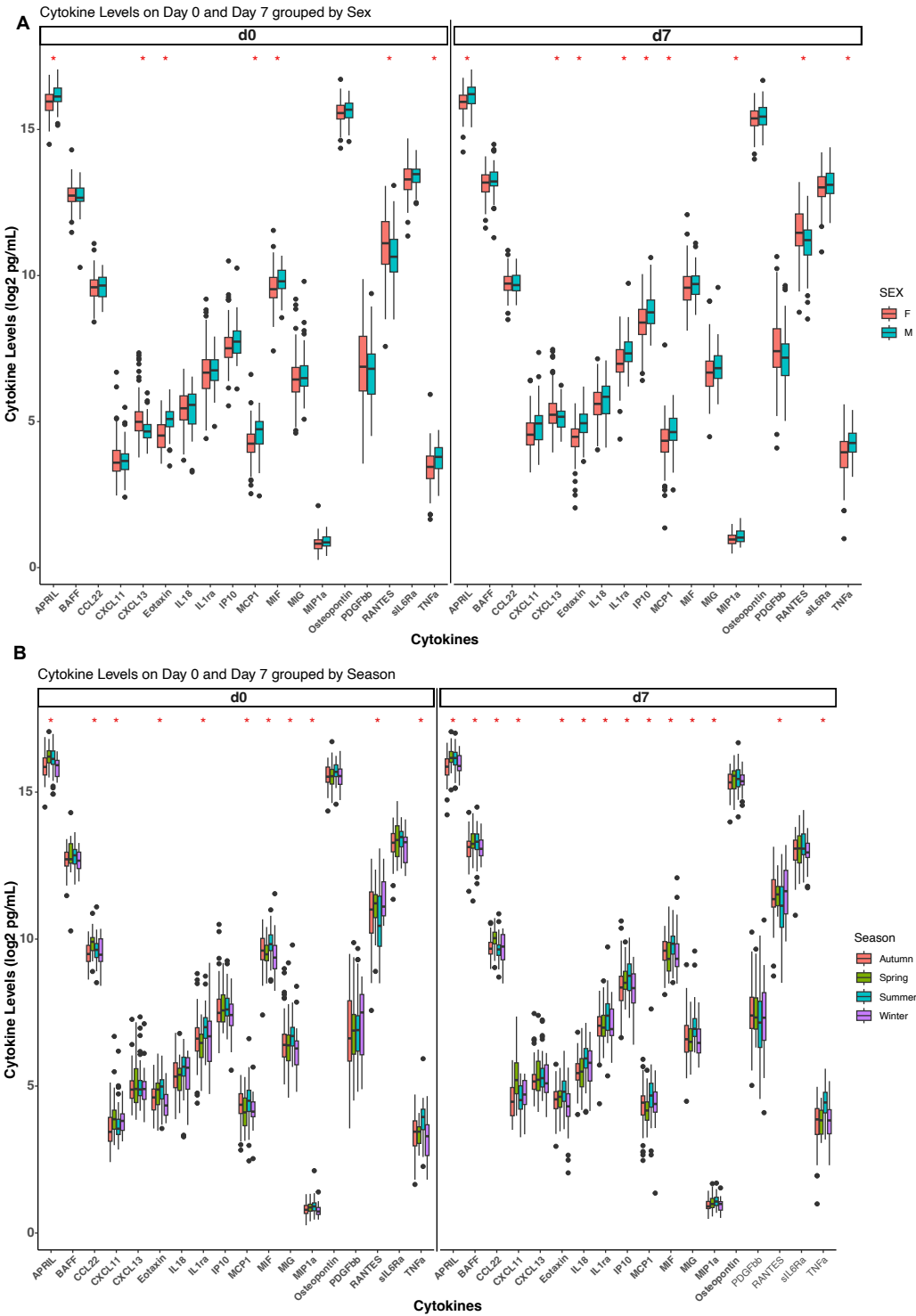
Figure 27.Sex and the season when the vaccine is given are influencing the early cytokine levels after vaccination with YF17D.

A) Cytokine levels on day 0 and day 7 grouped by sex B) Cytokine levels on day 0 and day 7 grouped by seasons. The x-axis represents measured cytokines, the y-axis represents the cytokines' concentration. Box plots indicate medians (center lines) and first and third quartiles. One-Way ANOVA test with Dunnett's test, n = 3). Error bars indicate means and standard deviations. The red star indicates significant results after correction for multiple hypothesis testing using FDR method (FDR <0.05).

4.4.2 Confounding factors affecting the transcriptomic response in monocytes after vaccination with YF17D

The variability in transcriptomic responses has been examined. As demonstrated earlier, there hasn't been any effect of age, BMI, or seasons on expression (refer to Figure 17). Qualitatively, almost all vaccinees exhibit changes in gene expression following vaccination. A sex-specific differential gene expression analysis has been performed, yielding 6,699 DEGs in females and 4,853 DEGs in males. Additionally, a pathway enrichment analysis was conducted to investigate biological implications associated with the identified sex-specific DEGs using GSEA applied to the Hallmarks gene set collection. Both groups displayed up-regulation of IFN type I and II, complement, and inflammatory response. Females additionally exhibited an activation of the IL6-JAK-STAT pathway, which has not been detected in males (Figure 28).

GSEA: Hallmark

A

Females

B
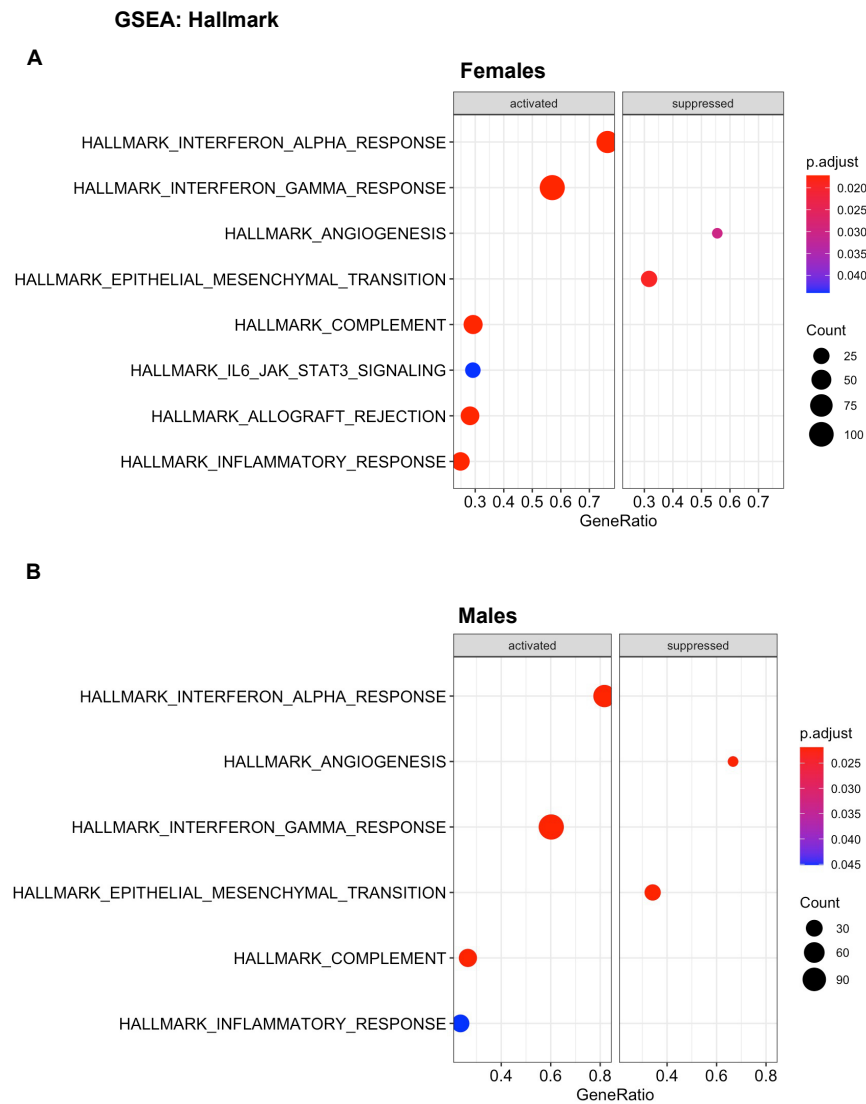
Males

Figure 28. GSEA enrichment pathway analysis in monocytes between males and females after vaccination with YF17D.

The analysis was conducted with the clusterProfiler package in R using the MSigDB and Hallmarks collection. The dot plots illustrate the most significant pathways. A) pathways activated or suppressed in females B) Pathways activated or suppressed in males. The x-axis represents the Gene Ratio, the number of DEGs compared to the background set of genes, the y-axis corresponds to specific pathways or terms. The most significant results are ranked in terms of adjusted p-values (where red depicts the lowest p-value) and gene count. The count indicates the number of genes involved in each pathway.

4. 5 Factors influencing the adaptive immune response to YF vaccination

4.5.1 Antibody and T cell response to YF17D vaccination

Neutralizing antibodies are considered to be a critical indicator of vaccine immunogenicity (Bookchin and Schumacher, 2000). In order to evaluate immune protection after YF17D vaccination, neutralizing antibody titers were determined for pre- and post-vaccination sera by Lisa Lehmann (disclaimer page 7) using the FluoRNT assay (Scheck *et al.*, 2022). All 250 vaccine recipients developed protective titers against YF17D as early as day 14 that further increased by day 28 pv. Protection against YF was defined as the neutralization of 80% of the virus in a >1:10 serum dilution (Wieten *et al.*, 2016).

Figure 29 shows that stratifying neutralization efficacy by sex revealed no statistically significant differences between the vaccine recipients. Additionally, the impact of TBE pre-immunity was investigated since TBEV belongs to the flavivirus family, and pre-existing antibodies could potentially be cross-reactive and affect the antibody response to yellow fever. Most of the cohort were vaccinated against TBEV (66,4%), however, neutralization in both the TBE-positive and naive individuals showed no difference, indicating that TBE pre-immunity does not alter the overall neutralizing response to YF17D in the first 28 days when neutralizing activity is still mediated mainly via IgM. Described in more detail in Santos-Peral et al. (Santos-Peral *et al.*, 2024).
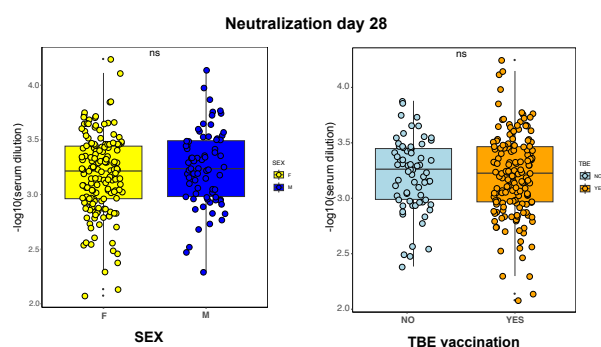
Figure 29.Neutralizing antibody titer after YF-17D vaccination.
Neutralizing antibodies were measured in serum by FluoRNT on days 0, 14, and 28 post-vaccinations. The NT80 titer was defined as the serum dilution, which caused an 80% reduction of YF-17D Venus fluorescence. A) Neutralization grouped by sex on day 28 B) Neutralization grouped by TBE vaccination status on day 28. Statistical significance of differences between the two groups was determined using Wilcoxon Rank-Sum test, n=245. Box plots indicate medians (center lines) and lower and upper hinges corresponding to first and third quartiles. Non-significant if p-values > 0.05 (ns).

Additionally, the functionality and number of YFV17D-specific CD4+ and CD8+ T cells induced by the vaccine have been measured as an additional determinant of vaccination success. Apart from neutralization, T cells are equally important elements of antiviral immunity and immune protection (Monath, 2001). Quantification of the number and functionality of the antigen-specific T cell response was measured by Antonio Santos del Peral (see disclaimer page 7) with an *ex vivo* re-stimulation assay using PBMCs from day 0 and day 28 post-vaccination, followed by intracellular cytokine staining (ICS), with live virus as the stimulating antigen. This approach, similar to the one used by Miller et al. (2008) with the vaccinia virus (Miller *et al.*, 2008) allows the simultaneous detection of antigen-specific CD4+ and CD8+ T cell subsets. The frequency of antigen-specific T cells was measured by the detection of IFN-γ, TNFα, IL-2, and IL21 together with degranulation markers like CD107a and the activation-induced marker CD40L (CD154) allowing the accurate detection of antigen-specific T cells rather than bystander activated CD4+ T cells. To further characterize the activation and composition of the T cell compartment before and after the vaccination in addition to the restimulation assay, an extensive flow cytometry panel comprising 26 different T cell parameters was used to analyze PBMCs from days 0, 7,14, and 28 post-vaccination (Santos del Peral submitted, Dissertation; Santos-Peral, Zaucha *et al.* submitted). The list of all measured cell populations and the flow cytometry panel used for the restimulation assay and the extensive T cell characterization are described in the supplementary tables (Supplementary Tables 2, 3, and 4).

4.5.2 High and low responders' classification

To investigate the mechanisms driving variation in immune responses to the YF17D vaccine virus across individuals, the subjects were classified based on vaccination endpoints, including neutralization levels and the abundance of CD4+ and CD8+ T cells on day 28 pv. Given that all individuals developed neutralizing titers and antigen-specific T cells, it was difficult to distinguish between high and low responders. To address this, unsupervised hierarchical clustering was performed (see Figure 30) using the neutralizing antibody response and parameters of the CD8+ and CD4+ T cell compartment separately. These three main vaccine-response compartments were then used to form a composite score that categorized the individuals as high, low, and average responders. In total, 46 individuals were classified as high responders and 43 as low responders to YF17D vaccination (Santos-Peral, Zaucha *et al.* submitted).
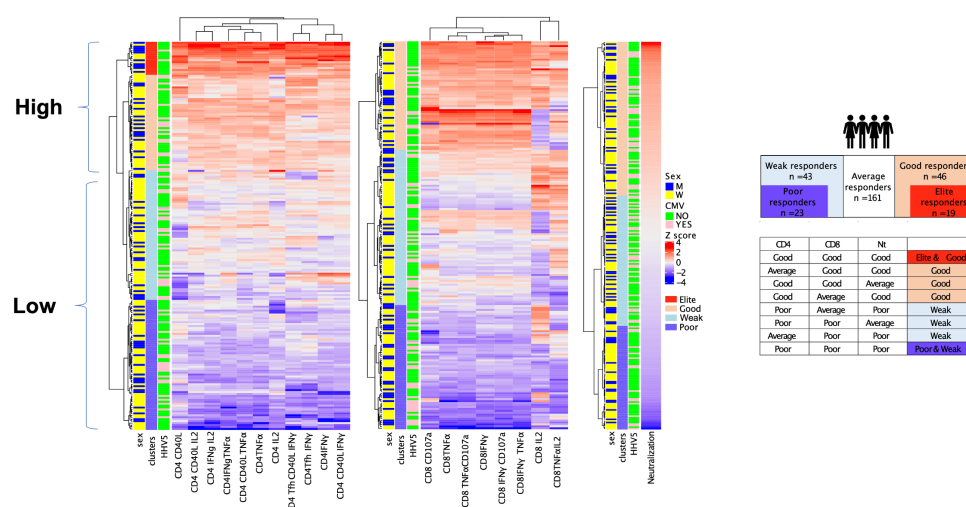
Figure 30.The classification of high and low responders.

The individuals were grouped into high (further subcategorized into Good and Elite) and low (further subcategorized into Weak and Poor) responders based on the hierarchical clustering. High responders are depicted in red and orange, while low responders are marked in light or dark blue, (left). The color gradations signify higher (red) or lower (blue) levels of cells and antibodies. Unsupervised hierarchical clustering was performed using Ward's method (Ward.D2) and visualized with the ComplexHeatmap package in R.

4.5.3 Transcriptional profiles pre- and post-vaccination

To investigate the sources of immune response variability, we analyzed expression profiles across individuals.

To analyze interindividual differences in gene expression, unsupervised hierarchical clustering was performed on the pre-vaccination transcriptional expression profiles. Three distinct clusters of individuals were identified (endotypes), which were defined based on the baseline expression of gene sets derived from the MsigDB Hallmarks collection using Gene Set Variation Analysis (GSVA) (Subramanian *et al.*, 2005). The expression data were normalized and corrected for batch effects and the optimal number of clusters was defined using the NbClust function.

One of the identified endotypes exhibited pronounced expression of numerous pro-inflammatory genes, including pathways such as complement activation, 'IL6_JAK_ STAT3_SIGNALING', 'TNFA_SIGNALING_VIA_NFKB', 'TGF_BETA_SIGNALING', 'INFLAMMATORY_RESPONSE' and 'IL2_STAT5_SIGNALING', which was labeled as

the 'high inflammatory endotype' (high inflam.) Another endotype exhibited low expression of pro-inflammatory gene expression alongside with elevated levels of 'MYC_TARGETS' and 'E2F_TARGETS', as well as pathways associated with glycolysis. Consequently, it was termed as the 'low inflammatory endotype' (low inflam.). Lastly, the third endotype displayed a mixture of inflammatory gene expression and thus called the 'moderate inflammatory endotype' (moderate inflam.) (Figure 31A).

A

Pre-vaccination transcriptomic profile

B

Sex distribution within Endotypes
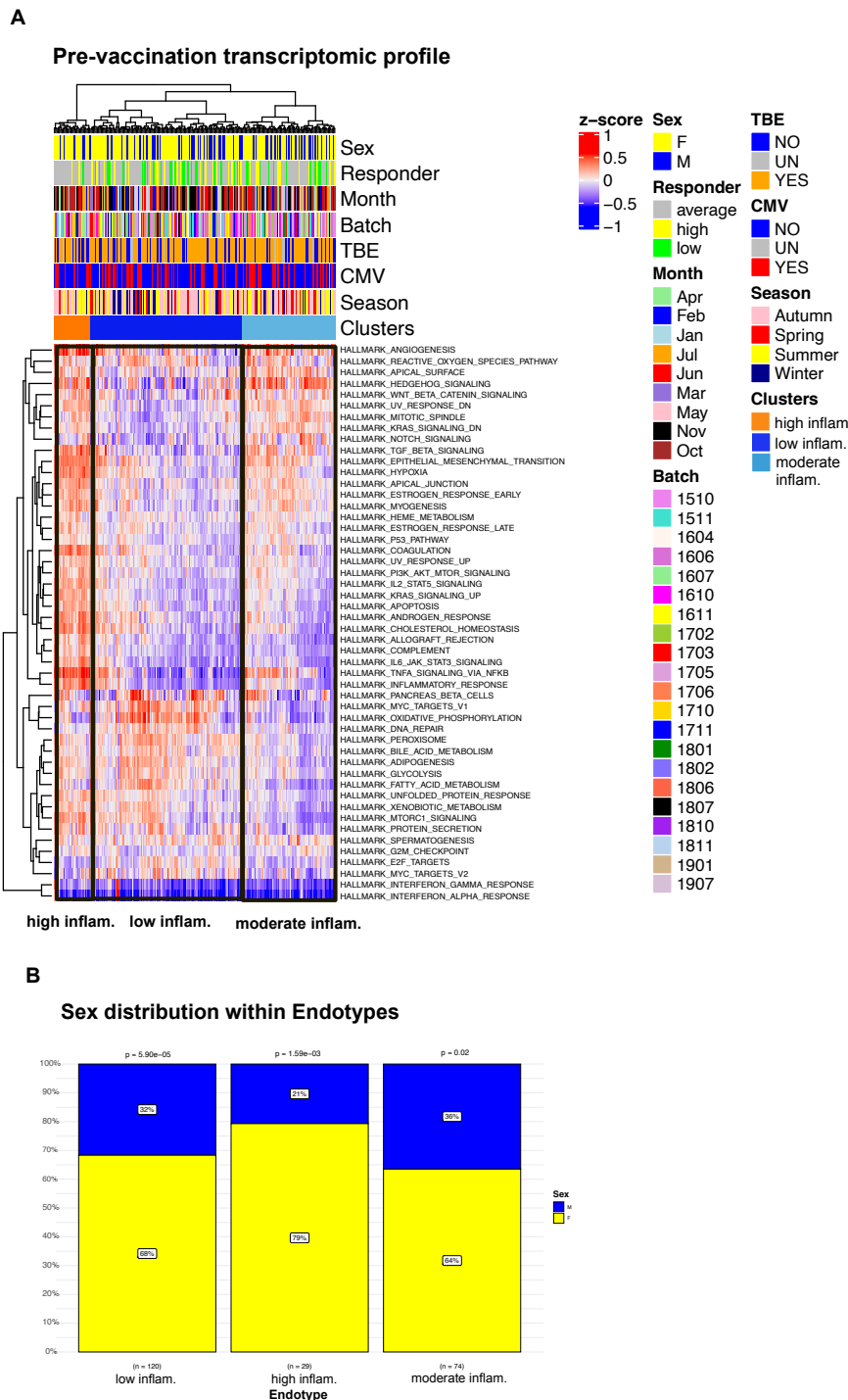
Figure 31.Pre-vaccination transcriptomic profiles identify three clusters (endotypes) with in the individuals of the vaccine cohort.

A) The transcriptomic activity of gene sets was estimated using Gene Set Variation Analysis (GSVA). A heatmap of GSVA scores was constructed using hierarchical clustering with Ward's method (Ward. D2) and the squared Euclidean distance metric. defining three clusters also called endotypes characterized by high, low and moderate activation of inflammatory genes. Various confounding factors were included in the analysis, including sex, CMV seropositivity, TBE status, responder classification, as well as seasons, months of collection, and batch. B) The sex distribution across the

endotypes defined in A. Statistical significance was evaluated using the Chi-squared to determine if the variables (the sex and endotypes) were non-randomly associated (n = 223).

The investigation explored the impact of batch effects and various confounding factors including sex, seasonality, CMV seropositivity, and TBE pre-immunity, as well as responder grouping on gene expression. The analysis indicated that TBE status, CMV seropositivity, and seasonality did not show a noticeable effect on the endotypes. However, there was an overrepresentation of females in the high inflam. endotype (χ^2 p value = 1.59e-03) (Figure 31B).

The clusters identified at baseline were carried over for the visualization of post-vaccination (day 7) expression (Figure 32A). The constructed heatmap highlights the strong up-regulation of IFN alpha and gamma signaling compared to other pathways. To determine whether the IFN pattern differs between high and low responders, the type I and II IFN pathways were plotted however, the differences between those groups were not significant (Figure 32B).
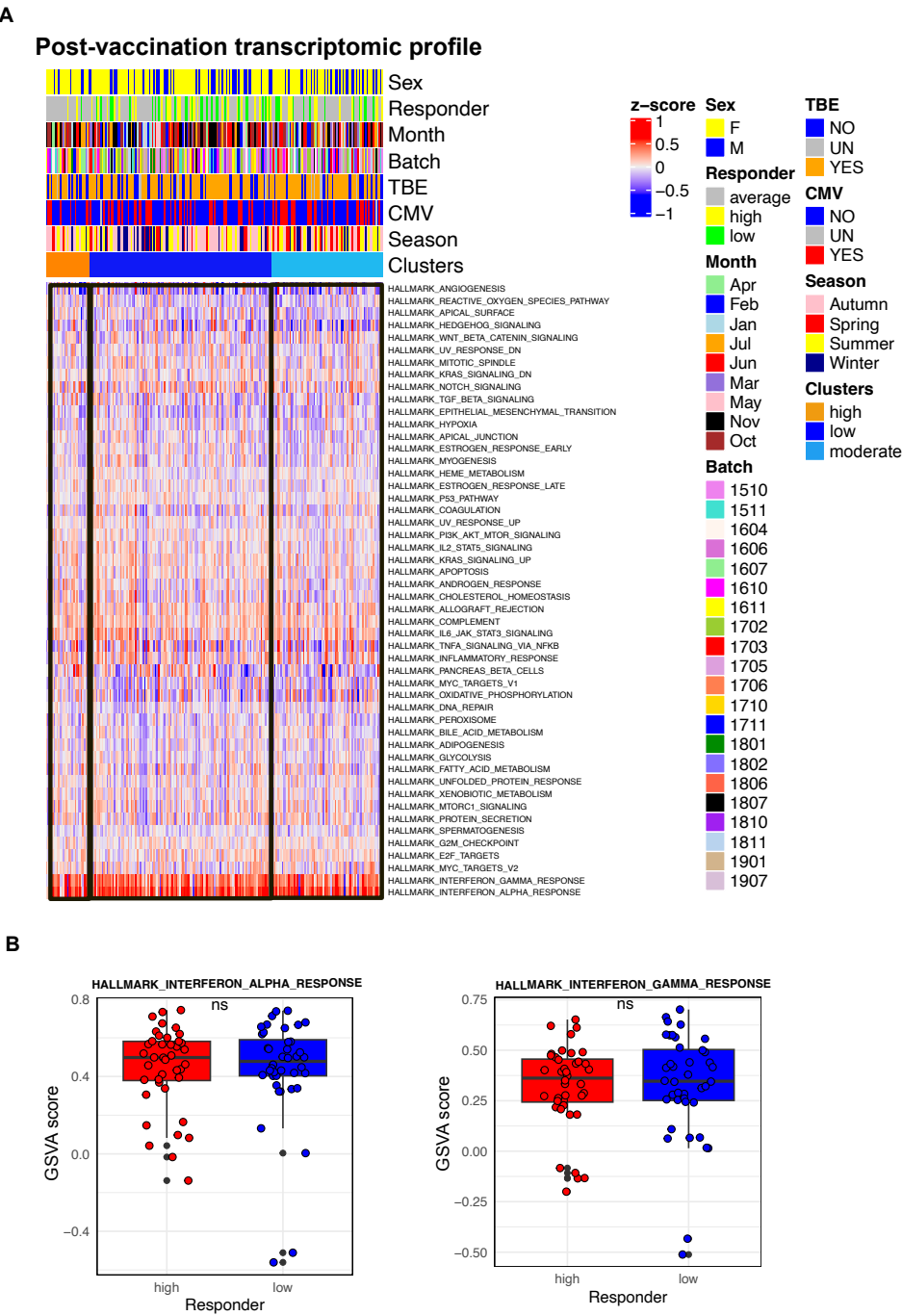
Figure 32.Groupings of individuals based on pre-vaccination transcriptional profiles/endotypes in monocytes do not correlate with post-vaccination transcriptomic profiles.

A) A heatmap of GSVA scores was constructed using pre-defined pre-vaccination clusters (n=223) B) The differences in IFN pathways between high and low responders post-vaccination. Statistical significance between groups was calculated using the Wilcoxon rank-sum test, n=223. Box plots indicate medians (center lines) and lower and upper hinges corresponding to the first and third quartiles. Non-significant if p-values > 0.05 (ns).

Associations between pre-vaccination endotypes and subsequent variations in immune responses were explored. The endotypes exhibited minor changes, with the high inflam. endotype displaying a slight upregulation of neutralizing antibodies (see Figure 33A) and activated CD38+ Ki-67+ CD8+ T-cell levels (Figure 33C) on day 28. However, the observed differences between the groups did not reach statistical significance.
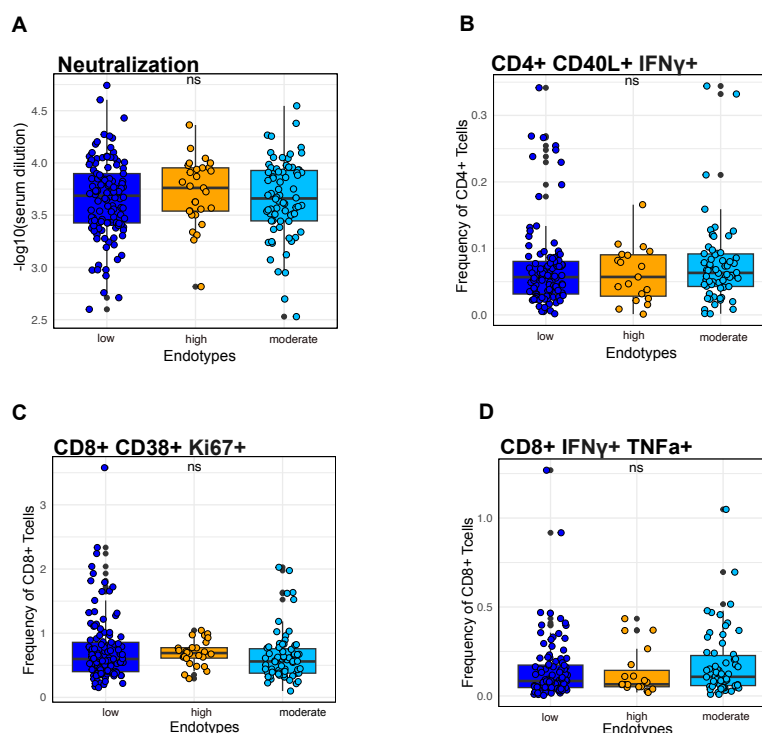
Figure 33. Influence of pre-vaccination endotypes on the immune response to YFV17D.

Box plots show differences in the response. Each endotype is marked in a different color. A) Neutralization on day 28 B) CD4+ CD40L+ IFN-γ+ C) CD8+ CD38+ Ki67+ D) CD8+ IFN-γ+ TNFa+, measured on day 28. Statistical significance between groups was calculated using the Kruskal-Wallis test with Benjamini-Hochberg's correction, n=223). Box plots indicate medians (center lines) and first and third quartiles. Significant if adjusted p-values < 0.05.

4.5.4 Association of gene signatures with the immune response

Previous results revealed variability in the baseline status across individuals. To get an insight into the baseline gene expression and its association with the adaptive immune response, Weighted Gene Co-expression Network Analysis (WGCNA) was conducted (Langfelder and Horvath, 2008). This method allows for the identification of patterns and relationships among co-expressed genes called modules using unsupervised

hierarchical clustering and enables the correlation of detected modules with external traits, aiding in the understanding of their relationships within the context of biological networks.

As depicted in Figure 34, genes were clustered into four major modules: blue, turquoise, yellow, and green (Figure 34A). The expression of each module was correlated with the immune response including neutralization and T cell responses. The green module exhibited a weak correlation with neutralizing antibodies on day 14 (R= 0.25, p =0.0002) and a negative correlation (R= -0.2, p =0.003) was detected with activated CD4$^+$ T cells expressing CD38 and Ki67 on day 28 (Figure 34B and C).

The green module consists of 984 genes. The 10 most significantly associated genes with this module were solute carrier (SLC) family SLC35A1 and SLC40A1, asparaginyl-tRNA synthetase 1 (NRS1), sorting nexin (SNX1/SNX27), coenzyme Q (COQ5/COQ9), vacuolar protein sorting-associated protein 35 (VPS35), methionine adenosyltransferase 2B (MAT2B) and additionally, other significant genes were detected including aldehyde dehydrogenase genes (ALDH9A1/ALDH3A2), family with sequence similarity (FAM118B/FAM222B/FAM86C1), and additional members of SLC family SLC5A9, SLC6A12, SLC9A3, SLC25 (A1, A3, A12, A13, A17, A20, A37), SLC28A3, SLC35 (B3, B4, C1, E3), SLC29A3, SLC37A4, SLC38A6, SLC46A2, FOS like 2 (FOSL2), TNF receptor superfamily member 12A (TNFRSF12A), HLA-DQB1, and CD200 receptor 1 (CD200R1).

A

Gene dendrogram day 0

Modules

B

Module–neutralization relationships

C

Module–T cell relationships
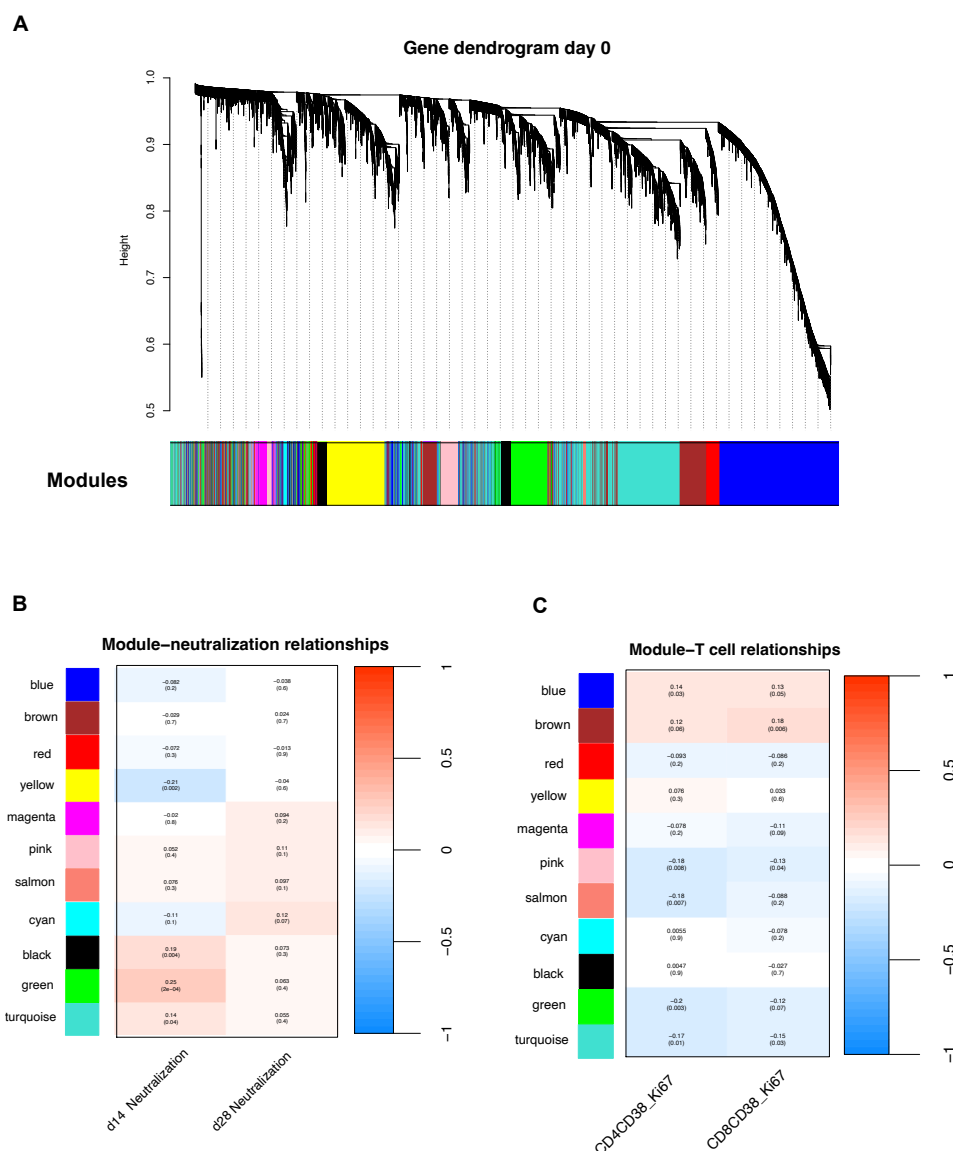
Figure 34. The WGCNA analysis of co-expressed genes at baseline and association of gene modules with vaccine responses.

A) The gene dendrogram at the baseline was constructed using WGCNA (hierarchical clustering and average linkage method) in R. The y-axis represents "Height", which is a measure of dissimilarity/distance between clusters (a higher height indicates lower similarity) and the x-axis represents assigned modules of co-regulated genes determined by the dynamic tree cut function in in R. The heatmaps show the correlation of gene modules with traits including B) neutralizing antibody levels and C) number of activated (CD38+, Ki67+) CD4+ and CD8+ T cells respectively on day 28. Each row corresponds to a genes' module and each column to a trait. Each cell depicts Pearson's correlation (R and p-value, n=223).

Additionally, we performed a correlation analysis of the detected baseline expression modules with other T-cell characteristics (Figure 35) measured on day 28 after

vaccination. The analysis revealed a weak positive correlation between the baseline expression levels of the brown module which comprises 1221 genes and the number of CD107a^{+} CD8^{+} T cells (R = 0.2, p = 0.003) and a modest correlation with CD107a+ central memory (CM) CD8^{+} T cells (R = 0.3, p = 0.000005) on day 28. The top associated genes with the brown module were glutamate-ammonia ligase (GLUL), ariadne RBR E3 ubiquitin protein ligase 2 (ARIH2), SLC15A4, mitogen-activated protein kinase 1 interacting protein 1 like (MAPK1IP1L), MEFV innate immunity regulator/pyrin MEFV, basic leucine zipper and W2 domains 1 (BZW1), golgi transport 1B (GOLT1), MAP1LC3B and SLC3A2. Other significantly associated genes of the brown module include members of the SLC family (SLC7A5, SLC10A3, SLC25A25, SLC17A5, SLC26A11, SLC41A2), ZNF394 (zinc finger protein 394), CD48, CD86, eukaryotic translation initiation factor 1A domain-containing (EIF1AD) neuraminidase 4 (NEU4), E2F3 (E2F transcription factor 3), HLA-DRA, HLA-DPA1 and CLEC7A.

Furthermore, we observed a correlation between effector memory (EM) CD4^{+}/CD8^{+} T cells secreting IL2 cytokine on day 28 post-vaccination with a cyan module (R= 0.28, p = 0.00002) consisting of eukaryotic translation elongation factor 2 (EEF2), N-sulfoglucosamine sulfohydrolase (SGSH), F-box and leucine-rich repeat protein 18 (FBXL18), Plectin (PLEC), Rho/Rac guanine nucleotide exchange factor 2 (ARHGEF2), growth arrest-specific 7 (GAS7), pre-mRNA processing factor 8 (PRPF8), nischarin (NISCH), low-density lipoprotein receptor-related protein 1 (LRP1), NCK-associated protein 5-like (NCKAP5L) and yellow module (R= 0.21, p = 0.002) that includes REL proto-oncogene (REL), ATPase 13A3 (ATP13A3), Multiple epidermal growth factor-like domains protein 9 (MEGF9), chromosome 16 open reading frame 72 (C16orf72), cytoplasmic polyadenylation element-binding protein 4 (CPEB4), general transcription factor II-I repeat domain-containing protein 1 (GTF2IP1), frizzled-2 (FZD2), SMAD ubiquitination regulatory factor 1 (SMURF1), zyg-11 family member B (ZYG11B), purine-rich element-binding protein B (PURB) as well as SLC family genes (SLC45A4, SLC25A33, SLC2A13, SLC25A43, SLC22A15, SLC35D2, SLC25A28).

Additionally, negative correlations were detected between these T cell populations and other baseline gene modules, specifically CM CD107^{+} CD8^{+} T cells within the red, black, and turquoise modules. Moreover, EM CD8^{+} T cells secreting IL2 cells showed a negative correlation with the green module.

Figure 35.Correlations between baseline WGCNA modules and T cell levels measured on day 28.

The heatmap of correlation of modules on day 7 pv with T cell levels. Each row corresponds to a genes' module and each column to a trait. Each cell depicts Pearson's correlation (R and p-value).
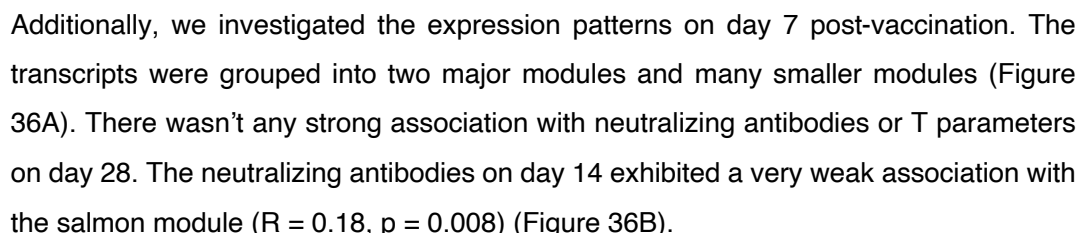
To gain further insight into the function of the modules, pathway enrichment was performed on each gene module using GSEA applied to 7,233 C2 curated gene sets from MSigDB. None of the modules showed statistically significant functional enrichment after correction for false discoveries (FDR < 0.05). However, interestingly, the green module was associated with pathways including 'KEGG antigen processing and presentation' and 'REACTOME interferon-gamma signaling,' whereas the brown module was associated with 'BIOCARTA cytokine pathway', 'REACTOME C-type lectin receptors', and 'BIOCARTA inflammatory pathway' (data not shown).

Additionally, we investigated the expression patterns on day 7 post-vaccination. The transcripts were grouped into two major modules and many smaller modules (Figure 36A). There wasn't any strong association with neutralizing antibodies or T parameters on day 28. The neutralizing antibodies on day 14 exhibited a very weak association with the salmon module (R = 0.18, p = 0.008) (Figure 36B).

Figure 36. The WGCNA analysis of co-expressed genes on day 7 pv and association of the identified gene modules with vaccine responses.

A) The gene dendrogram post-vaccination was constructed using WGCNA (hierarchical clustering and average linkage method) in R. The y-axis shows "Height" which represents dissimilarity/distance between clusters (a higher height indicates lower similarity) and the x-axis represents assigned modules of co-regulated genes determined by dynamic tree cut function in in R. The heatmaps show correlations of gene modules with traits including B) neutralizing antibody levels and C) T cell levels on day 14 and day 28 respectively and C) the number of activated (CD38+, Ki67+) CD4 and CD8 T cells respectively on day 28. Each row corresponds to a genes' module and each column to a trait. Each cell depicts Pearson's correlation (R and p-value, n=223).

Similarly, no correlation was detected with other T-cell populations (Figure 37). The most significantly associated with the salmon module were innate and antiviral genes including IFIT1, RSAD2, IFIT3, USP18, PARP9, IFIT2, CXCL10, TRIM22, MX1, SAMD9.

.

Figure 37.Correlations between WGCNA modules on day 7 pv and T cell levels parameters on day 28.

The heatmap of correlation of modules on day 7 pv with T cell parameters on day 28 after vaccination. Each row corresponds to a genes' module and each column to a trait. Each cell depicts Pearson's correlation (R and p-value)

4.5.5 Differences between high and low responders

To gain a deeper understanding of the differences between high and low responders, we conducted a DGE analysis between these groups, following the methodology previously employed using the limma-voom method as described previously. The high and low responders were set as the contrast groups. The analysis identified three candidate DEGs at baseline and seven DEGs post-vaccination between the high and low responders, although the adjusted p-values did not reach significance. The top DEGs at baseline included SYT1(Synaptotagmin-1), NEU4, and a lncRNA with an unknown function. Post-vaccination, the top DEGs included CD200R1. PPAN (Peter pan homolog), ALDH7A1 (Aldehyde dehydrogenase 7 family member A1), FAM225B –

lncRNA; a novel transcript C11orf54-MED17, RGPD6 (RANBP2 like and GRIP domain containing 6) and AMOTL1(Angiomotin like 1) gene (Table 5).

Genes	logFC	P-value	adj.P-value
Day 0			
SYT1	1.34	0.001345782	0.9815869
ENSG00000288879 lncRNA	-1.00	0.004957486	0.9815869
NEU4	-1.05	0.009246477	0.9815869
Day 7			
CD200R1	1.05	0.005180166	0.9997645
PPAN	1.00	0.005259102	0.9997645
ALDH7A1	1.02	0.005822203	0.9997645
FAM225B lncRNA	1.28	0.008872392	0.9997645
C11orf54-MED17	1.31	0.008961976	0.9997645
RGPD6	-1.19	0.001264484	0.9997645
AMOTL1	-1.02	0.001378598	0.9997645

Table 4.The DEGs on day 0 before vaccination and day7 after vaccination in peripheral blood monocytes between high and low responders.

The table shows the logFC, p-value and adjusted p-value for each gene detected by DEG analysis between high and low responders.

4.6 Quantitative trait loci (QTL) studies

4.6.1 Association of genetic variants with cytokine production and vaccine response parameters after vaccination with YF17D

To study the genetic impact on the variability in immune responses, we genotyped 247 vaccinees using the Infinium Global Screening Array-24 v3.0 SNP chip (Illumina).

To identify genetic loci that influence cytokine production, neutralizing antibody titers, virus-specific IgM and IgG titers, and cellular responses (T cells, B cells, Antigen-presenting cells) upon YF vaccination, the genome-wide SNP genotypes have been evaluated for associations with these quantitative traits using the SNPTEST software. Before association, data have been corrected for confounding factors including age, gender, seasonality, BMI, and TBE vaccination (Figure 38A).
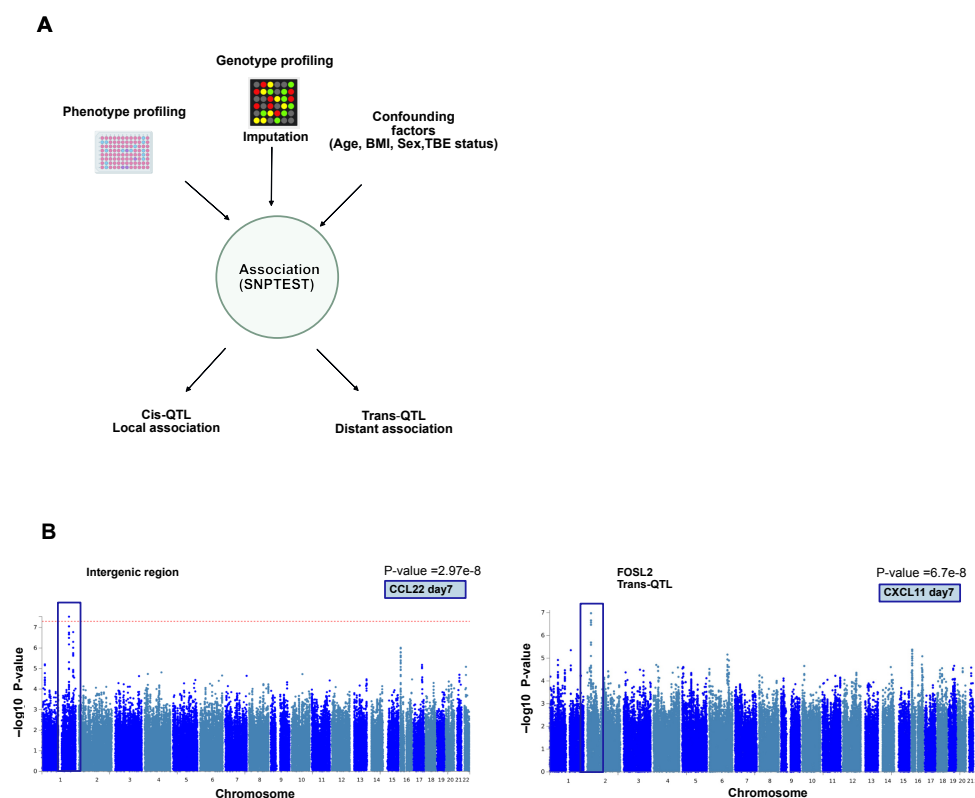
Figure 38.QTL Mapping.

A) Schematic associations between genotype and phenotype data (cytokine abundance after vaccination). B and C) Manhattan plots showing genome-wide association of genetic variants with CCL22 (B) and CXCL11 (C) measured on day 7 post-vaccination in the plasma of vaccinees. The x-axis shows genomic positions. The y-axis indicates the strength of the association, represented as -log10 transformed P-values. Each dot represents a single-nucleotide polymorphism (SNP) at the given locus (n=247).

These analyses identified one genome-wide (p < 5x10e-8) significant QTL and one interesting QTL candidate, which has not reached genome-wide significance (p-value=6.7e-8) (Figure 38B). The former locus, located in an intergenic region, was found to be significantly associated with CCL22 levels. The other locus, located in the intronic region of the FOSL2 gene sequence, was associated with CXCL11 levels. Association with neutralization also shows a suggestive but not significant signal coming from an intergenic region. The other QTLs detected exhibited low effect sizes, with p-values > 10e-7, not sufficient to achieve genome-wide significance (Table 6).

Trait	SNP	Chromosome	P-value	Casual Gene
CCL22 day7	1:199567304:T:C	1	2.97e-8	Intergenic region
CXCL11 day7	2:28408296:C:T	2	6.7e-8	FOSL2
Neutralization day14	13:73154223:G:A	13	9.14e-8	Intergenic region
Virus IgG day28	11:21377151:A:G	11	1.28e-6	NELL1
IgM day7	4:99473785:A:G	4	4.49e-6	TSPAN5
Monocyte CD14^{++} CD16$^-$ Siglec1$^+$ day7	12:113514194:C:T	12	2.46e-6	DTX1

Table 5.The detected QTLs post-vaccination.

The tables display the chromosome position and p-value for each association.

Analysis of genetic variations revealed an association between a SNP located in the FOSL2 locus and CXCL11 levels in response to YF17D vaccination. Depending on their allele composition individuals carrying this SNP demonstrated altered levels of CXCL11 compared to those without the variant, suggesting a potential regulatory role of this genetic variant on CXCL11 expression. The SNP thereby influenced both the baseline levels of CXCL11 in plasma prior to vaccination and even more so the CXCL11 levels induced by vaccination with YF17D (Figure 39A).

To validate the influence and functional consequences of FOSL2 expression on the YF17D-induced cytokine response 1205Lu cells deficient for FOSL2 were generated using CRSPR-Cas9 gene editing and infected *in vitro* with YF17D. Infecting cells deficient in FOSL2 resulted in a noticeable increase in the expression levels of interferon-beta (IFN-β) and CXCL10 compared to wild-type (WT) controls (Figure 39B). This observation confirms the regulatory role of FOSL2 in modulating the cytokine milieu post-vaccination.

A

B
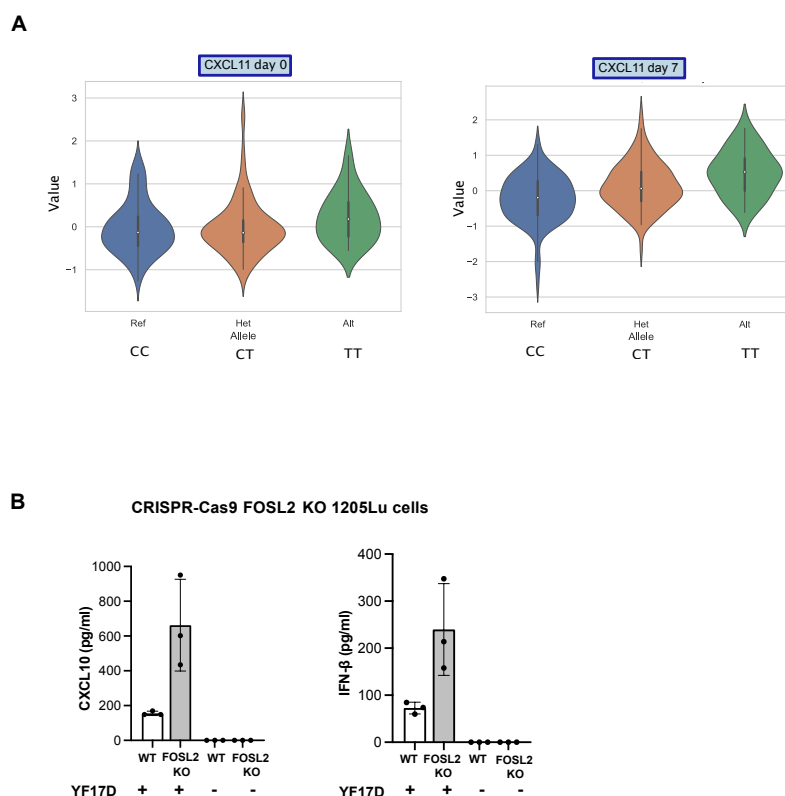
Figure 39. Variance in FOSL2 expression influences the cytokine production after infection with YF17D.

A) Violin plots showing CXCL11 levels influenced by the trans-QTL candidate in the FOSL2 gene (n=247) B) Wild-type (WT) and FOSL2 CRISPR-knockout (KO) 1205Lu cells were infected with Venus-YF17D at MOI 5. The CXCL10 and IFN-β abundance in the culture supernatant was measured by ELISA at 48h post-infection. Error bars represent means and standard deviations (n=3).

4.6.2 Expression quantitative trait loci (eQTL) study identify genetic variants influencing the transcriptional response of monocytes to vaccination with YF17D (response eQTL)

To further investigate the genetic influence on the response to the YF17D vaccine, RNA-seq data from the isolated monocytes before and 7 days after vaccination were integrated with the SNP data of the cohort and cis-eQTL mapping was performed (within 1 Mbp of the transcription start site (TSS) of each gene) using the FastQTL software (Ongen *et al.*, 2016), following the GTEx pipeline (Aguet *et al.*, 2017, 2023). The association identified 2389 and 2194 eGenes (genes associated with at least one cis-eQTL) at baseline and post-vaccination, respectively. To determine which cis-eQTLs are

specifically related to the response to YF17D infection, we employed a tool called mashr (Urbut *et al.*, 2019) to identify genetic loci that affect the magnitude of gene activation upon vaccination. Mashr first analyzes each timepoint separately to get initial effect estimates. Then, it uses the Empirical Bayes technique to learn patterns from these initial estimates and leverage those patterns to produce more reliable effect estimates and significance measures for each unit across all conditions. Response eQTLs (res-eQTLs) were defined as those showing significant differences in effect size (with a local false sign rate (LSFR)< 0.05) between day 7 and baseline conditions.

Using this method, in total, 36 res-eQTLs (Figure 40) were identified as significantly induced in response to the vaccination. The loci most strongly associated with response to YF17D infection include regulatory regions affecting the following genes: GrpE-like 2, mitochondrial (GRPEL2); eukaryotic translation initiation factor 2B subunit delta (EIF2B4); methyltransferase like 4 (METTL4); RNA polymerase II subunit K (POLR2K); Ubiquitin carboxyl-terminal hydrolase isozyme L3 (UCHL3); RAP1B, member of RAS oncogene family (RAP1B); heterogeneous nuclear ribonucleoprotein A3 (HNRNPA3); and megalencephalic leukoencephalopathy with subcortical cysts 1 protein (MLC1).

A
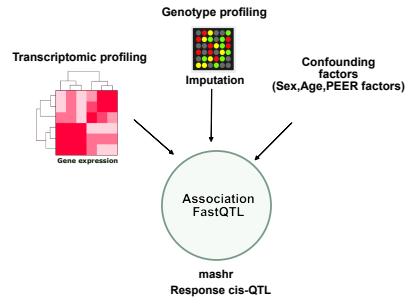
B

|	Variant mashr	LSFR d0	LSFR f7	GENEID	GENENAME
1	ENSG00000164284_5_150223261_C_T	0.10063987	0.001417287	ENSG00000164284	GRPEL2
2	ENSG00000115211_2_27383116_G_A	0.31638762	0.001858166	ENSG00000115211	EIF2B4
3	ENSG00000101574_18_2513460_C_T	0.05879328	0.003483445	ENSG00000101574	METTL4
4	ENSG00000147669_8_100100355_T_C	0.23036717	0.004292638	ENSG00000147669	POLR2K
5	ENSG00000118989_13_75567585_C_A	0.06501969	0.005342988	ENSG00000118939	UCHL3
6	ENSG00000127314_12_68444233_C_T	0.10178969	0.006926954	ENSG00000127314	RAP1B
7	ENSG00000170144_2_177223416_A_C	0.13635562	0.017536848	ENSG00000170144	HNRNPA3
8	ENSG00000100427_22_49445015_G_A	0.20857556	0.018485800	ENSG00000100427	MLC1
9	ENSG00000196151_2_159290634_T_C	0.05520920	0.023358506	ENSG00000196151	WDSUB1
10	ENSG00000123975_9_90206164_C_T	0.11229428	0.026174095	ENSG00000123975	CKS2
11	ENSG00000115009_2_227725924_G_A	0.14648095	0.028691874	ENSG00000115009	CCL20
12	ENSG00000197756_2_217372167_G_C	0.15318985	0.030853972	ENSG00000197756	RPL37A
13	ENSG00000204681_6_29908998_G_A	0.17134471	0.031268944	ENSG00000204681	GABBR1
14	ENSG00000132256_11_5680869_G_A	0.09615545	0.032128823	ENSG00000132256	TRIM5
15	ENSG00000166848_16_74763446_C_T	0.21325360	0.032840333	ENSG00000166848	TERF2IP
16	ENSG00000103653_15_74915307_A_G	0.06215203	0.033688423	ENSG00000103653	CSK
17	ENSG00000137818_15_68844535_A_C	0.05394085	0.033873287	ENSG00000137818	RPLP1
18	ENSG00000283228_2_152088264_C_T	0.36420036	0.035170655	ENSG00000283228	CACNB4
19	ENSG00000107949_10_126088475_C_T	0.05605108	0.036915978	ENSG00000107949	BCCIP
20	ENSG00000163823_3_46109445_G_A	0.8376183	0.037662620	ENSG00000163823	CCR1
21	ENSGO0000166016_11_34585067_C_A	0.24700677	0.037821638	ENSG00000166016	ABTB2
22	ENSG00000148834_10_103712215_A_G	0.05441028	0.042865220	ENSG00000148834	GSTO1
23	ENSG00000107201_9_32325283_A_G	0.20153444	0.043412456	ENSG00000107201	DDX58
24	ENSG00000143727_2_110819_C_T	0.06147358	0.043435466	ENSG00000143727	ACP1
25	ENSG00000133247_19_55270456_A_T	0.06162387	0.044805439	ENSG00000133247	KMT5C
26	ENSG00000213995_13_110638900_G_A	0.05442214	0.045164147	ENSG00000213995	NAXD
27	ENSG0800000181523_17_80550956_C_T	0.05274432	0.045914794	ENSG00000181523	SGSH
28	ENSG00000204356_6_32247992_G_C	0.05196628	0.046322822	ENSG00000204356	NELFE
29	ENSG00000137959_1_79193451_T_G	0.05729389	0.046428156	ENSG00000137959	IF44L
30	ENSG00000285410_15_50297203_G_A	0.05587189	0.046815820	ENSG00000285410	GABPB1-IT1
31	ENSG00000164074_4_128237286_T_C	0.05473669	0.047180833	ENSG00000164074	ABHD18
32	ENSG00000105676_19_18276095_A_C	0.05105614	0.047441415	ENSG00000105676	ARMC6
33	ENSG00000107957_10_103666921_A_G	0.05032475	0.047570106	ENSG00000107957	SH3PXD2A
34	ENSG00000110435_11_34941912_T_C	0.29419349	0.049429880	ENSG00000110435	PDHX
35	ENSG00000113742_5_174182271_A_G	0.14107438	0.049538483	ENSG00000113742	CPEB4
36	ENSG00000104951_19_49024082_C_T	0.05842222	0.049618318	ESNG00000104951	IL4I1

Figure 40.Immune response eQTLs detected in peripheral blood monocytes 7 days after YF17D infection.

A) eQTL analysis was performed to identify genetic variants associated with gene expression levels measured by RNA sequencing. SNPs and gene expression profiles of the corresponding samples were used as input. The analysis was carried out in two steps: (1) Cis-eQTL mapping using FastQTL to identify local SNPs influencing the expression of nearby genes was performed for day 0 (n=227) and day 7 separately (n=217). (2) Mashr software was then employed to detect regulatory SNPs (res-

eQTL) affecting gene expression in response to YF17D. B) A total of 36 res-eQTL was found to be significantly induced on day 7 compared to the baseline (LFSR, equivalent to FDR) of < 0.05.

Individuals carrying the alternative allele showed elevated levels of GRPEL2 expression, whereas individuals homozygous for the alternative allele exhibited lower levels of EIF2B4 expression (Figure 41).
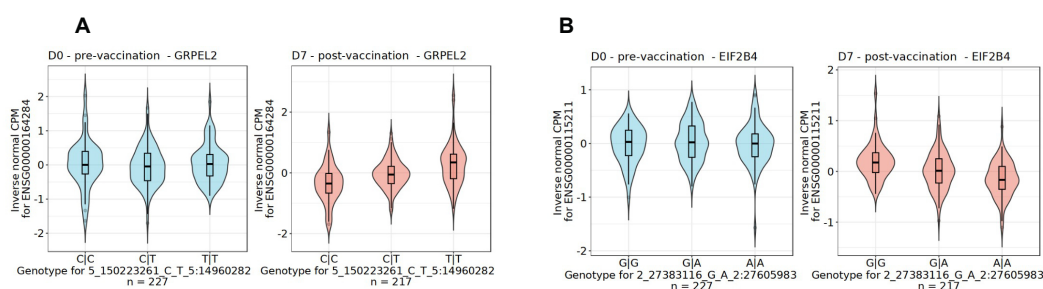
Figure 41.Differences in transcriptomic levels are influenced by genetic variation.

A) Violin plots showing expression levels of GRPEL2 and B) EIF2B4 in monocytes before and 7 days after vaccination with YF17D influenced by res-QTLs.

The analysis additionally detected cis-eQTLs influencing the expression of immune genes, including chemokine (C-C motif) ligand 20 (CCL20), tripartite motif-containing protein 5 (TRIM5), C-C chemokine receptor type 1 (CCR1), DExD/H-box helicase 58 (DDX58/RIG-I), interferon-induced protein 44-like (IFI44L), and interleukin-4 induced gene 1 (IL4I1), indicating their involvement in interindividual differences in response to viral infections. It is worthwhile to highlight that we detected a response eQTL in DExD/H-box helicase 58 coding for RIG-I the sensor we found to be the main pattern recognition receptor triggering the interferon response after infection with the YF17D. Individuals carrying the alternative allele in RIG-I or IFI44L loci showed elevated expression levels of these genes (see Figure 42).
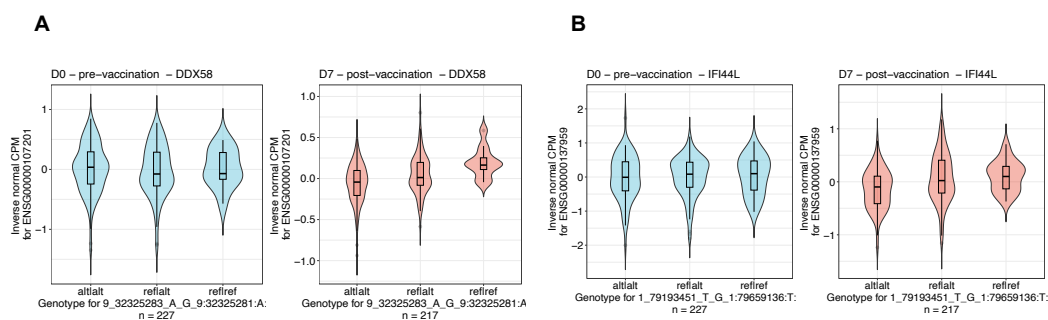
Figure 42.Differences in transcriptomic levels of immune genes are influenced by genetic variation.

A) Violin plots showing expression levels of DDX58 and B) IFI44L in monocytes before and 7 days after vaccination with YF17D influenced by res-QTLs.

5. Discussion

The YF vaccine, YF17D is one of the most potent vaccines ever developed. It induces a transient viral infection, leading to life-long immune protection, yet the underlying molecular mechanisms conferring such a strong and lasting immunity remain poorly understood (Theiler and Smith, 1937; Poland *et al.*, 1981). It is hypothesized that the effectiveness of YF17D vaccination relies heavily on innate sensing and the type I IFN response, which influences the strength of the subsequent adaptive immune response (Pulendran, 2009). Within this thesis, I aimed to characterize the molecular features of YF17D triggering the interferon response and uncover gene signatures associated with effective adaptive immunity, along with factors influencing interindividual variation in the immune response to YF17D across individuals.

The project employed a combination of experimental cellular biology to identify the main innate immune sensors, and pathways triggered by YF17D and a systems immunology approach to investigate the interplay of innate and adaptive immunity in the antiviral response, using the YF17D vaccine as a controlled perturbation model in a human cohort of 250 vaccinees. Through the vaccination, it was possible to mimic a natural viral infection under controlled conditions and thereby synchronize the perturbation, to better study the kinetics of the developing immune response. The study integrated data from different modalities including RNA sequencing, genotyping, flow cytometry and multiplex cytokine assays in order to find early or pre-existing signatures influencing and predicting

the strength of the adaptive antiviral immune response and to explain interindividual variability of the responses.

5.1 YF17D is preferentially sensed by the RLR pathway

The study aimed to uncover the receptors and pathways involved in sensing the YF17D infection. To achieve this, we conducted *in vitro* experiments using both murine and human cells and cell lines lacking one or multiple pattern recognition receptors and adaptors. These experiments revealed that predominantly RLR and MAVS signaling control the IFN-mediated restriction of the YF17D infection, with RIG-I playing a significant role in viral sensing early on and MDA5 contributing mainly at later timepoints in murine and human cell lines. Similar results were observed in human monocyte-derived dendritic cells (mo-DCs) where silencing MAVS with siRNA substantially impaired the ability of YF17D to stimulate IFN-β production, underscoring the high dependence of this response on MAVS and minor contribution of TLR signaling (data generated by Prof. Anne Krug group's, part of Zaucha, Winheim et al. manuscript in preparation).

Previous studies have demonstrated the activation of both TLRs (Querec *et al.*, 2006) and RLRs (Bruni *et al.*, 2015) in response to YF17D, whereas this study indicated only a minor contribution of TLRs, which might result from the differences in the used cell types. It has been shown that virus replication in plasmacytoid DCs (pDCs) triggers RIG-I-dependent IFN production, while interactions with other infected cells activate the TLR-dependent pathway (Bruni *et al.*, 2015; Sinigaglia *et al.*, 2018).

Interestingly, apart from RIG-I, MDA5 also contributes to the type I IFN response. The results have shown that the loss of both results in a severe impairment of the immune response.

Additionally, the study has investigated the specific viral RNA species recognized by RLRs showing that YF17D infection leads to the formation of dsRNA intermediates with 5' phosphate moieties. It was shown previously that RIG-I preferentially recognizes short dsRNAs with 5'- di- and tri-phosphate groups while ligands of MDA5 are long dsRNAs (Hornung *et al.,* 2006; Kato *et al.,* 2008; Schmidt *et al.,* 2009; Goubau *et al.,* 2014). Interestingly, we observed distinct activities of RIG-I and MDA5. RIG-I predominance was evident in the early phase (24 h post-infection), characterized by the accumulation of dsRNA RIG-I ligands with phosphate moieties at the 5' end. Conversely, at a later

timepoint (72 h post-infection), greater activity of MDA5 was observed, indicating the formation of longer dsRNA independent of phosphate moieties. Knocking out RIG-I and MDA5 confirmed that viral species are preferentially sensed by RIG-I at early timepoints, consistent with reports for West Nile Virus infections (Errett *et al.*, 2013). However, MDA5 KO did not show clear dominance at later timepoints, suggesting both RIG-I and MDA5 involvement in sensing YF17D at later stages.

5.2 Cytokine responses are influenced by sex and seasonality

It has been shown that cytokine responses play an important role in the antiviral immune (Querec *et al.*, 2006).

In this study, I have found that YF17D vaccination induces a robust and transient cytokine response post-vaccination. The data highlight significant changes in cytokine levels from baseline to post-vaccination timepoints showing an increase of cytokines levels on day 3, peaking on day 7, followed by a decrease at later timepoints: on days 14 and 28.

The Bio-Plex assay analysis allowed for the identification of changes in 18 distinct pro-inflammatory cytokines/chemokines in plasma samples. Previous research by Querec et al., on human blood samples, confirmed the significant upregulation of only two pro-inflammatory chemokines/cytokines IP10/CXCL10 and IL-1a across 15 individuals. These cytokine levels peaked on day 7 after vaccination (Querec *et al.*, 2009). Another study showed an upregulation of CCL3/MP-1a, IL6, IP10/CXCL10 in PBMCs isolated from four patients stimulated with YF17D (Bidet *et al.*, 2019). This study detected additional pro-inflammatory cytokines and chemokines, including Eotaxin, IL-1ra, IL-18, CXCL11, CXCL13, MIG, PDGF-bb, RANTES, TNF-α, CCL22, APRIL, and BAFF. While all measured type I, II, and III IFNs have not reached the lowest limit of quantification, the study confirmed the activation of multiple cytokines and chemokines including several interferon-induced chemokines like CXCL10 and CXCL11 post-vaccination.

5.3 YF17D activates a broad and robust transcriptomic response

In this study, I adapted and optimized the single-cell SmartSeq2 method for bulk RNA sequencing to characterize transcriptomic signatures in response to YF17D. Based on

the result of a pilot study performed together with the group of Prof. Anne Krug (LMU), isolated peripheral blood monocytes were chosen for bulk RNA-seq as they had the highest transcriptomic changes post-vaccination in the pilot study.

The comprehensive analysis of 244 individuals revealed a total of 8,132 differentially expressed genes post-vaccination. Among the most significantly differentially expressed genes were IFI44L, SIGLEC1, XAF1, OAS2, EPSIT1, USP18, MX2, RSAD2, LY6E, IFI44, EIF2AK2, MX1, FIT3, SPATS2L, IFI6, IFIT1, IRF7, and OAS3 (ranked starting with the highest adjusted p-value). Many of these genes have been previously identified and described within the context of yellow fever infection where most of them were associated with antiviral signaling (Gaucher *et al.*, 2008; Querec *et al.*, 2009) and inhibition of viral replication (Schoggins *et al.*, 2011). The downregulated genes including DANCR, ITGAE, EIF4B, and EIF3L have also been previously described to be DE in other vaccination studies (Gaucher *et al.*, 2008; Querec *et al.*, 2009; de Lima *et al.*, 2019). The previous work found DANCR to be upregulated in an influenza study (de Lima *et al.*, 2019) whereas EIF4B was downregulated after YF17D vaccination (Gaucher *et al.*, 2008). Differences in the expression of DANCR in our study versus the influenza study could be caused by differences in the analyzed cell type: isolated monocytes in our study versus whole blood and unseparated PBMCs in the study from de Lima.

5.4 Vaccination with YF17D activates multiple pathways associated with the innate and adaptive immunity

To gain a deeper understanding of the function of the identified genes, Gene Ontology Biological Process and Reactome pathway enrichment analyses were conducted. The GO analysis indicated the upregulation of 96 pathways, the most activated pathways being 'defense responses to viruses', 'type I and II IFN responses', 'antigen processing and presentation via MHC class I', 'and negative regulation of viral genome replication'. Similar findings were observed based on the Reactome and MSigDB Hallmarks collection, emphasizing the significant upregulation of interferon along with complement and inflammation signaling, which all appear to play pivotal roles in the early immune response.

The previous study by Querec et al. (2009) demonstrated the activation of several pathways, including antiviral and interferon signaling, complement, antigen processing, signal transduction, ISGylation, chemotaxis, and cell adhesion processes (Querec et al.,

2009). Hou et al. (2017) reported a robust activation of innate signaling, particularly type I IFN, pattern recognition receptors, and RIG-I-like receptors, along with IRF signaling on day 7 post-vaccination (pv) (Hou et al., 2017). Similarly, Bidet et al. (2019) showed that the IFN pathway exhibited the strongest upregulation in peripheral blood mononuclear cells (PBMCs) in response to YF17D stimulation (Bidet *et al.*, 2019). Although interferons by themselves could not be measured post-vaccination on protein or transcript levels, in any of the studies described above, the data demonstrate the activation of robust IFN type I and II signatures. This indicates the upregulation of the JAK-STAT pathway and signaling through the IFN receptors IFNAR 1/2 (type I IFNs) and IFNGR 1/2 (type II) post-vaccination. This could be due to the chosen timepoint of the measurements, conducted on day 7 pv. However, Hou et al. did not detect any upregulation of INF transcripts as early as 4h pv, suggesting very low, transient levels of IFN below the detection range, which was also the case in my study.

In my study, the GO term 'defense response to virus' encompasses the largest cluster of genes involved in type I IFN and type II IFN signaling, highlighting the transcription factors STAT1, STAT2, and IRF1/2/3/5/7/9 as hub genes. This is in agreement with the findings of Hou et al. who identified STAT1 as a central gene, and Gaucher et al. who reported the upregulation of STAT1, IRF1, IRF7, and IRF8 following YF17D vaccination (Gaucher *et al.*, 2008; Hou *et al.*, 2017). Similarly, Querec et al. demonstrated activation of IRF7 and STAT1 transcription factors. Moreover, additional genes which I found upregulated in my dataset and are part of the interferon signaling cluster were OAS1/3, OASL, MX1/2, ADAR, IFI6, IFIT1/3/27, ISG15/20, TREX1, RNASEL, IFITM1/3, BST2, GPB1/3, TRIM22/25/34/56, most of which have been previously described as ISGs involved in interferon and antiviral signaling and ISGylation processes (Querec *et al.*, 2009; Schoggins and Rice, 2011). Previous studies have shown that IFITM2/3 can impede viral binding, entry, and uncoating, exhibiting antiviral properties against flaviviruses including WNV and DENV (Jiang *et al.*, 2010). Schoggins et al. demonstrated variability in the specificity of ISGs showing YF-specific inhibition of viral replication by IFI6 and TREX1 and demonstrated a broader range of antiviral effects of e.g. IFITM3 (Schoggins *et al.*, 2011). Furthermore, ISG15 has been shown to be essential in ISGylation processes necessary for RLR signaling activity (Diamond and Kanneganti, 2022). Many of these upregulated genes are also part of the *negative regulation of viral replication pathway* including RSAD2, EIF2AK2, MX1, IFIT1/5, OAS1/3, OASL, RANSEL, ISG15/20.

In addition, our analysis inferred an upregulation of the transcription factors STAT1, STAT2, IRF1, and IRF9, which together with IFN receptors (IFNAR and IFNGR) expression confirms the upregulation of type I and II IFN pathways, which, in turn, activates ISGs post-vaccination. Additionally, the 'defense response to virus' cluster has pointed to the importance of CXCL10 and CXCL9 in antiviral function which plays a critical role in the response to various pathogens (Liu *et al.*, 2011).

Moreover, genes shared between IFN modules and antigen processing, and presentation were predominantly HLA and B2M genes, integral for antigen processing and critical for adaptive immunity activation. The analysis also revealed the activation of pathways involved in adaptive immunity including positive regulation of B cell-mediated immunity and T cell-mediated cytotoxicity (but due to our method we are restricted to pathways that exist in monocytes: the identified genes can also only be ligands for receptors on B and T cells or receptors for ligands on T and B cells).

The Reactome analysis identified an interesting cluster of genes, including the Siglec family, CLEC2B, and CD40 in the 'immunoregulatory interactions between lymphoid and non-lymphoid' module that interact with IFNs and antigen processing clusters. SIGLEC1/CD169, a cell adhesion, type I IFN stimulated molecule, expressed on DCs, macrophages, and monocytes facilitating lymphocyte binding, emerged as one of the most upregulated genes and has previously been shown to induce effector and memory CD8$^+$ T cell response (van Dinther *et al.*, 2018). CLEC2B encodes a C-type lectin member, and while its precise function remains unclear, another member of this family, CLEC5A, expressed in myeloid cells, has been linked to binding DENV and activating the inflammatory response. The study has found an increase in activated monocytes expressing CLEC5B$^+$ after YF17D vaccination, which correlated with later responses of CD4$^+$ and CD8$^+$ T cells. Additionally, CLEC5B expression was shown to be positively correlated with CXCL10 chemokine and IL-6 cytokine expression, as well as with IFN-γ pathways, (Azamor *et al.*, 2021). Additionally, CD40, a member of the tumor necrosis factor receptor family, expressed on APC cells was identified in this cluster. CD40 serves as the co-stimulatory molecule that interacts with the CD40 ligand (CD40L) on T cells. The CD40 signaling activation results in cytokine and IFN-γ production and the upregulation of MHC II expression leading to the enhancement of T cell -and B cell-mediated immunity (Rogers *et al.*, 2021).

The activation of this cluster of genes suggests their involvement in the interactions between and regulation of adaptive immune cells by myeloid cells, highlighting the interplay between innate and adaptive immunity necessary for establishing strong

immune protection. Moreover, our findings show the pivotal role of IFNs in the antiviral immune response, and the significance of IFN-γ and type I IFN in enhancing MHC expression (HLA, B2M, TAP genes) and antigen presentation. Previous studies have demonstrated that the SARS-CoV-2 infection significantly reduces MHC class I genes HLA-A/B/C and B2M by up to 66%, indicating viral targeting of the MHC class I pathway through STAT1-IRF1 signaling by an escape mechanism of SARS-Cov-2 (Yoo *et al.*, 2021). Similarly, the downregulation of IFN-γ-stimulated B2M, HLA class I, and II genes, was observed in mild but particularly in ICU-bound patients with severe outcomes, suggesting a crucial role for IFN-γ in immune response modulation. Additionally, the same study has shown that an early transient IFN type I response is beneficial, whereas prolonged activation can lead to hyper-inflammation in COVID-19 patients (Kim *et al.*, 2021). The study by Arunachalam et al. showed reduced HLA-DR expression but also a lack of type I IFNs in severe COVID-19 patients (Arunachalam *et al.*, 2020). Several pathogenic flaviviruses, such as dengue virus (DENV), West Nile virus (WNV), and hepatitis C virus (HCV), have been reported to employ strategies to target and evade the host interferon (IFN) response (Jones *et al.*, 2005; Keller *et al.*, 2006; Loo *et al.*, 2006; Muñoz-Jordán and Fredericksen, 2010). In contrast, infection with the live-attenuated yellow fever vaccine strain YF17D is less effective in downregulating IFN signaling pathways (Querec *et al.*, 2006).

Collectively, the presented data show that an early and balanced IFN response elicited by YF17D appears to be critical for its effective immune stimulation and antigen presentation. The transient type I and II IFN upregulation are thereby necessary for establishing the antiviral immune response. Furthermore, the stimulation of interferons plays a pivotal role in enhancing MHC class I and II presentation through STAT1, ultimately activating CD4+ and CD8+ T cells. This cascade of events further enhances antibody production.

5.5 Intrinsic and non-genetic factors influence the variability early in the immune response

Differences between sexes, along with other baseline characteristics, have been demonstrated to be associated with variations in susceptibilities to viral infections and immune responses (Klein and Flanagan, 2016).

This data revealed that cytokine levels are influenced by intrinsic factors such as sex and seasonality, as reported previously (Furman *et al.*, 2014; Brodin *et al.*, 2015; Klein and Flanagan, 2016). Regarding sex-based differences, the findings indicate that males exhibit elevated levels of pro-inflammatory cytokines—such as APRIL, Eotaxin, TNF-α, MIF, MIP1a, and MCP1—compared to females on day 7 pv. Additionally, males show up-regulated levels of most of these cytokines already at baseline. This observation aligns with other studies that have demonstrated increased production of monocyte-derived pro-inflammatory cytokines (IL-1b, TNF-α, IL-6) in males after *in vitro* stimulation (Swertz *et al.*, 2016) or elevated levels of circulating cytokines, including TNF-α, in COVID-19 male patients, associated with higher severity and mortality in this group (Hu *et al.*, 2022). Additionally, a higher expression of inflammatory cytokines in males infected with SARS-CoV-2 at baseline was described by Liu et al.,(2020).

The effect of BMI was also investigated in this study; however, we have not detected any influence of BMI on cytokine levels. Other studies have reported associations of BMI with pro-inflammatory cytokines and induced inflammation (Swertz *et al.*, 2016; Dragon-Durey *et al.*, 2021). However, we cannot exclude the potential effect of BMI due to the homogeneity of BMI data, in our cohort where most individuals fall within the normal range of BMI. Similarly, we did not observe any impact of age, which is most likely attributed to the homogenous young age of the study subjects. Additionally, apart from sex-based differences, the results indicate a seasonal pattern in the production of several cytokines. APRIL, BAFF, CCL22, CXCL11, Eotaxin, IL-18, IL1ra, CXCL10, MCP1, MIF, MIG, MIP1a, RANTES, and TNF-α showed increased levels primarily in the spring and summer already at baseline and on day 7 pv. This trend aligns with other research indicating an upregulation of pro-inflammatory cytokines during the summer months (Swertz *et al.*, 2016).

Furthermore, in this study, I sought to find differences in the transcriptomic response between individuals. The analysis revealed a minimal influence of sex on the transcriptomic response. A disparity in the number of differentially expressed genes was observed between females and males, with females exhibiting a greater number of DEGs by 1846. This aligns with findings by Klein et al. who also noted an increased number of DEGs, particularly involved in innate and interferon signaling, among females after YF17D vaccination (Klein *et al.*, 2010). Similarly, Liu et al. reported upregulated IFN gene expression in COVID-19 females. (Liu *et al.*, 2020). However, Takahashi et al. found no

variation in protein levels of type I, II, and III IFN between sexes (Takahashi *et al.*, 2020).In this study, differences in the IFN expression were not observed. The alterations in antiviral signaling, particularly the total number of DEGs and the upregulation of the JAK-STAT3 pathway, can be attributed to the disparity in the number of recruited males and females, with the latter group being significantly more numerous. Although both groups exhibited the upregulation of IFN signaling, however expression of IFN genes, or their protein levels in plasma could not be measured in our study.

5.6 Association of early and late immune responses

5.6.1 Differences in transcriptional profiles does not explain the variability in the adaptive response

In order to comprehensively examine differences between individuals in terms of gene expression, a transcriptional expression profile was created using Hallmarks GSEA, distinguishing three endotypes – high inflam., low inflam., and moderate inflam. - based on the baseline expression status. The investigation aimed to assess whether the differences in expression between the endotypes observed at baseline before the vaccination were associated with changes in the immune response and protection. The defined endotypes exhibited slight differences in neutralizing antibody levels and CD8+ T cell responses; however, these differences were not statistically significant.

Fourati et al. identified three profiles of gene expression by analyzing data from 820 participants across multiple studies vaccinated with 13 different vaccines. The high-inflammatory endotype exhibited the upregulation of similar pathways, including 'TNFA_SIGNALLING_VIA_NFKB', 'IL6_JAK_STAT3', complement, and inflammatory response. The inflammatory low endotype showed downregulation of pro-inflammatory pathways and activation of 'MYC_TARGETS' and 'E2F_TARGETS' signaling, similar to what was observed in our YF cohort. Our study found that these groups did not differ in terms of neutralization or T-cell responses to YF17D, whereas Fourati et al.'s study detected differences in the CD4+ Th2 responses, showing the induction of Th2 cells in the pro-inflammatory endotype (Fourati *et al.*, 2022).

The clustering performed revealed that only sex has a slight impact on basal gene expression, with females tending to cluster in the 'high inflam. endotype'. The data collectively show that females exhibit a higher basal innate and inflammatory gene expression, while males have a greater upregulation of basal pro-inflammatory cytokine levels. However, these basal transcriptomic differences in monocytes do not influence the immune response, like we did not find sex differences to impact the development of neutralizing antibody levels.

Moreover, all individuals in our study exhibit down-regulation at baseline and strong up-regulation of type I and type II IFN signatures on day 7 post-vaccination, a pattern that was not observed in the Fourati study. The authors observed differences between endotypes in terms of the inflammatory response, as well as in IFN pathways, with some individuals in the high inflammatory group exhibiting the upregulation of baseline expression of type I IFN signatures. The study used published data from 13 different vaccine studies and the observed differences might have arisen due to the high variability of the data set and potential batch effects that had not been completely removed or potentially, since some of these individuals might have had some upregulation of IFN signatures before vaccination. It would be interesting to investigate if the observed IFN patterns on the transcriptomic level pv correspond to IFN plasma or serum levels across individuals after YF17D vaccination, considering the differences between the sexes and defined endotypes. Previous research has shown that mRNA levels of cytokines often do not correlate with protein levels due to post-transcriptional modifications and cytokine secretion remodeling (Anderson, 2008).

Collectively, the results show differences in baseline gene expression across individuals, however, these differences did not influence the vaccination outcome in our study.

5.6.2 Baseline expression of WGCNA-identified modules correlates with the late immune response

To comprehensively characterize the baseline status of vaccinees, we conducted a WGCNA analysis. This analysis revealed two interesting gene modules correlating with antibody and T-cell responses. The green module showed a weak correlation with neutralizing antibodies, while the brown module correlated with antigen-specific CD8^{+} T

cell levels. Interestingly, both the green and brown modules included many members of the solute carrier (SLC) gene family. SLCs, encoding transporters of endogenous and exogenous compounds, consist of more than 400 members that can influence viral infection and entry (Schaller and Lauschke, 2019). Querec et al. correlated early expression (3 and 7 days after vaccination) of the SLC2A6 (a sugar transporter) gene with late CD8$^+$ T cell response to YF17D. Additionally, the study found an association of the number of virus-specific CD8$^+$ T cells with other SLC members, including SLC16A5, SLC25A13, and SLC39A11 (Querec *et al.*, 2009). These results underscore the importance of SLCs in regulating broad adaptive immunity.

The most significant gene associated with the green module was SLC35A1. Knocking out SLC35A1, a sialic acid transporter, resulted in increased infectivity and apoptosis following VSV infection, as demonstrated by Moskovskich et al. (Moskovskich *et al.*, 2019). SLC35A1 was not directly associated with influenza virus infection; however, it might indirectly influence host-virus interactions. Sialic acids, present on glycoproteins and glycolipids of cell surfaces, serve as attachment receptors for influenza, mediating viral cell entry. However, the mechanism of involvement of solute carriers, especially SLC35A1, in viral infections remains elusive (Gillespie *et al.*, 2016; Moskovskich *et al.*, 2019). Additionally, the TNFRSF12A gene was associated with this module. Previous research has correlated the expression of another member of this superfamily, TNFRSF17, a TNF receptor superfamily recognizing B-cell activating factor (BAFF), with antibody responses (Querec *et al.*, 2009). The TNFRSF12A gene is involved in apoptotic signaling and was found to be upregulated in influenza-infected mice but not in SARS-CoV-2 -infected mice, however, its function is not well understood in the context of antiviral immunity (Wang *et al.*, 2023). In addition, the baseline expression of aldehyde dehydrogenase 7 family, member A1 (ALDH7A1), an enzyme metabolizing aldehydes was also correlated with this module. Previous studies have identified other members of this family, such as ALDH16A1 and ALDH3B1, as being associated with CD8$^+$ T cells highlighting the involvement of this family in immune regulation (Querec *et al.*, 2009).

The brown module exhibited a mild correlation with CD8$^+$ T cell responses, with GLUL emerging as the most significantly associated gene, belonging to the glutamine synthetase family. Previous research has identified a co-expression of ACE2 with GLUL and SLC6A14, indicating a correlation between ACE2 expression and elevated levels of glutamine associated with GLUL expression (Stewart *et al.*, 2020). Moreover, the solute

carrier genes were also found within the brown module, one of the most associated was the SLC15A4 gene, which is an endolysosome resident, peptide transporter linked to inflammation and autoimmune diseases (Zhang *et al.*, 2023). SLC15A4 is expressed in immune cells and was found to be involved in the trafficking and co-localization of TLRs and ligands to endosomes (Rimann *et al.*, 2022). Additionally, the brown module encompassed family with sequence similarity 225 member B (FAM225B), neuraminidase 4 (NEU4), and translation initiation factor 1A domain containing (EIF1AD) are involved in the regulation of protein synthesis. The early expression of EIF2AK, another member of this family, was correlated with the abundance of YF17D-specific CD8$^+$ T cells (Querec et al., 2009). Furthermore, the baseline expression of molecules including, CD48 involved in adhesion and activation on antigen-presenting cells (APCs) and T cells (McArdela *et al.*, 2019), CD86 – an activation marker and co-stimulatory molecule in APCs (Banchereau and Steinman, 1998), and MHC class II genes (HLA-DRA, HLA-DPA), alongside with CLEC7A expressed on myeloid cells, was associated with this module and its correlation to in YF17D specific CD8+ T cell response development.

These results demonstrate that baseline co-expression of genes from the green and brown modules correlate with later responses. On day 7, the genes that were weakly associated with neutralization were antiviral genes and ISGs, which were activated upon infection, while baseline genes found to be involved in shaping immunity were not well-known in the context of viral infections. Interestingly, we found genes encoding many cell-adhesion molecules, as well as genes related to the processing and recognition of sialic acids, including SLC35A1, NEU4, along with various members of solute carrier transporters, or enzymes including aldehyde dehydrogenase, and glutamine synthetase. Additionally, SIGLEC-1, a member of the Siglec family that contributes to pathogen uptake and presentation was the second most DE gene post-vaccination (Varki and Angata, 2006).

This collectively suggests that pre-vaccination signatures are associated with the activation of later adaptive immunity after YF17D vaccination.

5.6.3 Baseline transcriptional gene signatures associate with the magnitude of the immune response

To investigate the transcriptional differences between high and low responders, a differential gene expression analysis was performed between those groups. Although results were not statistically significant, the data suggested differences in the expression of several genes both at baseline and on day 7 post-vaccination.

Interestingly, the top variable gene -NEU4 was associated with the WGCNA-brown gene expression module at baseline that correlated with CD8+ T cell responses. NEU4, located on chromosome 2 is a human neuraminidase enzyme also known as sialidase responsible for hydrolyzing sialic acid residues from glycoproteins and glycolipids. Although its function is not well understood, NEU4 has been reported to be involved in various processes, including apoptosis, inflammation, and lysosomal storage disorders (Okun *et al.*, 2023) as well was found to be the most significant eQTL after LPS stimulation of monocytes (Kim *et al.*, 2014). Additionally, NEU1, another member of neuraminidases, located on chromosome 6 within the MHC locus, has been found to be involved in immune response regulation and modulation of inflammation (Pshezhetsky and Hinek, 2011). Recently, it has been implicated in the activation of TLRs (Amith *et al.*, 2010). This data shows that human NEU4 baseline expression is downregulated in high responders compared to low responders, suggesting its role in modulating immunity across individuals.

Post-vaccination, the detected DEGs included CD200R1, ALDH7A1, and FAM225B, which, interestingly, were also part of the green module that correlated with neutralization. All of them showed upregulation on day 7 pv in high responders as compared with the low responders. CD200R1 is an immunomodulatory receptor that regulates pro-inflammatory cytokines (Vaine and Soberman, 2014). The dysfunction of ALDH7A1 has been associated with osteoporosis and Huntington's disease (Lu *et al.*, 2022) whereas FAM225B, a long non-coding RNA, was differentially expressed in asthmatic patients inoculated with the Rhinovirus (HRV). Another member of this family, FAM225A, was found to be differentially expressed in response to live influenza vaccination, whereas, the expression of yet another member-FAM30A was correlated with the antibody response (de Lima *et al.*, 2019). However, beyond these observations, the function of these genes is not well characterized, nor has their involvement in antiviral immunity been confirmed.

These data demonstrate the potential for these transcriptional signatures to predict vaccine immunogenicity allowing for the identification of high and low responders before vaccination.

5.6.4 Type II IFN signaling is associated with neutralization

Strikingly, the WGCNA-green module revealed enrichment in the IFN-γ signaling and antigen presentation pathways. While the result was not statistically significant, it suggests IFN-γ as a pivotal component in establishing the adaptive immune response. Li et al. observed a correlation between elevated antibody responses and the activation of type I interferon and cell-adhesion modules post-YF17D vaccination (Li *et al.*, 2014). It has been previously shown that YF17D activates robust type I IFN in pDCs (Querec *et al.*, 2006). In addition, the COVID-19 study by Edahiro et al. highlighted the role of INF-γ-mediated response in disease progression. Reduced expression of the IFN-γ response signatures, along with downregulation of the chemokine CXCL10 correlated with disease severity (Edahiro *et al.*, 2023). Furthermore, Saichi et al. observed upregulated inflammatory pathways, such as hypoxia and TNF signaling, and diminished interferon (IFN) signatures in severe COVID-19 cases. This dysregulated immune response leads to ineffective viral control due to compromised IFN-mediated antiviral mechanisms, while simultaneously driving excessive inflammatory reactions contributing to immunopathology (Saichi *et al.*, 2021).

Interestingly, this study observed the expression of many cell-adhesion molecules in monocytes, reinforcing T-cell activation. It also highlights the upregulation of both type I and II IFNs, suggesting their involvement in antiviral immunity but also in generating potent antibody responses through antigen processing and presentation, cell adhesion processes, chemokine, and cytokine secretion, as well as Tfh-cell responses. Although this study, along with others using human models, couldn't detect IFN levels in serum or plasma, other studies using murine models emphasized the importance of early IFN-γ (1-day pv) in eliciting high-quality adaptive responses to YF17D (Neves *et al.*, 2013) and in controlling the YFV vaccine strain infection (Lam *et al.*, 2018). Interestingly, IFN-γ restriction in the absence of type I IFN was limited to the attenuated YF17D strain, whereas the wild-type strain was not sensitive to IFN-γ, suggesting that the mechanism of attenuation increases sensitivity to IFN-γ (Lam *et al.*, 2018).

These results underscore the importance of IFN-γ as a critical mediator of early antiviral immunity, as well as highlight the necessity of early balanced type I and II IFN responses.

5.7 Genetics moderately influenced the studied quantitative traits and gene expression

It has been demonstrated that genetic factors can influence susceptibility to viral infections and vaccination, and the heritability between vaccines differs significantly, ranging from around 80% for measles to 39% for mumps in children to almost zero for the seasonal vaccination to influenza in elderly adults (Brodin *et al.*, 2015).

To investigate whether genetic factors influence immune responses, including cytokine production, antibodies, and APC levels, a QTL analysis was conducted. This study unveiled high interindividual differences in cytokine levels, including CCL22, CXCL11, CXCL13, PDGFbb, and RANTES. While two genetic loci were associated with cytokine levels—one on chromosome 1 in an intergenic region for CCL22 and another in the FOSL2 gene linked to CXCL11 cytokine levels on day 7—these findings suggest a limited genetic contribution. Existing research indicates that only 25% of immunological traits, such as cytokines, are heritable and attributable to genetic factors (Brodin *et al.*, 2015). FOSL2 is a member of the AP-1 transcription factor complex that plays an essential role in cell proliferation, differentiation, and apoptosis. Other studies have implicated it in regulating autoimmunity, and it has been demonstrated that the deregulation of its expression can lead to various disorders, including cancer, asthma, and rheumatoid diseases (Renoux *et al.*, 2020). Its role in antiviral immunity is not well understood. Recently, AP-1 was shown to be involved in TIV influenza (Wimmers *et al.*, 2021) and mRNA COVID-19 vaccination (Arunachalam *et al.*, 2021). Epigenetic changes in the AP-1 locus were associated with a reduction of its expression leading to elevated expression levels of IFN and antiviral signaling in myeloid cells. However, both vaccines for which this was reported are non-live. It would be intriguing to investigate the epigenetic changes induced by YF17D, particularly considering the association of the FOL2 gene with the WGCNA-green module associated with IFN-γ signaling and antigen presentation pathways, as demonstrated earlier in this study. Furthermore, cells lacking FOSL2 exhibited a higher induction of CXCL10 and IFN-β after infection with YF17D, suggesting a potential link between AP-1 member, FOSL2 and the immune response to live vaccines.

No QTLs associated with antibody and APC levels were identified; however, an interesting variant in the DTX1 locus appeared to affect monocytes expressing SIGLEC1^{+}. The DTX1 gene is highly expressed in germinal center B cells (Kizhakeyil *et al.*, 2022). Recently, a GWAS has implicated the cis-regulatory region near the OAS locus which has been identified as a severe disease risk locus indirectly interacting with the promoter of the DTX1 locus (Schmiedel *et al.*, 2021).

To identify genetic effects on the modulation of transcriptional response upon YF17D infection, cis-eQTL mapping was performed. The most significant res-eQTL, GRPEL2, is a gene involved in mitochondrial protein import and along with GRPEL1, has been found to be responsible for stress modulation (Srivastava *et al.*, 2017). Interestingly, another study has shown GRPEL1's involvement in the dengue virus replication processes. Gandikota et al. demonstrated that the dengue virus interacts with GRPEL1, cleaving it and reducing its levels, especially in severe dengue-infected samples (Gandikota *et al.*, 2020). The second most significant res-eQTL, EIF2B4, is a stress response gene belonging to the eukaryotic translation initiation factor family (Sidrauski *et al.*, 2015). This study has shown the association of other genes in this family with the immune response to YF17D vaccination. The analysis also identified several loci associated with innate immunity genes including RIG-I, IFI44L, TRIM5 - interferon-stimulated genes, chemokines, and cytokines: CCL20, IL4l1 as well as the chemokine receptor CCR1. All of these genes were differentially expressed post-vaccination, with IFI44L being the most significant DEG, while RIG-I has been found to be a primary sensor of YF17D. Other studies have found an association between polymorphisms in RIG-I, TRIM5, and IFI44L, and interindividual antibody levels in response to Rubella and MMR vaccines(Ovsyannikova *et al.*, 2015; Haralambieva *et al.*, 2018).

These data demonstrate the crucial role of these genes in modulating the immune response to virus infections and the contribution of genetic variants within these loci to interindividual variability in the immune response.

While several previous studies have investigated the host response to viruses or vaccines, such as the live-attenuated yellow fever vaccine strain YF17D, using peripheral blood mononuclear cells (PBMCs) (Querec *et al.*, 2009; Hou *et al.*, 2017), and whole blood samples (Gaucher *et al.*, 2008), our study focuses specifically on monocytes. This choice is motivated by the observation that YF17D can infect myeloid cells, including

monocytes, which exhibit substantial transcriptional changes upon infection, as supported by our findings and other studies (Lee *et al.*, 2022). By leveraging bulk RNA-seq and eQTL analysis in primary monocytes, we aim to uncover unique transcriptional signatures and regulatory networks governing the monocyte-specific antiviral response. Moreover, the use of purified monocytes eliminates potential biases arising from other cell types present in heterogeneous samples; however, cell-cell interactions could not be analyzed in this study.

6.   Summary and Outlook

This project provides a comprehensive overview of the immune response to YF17D vaccination. The YF17D vaccine strain, derived from the wild-type virus, is widely used to prevent yellow fever and to this very day, it is one of the most effective vaccines ever developed. However, despite its efficacy, the precise mechanisms underlying its effectiveness remain poorly understood. The live-attenuated YF17D vaccine is a safe viral infection model that can be used in the human system, providing insights into human antiviral immune responses.

The key findings of this study are:

- RLR and MAVS signaling predominantly control the IFN-mediated restriction of YF17D, with RIG-I playing a significant role in viral sensing.

- The YF17D vaccine elicits a robust and transient early cytokine and transcriptomic response, particularly associated with antiviral and interferon pathways. The vaccination activates multiple pathways including pathways functional modules categorized as defense responses to viruses, type I and II IFN responses, antigen processing and presentation, and interaction of lymphoid and myeloid cells. The study underscores the pivotal role of interferons in the early immune response and emphasizes the interplay between innate and adaptive immunity.

- The influence of intrinsic and non-genetic factors on immune traits is low and only at baseline status. However, these differences did not significantly impact the immune response.

- Baseline expression status of specific coregulated gene modules was found to weakly correlate with the immunogenicity of the vaccine (and has a potential to classify high and low responders).

- Genetics mildly influence the interindividual differences in the cytokine and transcriptomic responses.

Further research is essential to deepen our understanding of these findings. Particularly interesting is the validation of IFN levels in plasma or serum helping to disentangle the contribution of type I and type II interferons. This is important given that previous studies utilizing the YF17D virus model in human systems have not detected the expression of IFN-encoding genes or protein secretion. Interestingly, this study has revealed robust IFN-γ molecular signatures. It is noteworthy that previous reports have indicated that IFN-γ-mediated responses contribute to high vaccine immunogenicity and restrict viral replication in murine models (Neves *et al.*, 2013; Lam *et al.*, 2018). Delving deeper into this phenomenon could provide valuable insights, as IFN-γ appears to play a pivotal role in bridging innate and adaptive immunity.

Furthermore, additional investigation is necessary to explore the predictive molecular signatures identified in this study and validate them in an independent test set. While these genes have not been previously implicated in the context of antiviral immunity, they present intriguing candidates for biomarkers. This study underscores the complexity of the immune response, which is driven not by a single gene but by a multitude. This highlights the necessity for comprehensive and complex analysis in systems biology studies, as well as the development of models that can better capture the intricacies of immune responses.

7.   References

Aguet, F., Alasoo, K., Li, Y.I., Battle, A., Im, H.K., Montgomery, S.B., and Lappalainen, T. (2023) Molecular quantitative trait loci. *Nat. Rev. Methods Prim.* **3**:.

Aguet, F., Brown, A.A., Castel, S.E., Davis, J.R., He, Y., Jo, B., et al. (2017) Genetic effects on gene expression across human tissues. *Nature* **550**: 204–213.

Akondy, R.S., Johnson, P.L.F., Nakaya, H.I., Edupuganti, S., Mulligan, M.J., Lawson, B., et al. (2015) Initial viral load determines the magnitude of the human CD8 T cell response to yellow fever vaccination. *Proc. Natl. Acad. Sci. U. S. A.* **112**: 3050–3055.

Akondy, R.S., Monson, N.D., Miller, J.D., Edupuganti, S., Teuwen, D., Wu, H., et al. (2009) The Yellow Fever Virus Vaccine Induces a Broad and Polyfunctional Human Memory CD8+ T Cell Response. *J. Immunol.* **183**: 7919–7930.

Amith, S.R., Jayanth, P., Finlay, T., Franchuk, S., Gilmour, A., Abdulkhalek, S., and Szewczuk, M.R. (2010) Detection of Neu1 sialidase activity in regulating TOLL-like receptor activation. *J. Vis. Exp.* 24–26.

Anderson, P. (2008) Post-transcriptional control of cytokine production. *Nat. Immunol.* **9**: 353–359.

Arunachalam, P.S., Scott, M.K.D., Hagan, T., Li, C., Feng, Y., Wimmers, F., et al. (2021) Systems vaccinology of the BNT162b2 mRNA vaccine in humans. *Nature* **596**: 410–416.

Arunachalam, P.S., Wimmers, F., Mok, C.K.P., Perera, R.A.P.M., Scott, M., Hagan, T., et al. (2020) Systems biological assessment of immunity to mild versus severe COVID-19 infection in humans. *Science (80-.).* **369**: 1210–1220.

Azamor, T., da Silva, A.M.V., Melgaço, J.G., Dos Santos, A.P., Xavier-Carvalho, C., Alvarado-Arnez, L.E., et al. (2021) Activation of an effective immune response after yellow fever vaccination is associated with the genetic background and early response of ifn-γ and clec5a. *Viruses* **13**: 1–12.

Badia-I-Mompel, P., Vélez Santiago, J., Braunger, J., Geiss, C., Dimitrov, D., Müller-Dott, S., et al. (2022) decoupleR: ensemble of computational methods to infer

biological activities from omics data. *Bioinforma. Adv.* **2**: 1–3.

Banchereau, J. and Steinman, R.M. (1998) Dendritic cells and the control of immunity. *Nature* **392**: 245–252.

Barba-Spaeth, G., Longman, R.S., Albert, M.L., and Rice, C.M. (2005a) Live attenuated yellow fever 17D infects human DCs and allows for presentation of endogenous and recombinant T cell epitopes. *J. Exp. Med.* **202**: 1179–1184.

Barba-Spaeth, G., Longman, R.S., Albert, M.L., and Rice, C.M. (2005b) Live attenuated yellow fever 17D infects human DCs and allows for presentation of endogenous and recombinant T cell epitopes. *J. Exp. Med.* **202**: 1179–1184.

Bidet, K., Ho, V., Chu, C.W., Naim, A.N.H., Thazin, K., Chan, K.R., et al. (2019) Mimicking immune signatures of flavivirus infection with targeted adjuvants improves dengue subunit vaccine immunogenicity. *npj Vaccines* **4**:.

Boehmer, D.F.R., Formisano, S., de Oliveira Mann, C.C., Mueller, S.A., Kluge, M., Metzger, P., et al. (2021) OAS1/RNase L executes RIG-I ligand–dependent tumor cell apoptosis. *Sci. Immunol.* **6**: 1–15.

Bonaguro, L., Schulte-Schrepping, J., Ulas, T., Aschenbrenner, A.C., Beyer, M., and Schultze, J.L. (2022) A guide to systems-level immunomics. *Nat. Immunol.* **23**:.

Bookchin, D. and Schumacher, J. (2000) The Virus and the Vaccine. *Atl.* **10**: 94–98.

Brodin, P. and Davis, M.M. (2017) Human immune system variation. *Nat. Rev. Immunol.* **17**: 21–29.

Brodin, P., Jojic, V., Gao, T., Bhattacharya, S., Angel, C.J.L., Furman, D., et al. (2015) Variation in the human immune system is largely driven by non-heritable influences. *Cell* **160**: 37–47.

Bruni, D., Chazal, M., Sinigaglia, L., Chauveau, L., Schwartz, O., Desprès, P., and Jouvenet, N. (2015) Viral entry route determines how human plasmacytoid dendritic cells produce type i interferons. *Sci. Signal.* **8**: ra25.

Bruns, A.M. and Horvath, C.M. (2012) Activation of RIG-I-like receptor signal transduction. *Crit. Rev. Biochem. Mol. Biol.* **47**: 194–206.

Bruns, A.M., Leser, G.P., Lamb, R.A., and Horvath, C.M. (2014) The Innate Immune Sensor LGP2 Activates Antiviral Signaling by Regulating MDA5-RNA Interaction and Filament Assembly. *Mol. Cell* **55**: 771–781.

Bryant, J.E., Vasconcelos, P.F.C., Rijnbrand, R.C.A., Mutebi, J.P., Higgs, S., and Barrett, A.D.T. (2005) Size Heterogeneity in the 3' Noncoding Region of South American Isolates of Yellow Fever Virus. *J. Virol.* **79**: 3807–3821.

Cano-Gamez, E. and Trynka, G. (2020) From GWAS to Function: Using Functional Genomics to Identify the Mechanisms Underlying Complex Diseases. *Front. Genet.* **11**: 1–21.

Chan, C.P. and Jin, D.Y. (2022) Cytoplasmic RNA sensors and their interplay with RNA-binding partners in innate antiviral response: theme and variations. *Rna* **28**: 449–477.

Chan, Y.K. and Gack, M.U. (2016) Viral evasion of intracellular DNA and RNA sensing. *Nat. Rev. Microbiol.* **14**: 360–373.

Chathuranga, K., Weerawardhana, A., Dodantenna, N., and Lee, J.S. (2021) Regulation of antiviral innate immune signaling and viral evasion following viral genome sensing. *Exp. Mol. Med.* **53**: 1647–1668.

Chiang, J.J., Davis, M.E., and Gack, M.U. (2014) Regulation of RIG-I-like receptor signaling by host and viral proteins. *Cytokine Growth Factor Rev.* **25**: 491–505.

Chow, K.T., Gale, M., and Loo, Y.M. (2018) RIG-I and Other RNA Sensors in Antiviral Immunity. *Annu. Rev. Immunol.* **36**: 667–694.

Das, S., Abecasis, G.R., and Browning, B.L. (2018) Genotype imputation from large reference panels. *Annu. Rev. Genomics Hum. Genet.* **19**: 73–96.

Davis, M.M., Tato, C.M., and Furman, D. (2017) Systems immunology: Just getting started. *Nat. Immunol.* **18**: 725–732.

Diamond, M.S. and Kanneganti, T.D. (2022) Innate immunity: the first line of defense against SARS-CoV-2. *Nat. Immunol.* **23**: 165–176.

van Dinther, D., Veninga, H., Iborra, S., Borg, E.G.F., Hoogterp, L., Olesek, K., et al. (2018) Functional CD169 on Macrophages Mediates Interaction with Dendritic Cells for CD8 + T Cell Cross-Priming. *Cell Rep.* **22**: 1484–1495.

Dragon-Durey, M.A., Chen, X., Kirilovsky, A., Hamouda, N. Ben, Sissy, C. El, Russick, J., et al. (2021) Differential association between inflammatory cytokines and multiorgan dysfunction in COVID-19 patients with obesity. *PLoS One* **16**: 1–20.

Edahiro, R., Shirai, Y., Takeshima, Y., Sakakibara, S., Yamaguchi, Y., Murakami, T., et al. (2023) Single-cell analyses and host genetics highlight the role of innate immune cells in COVID-19 severity. *Nat. Genet.* **55**: 753–767.

Errett, J.S., Suthar, M.S., McMillan, A., Diamond, M.S., and Gale, M. (2013) The Essential, Nonredundant Roles of RIG-I and MDA5 in Detecting and Controlling West Nile Virus Infection. *J. Virol.* **87**: 11416–11425.

Fairfax, B.P., Humburg, P., Makino, S., Naranbhai, V., Wong, D., Lau, E., et al. (2014) Innate immune activity conditions the effect of regulatory variants upon monocyte gene expression. *Science (80-.).* **343**:.

Fairfax, B.P. and Knight, J.C. (2014) Genetics of gene expression in immunity to infection. *Curr. Opin. Immunol.* **30**: 63–71.

Flynn, E.D. and Lappalainen, T. (2022) Functional Characterization of Genetic Variant Effects on Expression. *Annu. Rev. Biomed. Data Sci.* **5**: 119–139.

Forlin, R., James, A., and Brodin, P. (2023) Making human immune systems more interpretable through systems immunology. *Trends Immunol.* **44**: 577–584.

Fourati, S., Tomalin, L.E., Mulè, M.P., Chawla, D.G., Gerritsen, B., Rychkov, D., et al. (2022) Pan-vaccine analysis reveals innate immune endotypes predictive of antibody responses to vaccination. *Nat. Immunol.*

Franco, L.M., Bucasas, K.L., Wells, J.M., Niño, D., Wang, X., Zapata, G.E., et al. (2013) Integrative genomic analysis of the human immune response to influenza vaccination. *Elife* **2**: 1–18.

Furman, D., Hejblum, B.P., Simon, N., Jojic, V., Dekker, C.L., Thiebaut, R., et al. (2014) Systems analysis of sex differences reveals an immunosuppressive role for testosterone in the response to influenza vaccination. *Proc. Natl. Acad. Sci. U. S. A.* **111**: 869–874.

Gandikota, C., Mohammed, F., Gandhi, L., Maisnam, D., Mattam, U., Rathore, D., et al. (2020) Mitochondrial Import of Dengue Virus NS3 Protease and Cleavage of GrpEL1, a Cochaperone of Mitochondrial Hsp70. **70**:.

Gaucher, D., Therrien, R., Kettaf, N., Angermann, B.R., Boucher, G., Filali-Mouhim, A., et al. (2008) Yellow fever vaccine induces integrated multilineage and polyfunctional immune responses. *J. Exp. Med.* **205**: 3119–3131.

Gilad, Y., Rifkin, S.A., and Pritchard, J.K. (2008) Revealing the architecture of gene regulation: the promise of eQTL studies. *Trends Genet.* **24**: 408–415.

Gillespie, L., Roosendahl, P., Ng, W.C., Brooks, A.G., Reading, P.C., and Londrigan, S.L. (2016) Endocytic function is critical for influenza A virus infection via DC-SIGN and L-SIGN. *Sci. Rep.* **6**: 1–11.

González-Navajas, J.M., Lee, J., David, M., and Raz, E. (2012) Immunomodulatory functions of type i interferons. *Nat. Rev. Immunol.* **12**: 125–135.

Goubau, D., Deddouche, S., and Reis e Sousa, C. (2013) Cytosolic Sensing of Viruses. *Immunity* **38**: 855–869.

Goubau, D., Schlee, M., Deddouche, S., Pruijssers, A.J., Zillinger, T., Goldeck, M., et al. (2014) Antiviral immunity via RIG-I-mediated recognition of RNA bearing 59-diphosphates. *Nature* **514**: 372–375.

Gould, E.A. and Solomon, T. (2008) Pathogenic flaviviruses. *Lancet* **371**: 500–509.

Gu, Z. (2022) Complex heatmap visualization. *iMeta* **1**: 1–15.

Hagan, T., Gerritsen, B., Tomalin, L.E., Fourati, S., Mulè, M.P., Chawla, D.G., et al. (2022) Transcriptional atlas of the human immune response to 13 vaccines reveals a common predictor of vaccine-induced antibody responses. *Nat. Immunol.*

Hänzelmann, S., Castelo, R., and Guinney, J. (2013) GSVA: Gene set variation analysis for microarray and RNA-Seq data. *BMC Bioinformatics* **14**:.

Haralambieva, I.H., Ovsyannikova, I.G., Kennedy, R.B., Larrabee, B.R., Zimmermann, M.T., Grill, D.E., et al. (2018) Genome-Wide Associations of CD46 and IFI44L Genetic Variants with Neutralizing Antibody Response to Measles Vaccine. **136**: 421–435.

Heinz, F.X. and Stiasny, K. (2012) Flaviviruses and flavivirus vaccines. *Vaccine* **30**: 4301–4306.

Hornung, V., Ellegast, J., Kim, S., Brzózka, K., Jung, A., Kato, H., et al. (2006) 5′-Triphosphate RNA is the ligand for RIG-I. *Science (80-.).* **314**: 994–997.

Hou, F., Sun, L., Zheng, H., Skaug, B., Jiang, Q.X., and Chen, Z.J. (2011) MAVS forms functional prion-like aggregates to activate and propagate antiviral innate immune response. *Cell* **146**: 448–461.

Hou, J., Wang, S., Jia, M., Li, D., Liu, Y., Li, Z., et al. (2017) A Systems Vaccinology

Approach Reveals Temporal Transcriptomic Changes of Immune Responses to the Yellow Fever 17D Vaccine. *J. Immunol.* **199**: 1476–1489.

Hu, H., Pan, H., Li, R., He, K., Zhang, H., and Liu, L. (2022) Increased Circulating Cytokines Have a Role in COVID-19 Severity and Death With a More Pronounced Effect in Males: A Systematic Review and Meta-Analysis. *Front. Pharmacol.* **13**: 1–15.

Huber, J.E., Ahlfeld, J., Scheck, M.K., Zaucha, M., Witter, K., Lehmann, L., et al. (2020) Dynamic changes in circulating T follicular helper cell composition predict neutralising antibody responses after yellow fever vaccination. *Clin. Transl. Immunol.* **9**: 1–16.

Janeway, C.A. and Medzhitov, R. (2002) INNATE IMMUNE RECOGNITION. *Annu. Rev. Immunol.* **20**: 197–216.

Jiang, D., Weidner, J.M., Qing, M., Pan, X.-B., Guo, H., Xu, C., et al. (2010) Identification of Five Interferon-Induced Cellular Proteins That Inhibit West Nile Virus and Dengue Virus Infections. *J. Virol.* **84**: 8332–8341.

Jones, M., Davidson, A., Hibbert, L., Gruenwald, P., Schlaak, J., Ball, S., et al. (2005) Dengue Virus Inhibits Alpha Interferon Signaling by Reducing STAT2 Expression. *J. Virol.* **79**: 5414–5420.

Kato, H., Sato, S., Yoneyama, M., Yamamoto, M., Uematsu, S., Matsui, K., et al. (2005) Cell type-specific involvement of RIG-I in antiviral response. *Immunity* **23**: 19–28.

Kato, H., Takeuchi, O., Mikamo-Satoh, E., Hirai, R., Kawai, T., Matsushita, K., et al. (2008) Length-dependent recognition of double-stranded ribonucleic acids by retinoic acid-inducible gene-I and melanoma differentiation-associated gene 5. *J. Exp. Med.* **205**: 1601–1610.

Kato, H., Takeuchi, O., Sato, S., Yoneyama, M., Yamamoto, M., Matsui, K., et al. (2006) Differential roles of MDA5 and RIG-I helicases in the recognition of RNA viruses. *Nature* **441**: 101–105.

Kawai, T. and Akira, S. (2011) Toll-like Receptors and Their Crosstalk with Other Innate Receptors in Infection and Immunity. *Immunity* **34**: 637–650.

Kawai, T., Takahashi, K., Sato, S., Coban, C., Kumar, H., Kato, H., et al. (2005) IPS-1,

an adaptor triggering RIG-I- and Mda5-mediated type I interferon induction. *Nat. Immunol.* **6**: 981–988.

Keller, B.C., Fredericksen, B.L., Samuel, M.A., Mock, R.E., Mason, P.W., Diamond, M.S., and Gale, M. (2006) Resistance to Alpha/Beta Interferon Is a Determinant of West Nile Virus Replication Fitness and Virulence. *J. Virol.* **80**: 9424–9434.

Kim-Hellmuth, S., Bechheim, M., Pütz, B., Mohammadi, P., Nédélec, Y., Giangreco, N., et al. (2017) Genetic regulatory effects modified by immune activation contribute to autoimmune disease associations. *Nat. Commun.* **8**:.

Kim, M.H., Salloum, S., Wang, J.Y., Wong, L.P., Regan, J., Lefteri, K., et al. (2021) Type I, II, and III Interferon Signatures Correspond to Coronavirus Disease 2019 Severity. *J. Infect. Dis.* **224**: 777–782.

Kim, S., Becker, J., Bechheim, M., Kaiser, V., Noursadeghi, M., Fricker, N., et al. (2014) Characterizing the genetic basis of innate immune response in TLR4-activated human monocytes. *Nat. Commun.* **5**: 1–7.

Kizhakeyil, A., Ghosh, S., Rojas-Neira, E., Deng, Q., Henderson, J., Showell, J., et al. (2022) DTX1 Controls Germinal Center B-Cell Development and Lymphomagenesis. *Blood* **140**: 1700–1701.

Klein, S.L. and Flanagan, K.L. (2016) Sex differences in immune responses. *Nat. Rev. Immunol.* **16**: 626–638.

Klein, S.L., Jedlicka, A., and Pekosz, A. (2010) The Xs and Y of immune responses to viral vaccines. *Lancet Infect. Dis.* **10**: 338–349.

Kleinert, R.D.V., Montoya-Diaz, E., Khera, T., Welsch, K., Tegtmeyer, B., Hoehl, S., et al. (2019) Yellow fever: Integrating current knowledge with technological innovations to identify strategies for controlling a re-emerging virus. *Viruses* **11**:.

Kohler, S., Bethke, N., Böthe, M., Sommerick, S., Frentsch, M., Romagnani, C., et al. (2012) The early cellular signatures of protective immunity induced by live viral vaccination. *Eur. J. Immunol.* **42**: 2363–2373.

Kotliarov, Y., Sparks, R., Martins, A.J., Mulè, M.P., Lu, Y., Goswami, M., et al. (2020) Broad immune activation underlies shared set point signatures for vaccine responsiveness in healthy individuals and disease activity in patients with lupus. *Nat. Med.* **26**: 618–629.

Kowalinski, E., Lunardi, T., McCarthy, A.A., Louber, J., Brunel, J., Grigorov, B., et al. (2011) Structural basis for the activation of innate immune pattern-recognition receptor RIG-I by viral RNA. *Cell* **147**: 423–435.

Kumar, H., Kawai, T., and Akira, S. (2011) Pathogen recognition by the innate immune system. *Int. Rev. Immunol.* **30**: 16–34.

Lam, L.K.M., Watson, A.M., Ryman, K.D., and Klimstra, W.B. (2018) Gamma-interferon exerts a critical early restriction on replication and dissemination of yellow fever virus vaccine strain. *npj Vaccines* **3**: 1–10.

Langfelder, P. and Horvath, S. (2008) WGCNA: An R package for weighted correlation network analysis. *BMC Bioinformatics* **9**:.

Law, C.W., Chen, Y., Shi, W., and Smyth, G.K. (2014) Voom: Precision weights unlock linear model analysis tools for RNA-seq read counts. *Genome Biol.* **15**: 1–17.

Lee, A., Scott, M.K.D., Wimmers, F., Arunachalam, P.S., Luo, W., Fox, C.B., et al. (2022) A molecular atlas of innate immunity to adjuvanted and live attenuated vaccines, in mice. *Nat. Commun.* **13**: 1–13.

Li, C., Lee, A., Grigoryan, L., Arunachalam, P.S., Scott, M.K.D., Trisal, M., et al. (2022) Mechanisms of innate and adaptive immunity to the Pfizer-BioNTech BNT162b2 vaccine. *Nat. Immunol.*

Li, S., Rouphael, N., Duraisingham, S., Romero-Steiner, S., Presnell, S., Davis, C., et al. (2014) Molecular signatures of antibody responses derived from a systems biology study of five human vaccines. *Nat. Immunol.* **15**: 195–204.

de Lima, D.S., Cardozo, L.E., Maracaja-Coutinho, V., Suhrbier, A., Mane, K., Jeffries, D., et al. (2019) Long noncoding RNAs are involved in multiple immunological pathways in response to vaccination. *Proc. Natl. Acad. Sci. U. S. A.* **116**: 17121–17126.

Lindenbach, B.D., Thiel, H.-J., and Rice, C. (2007) Flaviviridae: the viruses and their replication. *Fields Virol.* 1101–1151.

Linnik, J.E. and Egli, A. (2016) Impact of host genetic polymorphisms on vaccine induced antibody response. *Hum. Vaccines Immunother.* **12**: 907–915.

Liu, M., Guo, S., Hibbert, J.M., Jain, V., Singh, N., Wilson, N.O., and Stiles, J.K.

(2011) CXCL10/IP-10 in infectious diseases pathogenesis and potential therapeutic implications. *Cytokine Growth Factor Rev.* **22**: 121–130.

Liu, S., Cai, X., Wu, J., Cong, Q., Chen, X., Li, T., et al. (2015) Phosphorylation of innate immune adaptor proteins MAVS, STING, and TRIF induces IRF3 activation. *Science (80-.).* **347**:.

Liu, S., Chen, J., Cai, X., Wu, J., Chen, X., Wu, Y.T., et al. (2013) MAVS recruits multiple ubiquitin E3 ligases to activate antiviral signaling cascades. *Elife* **2013**: 1–24.

Liu, T., Balzano-Nogueira, L., Lleo, A., and Conesa, A. (2020) Transcriptional differences for covid-19 disease map genes between males and females indicate a different basal immunophenotype relevant to the disease. *Genes (Basel).* **11**: 1–14.

Loo, Y.-M., Fornek, J., Crochet, N., Bajwa, G., Perwitasari, O., Martinez-Sobrido, L., et al. (2008) Distinct RIG-I and MDA5 Signaling by RNA Viruses in Innate Immunity. *J. Virol.* **82**: 335–345.

Loo, Y.M. and Gale, M. (2011) Immune Signaling by RIG-I-like Receptors. *Immunity* **34**: 680–692.

Loo, Y.M., Owen, D.M., Li, K., Erickson, A.K., Johnson, C.L., Fish, P.M., et al. (2006) Viral and therapeutic control of IFN-β promoter stimulator 1 during hepatitis C virus infection. *Proc. Natl. Acad. Sci. U. S. A.* **103**: 6001–6006.

Lu, H.J., Chuang, C.Y., Chen, M.K., Su, C.W., Yang, W.E., Yeh, C.M., et al. (2022) The impact of ALDH7A1 variants in oral cancer development and prognosis. *Aging (Albany. NY).* **14**: 4556–4571.

Mair, F. and Liechti, T. (2021) Comprehensive Phenotyping of Human Dendritic Cells and Monocytes. *Cytom. Part A* **99**: 231–242.

Majewski, J. and Pastinen, T. (2011) The study of eQTL variations by RNA-seq: From SNPs to phenotypes. *Trends Genet.* **27**: 72–79.

McArdela, S.L., Terhorst, C., and Sharpe, A.H. (2019) Roles of CD48 in regulating immunity and tolerance. *Physiol. Behav.* **46**: 248–256.

McNab, F., Mayer-Barber, K., Sher, A., Wack, A., and O'Garra, A. (2015) Type I interferons in infectious disease. *Nat. Rev. Immunol.* **15**: 87–103.

Miller, J.D., van der Most, R.G., Akondy, R.S., Glidewell, J.T., Albott, S., Masopust,

D., et al. (2008) Human Effector and Memory CD8+ T Cell Responses to Smallpox and Yellow Fever Vaccines. *Immunity* **28**: 710–722.

Monath, T.P. (2001) Yellow fever: An update. *Lancet Infect. Dis.* **1**: 11–20.

Monath, T.P. and Vasconcelos, P.F.C. (2015) Yellow fever. *J. Clin. Virol.* **64**: 160–173.

Moskovskich, A., Goldmann, U., Kartnig, F., Lindinger, S., Konecka, J., Fiume, G., et al. (2019) The transporters SLC35A1 and SLC30A1 play opposite roles in cell survival upon VSV virus infection. *Sci. Rep.* **9**: 1–11.

Mukhopadhyay, S., Kuhn, R.J., and Rossmann, M.G. (2005) A structural perspective of the Flavivirus life cycle. *Nat. Rev. Microbiol.* **3**: 13–22.

Müller-Dott, S., Tsirvouli, E., Vazquez, M., Flores, R.O.R., Badia-i-mompel, P., Fallegger, R., et al. (2023) Expanding the coverage of regulons from high-confidence prior knowledge for accurate estimation of transcription factor activities. 1–16.

Muñoz-Jordán, J.L. and Fredericksen, B.L. (2010) How flaviviruses activate and suppress the interferon response. *Viruses* **2**: 676–691.

Murtagh, F. (1984) Ward's Hierarchical Agglomerative Clustering Method: Which Algorithms Implement Ward's Criterion? Ward's Hierarchical Agglomerative Clustering Method: Which Algorithms Implement Ward's Criterion? *J. Bacteriol.* **160**: 233–238.

Nakaya, H.I., Wrammert, J., Lee, E.K., Racioppi, L., Marie-Kunze, S., Haining, W.N., et al. (2011) Systems biology of vaccination for seasonal influenza in humans. *Nat. Immunol.* **12**: 786–795.

Nazarenko, A.S., Vorovitch, M.F., Biryukova, Y.K., Pestov, N.B., Orlova, E.A., Barlev, N.A., et al. (2023) Flaviviruses in AntiTumor Therapy. 1–16.

Neves, P.C.C., Santos, J.R., Tubarão, L.N., Bonaldo, M.C., and Galler, R. (2013) Early IFN-gamma production after YF 17D vaccine virus immunization in mice and its association with adaptive immune responses. *PLoS One* **8**: 1–16.

Okun, S., Peek, A., and Igdoura, S.A. (2023) Neuraminidase 4 (NEU4): new biological and physiological player. *Glycobiology* **33**: 182–187.

Oliveira, L.G. and Peron, J.P.S. (2019) Viral receptors for flaviviruses: Not only gatekeepers. *J. Leukoc. Biol.* **106**: 695–701.

Ongen, H., Buil, A., Brown, A.A., Dermitzakis, E.T., and Delaneau, O. (2016) Fast and efficient QTL mapper for thousands of molecular phenotypes. *Bioinformatics* **32**: 1479–1485.

Ovsyannikova, I.G., Larrabee, B.R., and Poland, G.A. (2015) Immune Responses To Measles and Rubella Vaccines. **66**: 663–669.

Parkin, J. and Cohen, B. (2001) An overview of the immune system. **357**: 1777–1789.

Patin, E., Hasan, M., Bergstedt, J., Rouilly, V., Libri, V., Urrutia, A., et al. (2018) Natural variation in the parameters of innate immune cells is preferentially driven by genetic factors resource. *Nat. Immunol.* **19**: 302–314.

Piasecka, B., Duffy, D., Urrutia, A., Quach, H., Patin, E., Posseme, C., et al. (2018) Distinctive roles of age, sex, and genetics in shaping transcriptional variation of human immune responses to microbial challenges. *Proc. Natl. Acad. Sci. U. S. A.* **115**: E488–E497.

Picelli, S. (2017) Single-cell RNA-sequencing: The future of genome biology is now. *RNA Biol.* **14**: 637–650.

Picelli, S., Faridani, O.R., Björklund, Å.K., Winberg, G., Sagasser, S., and Sandberg, R. (2014) Full-length RNA-seq from single cells using Smart-seq2. *Nat. Protoc.* **9**: 171–181.

Pichlmair, A., Schulz, O., Tan, C.P., Näslund, T., Liljeström, P., Weber, F., and Reis e Sousa, C. (2006) RIG-I–Mediated Antiviral Responses to Single-Stranded RNA Bearing 5'-Phosphates. *Science (80-.).* **314**: 997–1002.

Platanias, L.C. (2005) Mechanisms of type-I- and type-II-interferon-mediated signalling. *Nat. Rev. Immunol.* **5**: 375–386.

Plotkin, S. (2014) History of vaccination. *Proc. Natl. Acad. Sci.* **111**: 12283–12287.

Poland, J.D., Calisher, C.H., Monath, T.P., Downs, W.G., and Murphy, K. (1981) Persistence of neutralizing antibody 30-35 years after immunization with 17D yellow fever vaccine. *Bull. World Health Organ.* **59**: 895–900.

Poon, M.M.L., Byington, E., Meng, W., Kubota, M., Matsumoto, R., Grifoni, A., et al. (2021) Heterogeneity of human anti-viral immunity shaped by virus, tissue, age, and sex. *Cell Rep.* **37**: 110071.

Proutski, V., Gould, E.A., and Holmes, E.C. (1997) Secondary structure of the 3'

untranslated region of flaviviruses: Similarities and differences. *Nucleic Acids Res.* **25**: 1194–1202.

Pshezhetsky, A. V. and Hinek, A. (2011) Where catabolism meets signalling: Neuraminidase 1 as a modulator of cell receptors. *Glycoconj. J.* **28**: 441–452.

Pulendran, B. (2009) Learning immunology from the yellow fever vaccine: Innate immunity to systems vaccinology. *Nat. Rev. Immunol.* **9**: 741–747.

Pulendran, B., Oh, J.Z., Nakaya, H.I., Ravindran, R., and Kazmin, D.A. (2013) Immunity to viruses: Learning from successful human vaccines. *Immunol. Rev.* **255**: 243–255.

Querec, T., Bennouna, S., Alkan, S., Laouar, Y., Gorden, K., Flavell, R., et al. (2006) Yellow fever vaccine YF-17D activates multiple dendritic cell subsets via TLR2, 7, 8, and 9 to stimulate polyvalent immunity. *J. Exp. Med.* **203**: 413–24.

Querec, T.D., Akondy, R.S., Lee, E.K., Cao, W., Nakaya, H.I., Teuwen, D., et al. (2009) Systems biology approach predicts immunogenicity of the yellow fever vaccine in humans. *Nat. Immunol.* **10**: 116–125.

Reikine, S., Nguyen, J.B., and Modis, Y. (2014) Pattern recognition and signaling mechanisms of RIG-I and MDA5. *Front. Immunol.* **5**: 1–7.

Reimand, J., Isserlin, R., Voisin, V., Kucera, M., Tannus-Lopes, C., Rostamianfar, A., et al. (2019) Pathway enrichment analysis and visualization of omics data using g:Profiler, GSEA, Cytoscape and EnrichmentMap. *Nat. Protoc.* **14**: 482–517.

Renoux, F., Stellato, M., Haftmann, C., Vogetseder, A., Huang, R., Subramaniam, A., et al. (2020) The AP1 Transcription Factor Fosl2 Promotes Systemic Autoimmunity and Inflammation by Repressing Treg Development. *Cell Rep.* **31**:.

Rimann, I., Gonzalez-Quintial, R., Baccala, R., Kiosses, W.B., Teijaro, J.R., Parker, C.G., et al. (2022) The solute carrier SLC15A4 is required for optimal trafficking of nucleic acid–sensing TLRs and ligands to endolysosomes. *Proc. Natl. Acad. Sci. U. S. A.* **119**: 1–9.

Ritchie, M.E., Phipson, B., Wu, D., Hu, Y., Law, C.W., Shi, W., and Smyth, G.K. (2015) Limma powers differential expression analyses for RNA-sequencing and microarray studies. *Nucleic Acids Res.* **43**: e47.

Robinson, M.D., McCarthy, D.J., and Smyth, G.K. (2009) edgeR: A Bioconductor

package for differential expression analysis of digital gene expression data. *Bioinformatics* **26**: 139–140.

Robinson, M.D. and Oshlack, A. (2010) A scaling normalization method for differential expression analysis of RNA-seq data. *Genome Biol.* **11**: 1–9.

Rogers, K.J., Shtanko, O., Stunz, L.L., Mallinger, L.N., Arkee, T., Schmidt, M.E., et al. (2021) Frontline Science: CD40 signaling restricts RNA virus replication in Mϕs, leading to rapid innate immune control of acute virus infection. *J. Leukoc. Biol.* **109**: 309–325.

Rothenfusser, S., Goutagny, N., DiPerna, G., Gong, M., Monks, B.G., Schoenemeyer, A., et al. (2005) The RNA Helicase Lgp2 Inhibits TLR-Independent Sensing of Viral Replication by Retinoic Acid-Inducible Gene-I. *J. Immunol.* **175**: 5260–5268.

Saichi, M., Ladjemi, M.Z., Korniotis, S., Rousseau, C., Ait Hamou, Z., Massenet-Regad, L., et al. (2021) Single-cell RNA sequencing of blood antigen-presenting cells in severe COVID-19 reveals multi-process defects in antiviral immunity. *Nat. Cell Biol.* **23**: 538–551.

Santos-Peral, A., Luppa, F., Goresch, S., Elena Nikolova, E., Zaucha, M., Lehmann, L., et al. (2024) Prior flavivirus immunity skews the yellow fever vaccine response to cross-reactive antibodies with potential to enhance dengue fever vaccine response. *Nat. Commun.* 1–17.

Santos-Peral, A., Zaucha, M., Nikolova, E., Winheim, E., Goresch, S., Scheck, M.K., et al. Basal T-cell activation predicts yellow fever vaccine response independently of cytomegalovirus infection and sex-related immune variations (submitted).

Santos del Peral, A. Effect of Prior Flavivirus Immunity on the Response to the Yellow Fever 17D Vaccine. Dissertation, LMU München (submitted).

Satoh, T., Kato, H., Kumagai, Y., Yoneyama, M., Sato, S., Matsushita, K., et al. (2010) LGP2 is a positive regulator of RIG-I- and MDA5-mediated antiviral responses. *Proc. Natl. Acad. Sci.* **107**: 1512–1517.

Schaller, L. and Lauschke, V.M. (2019) The genetic landscape of the human solute carrier (SLC) transporter superfamily. *Hum. Genet.* **138**: 1359–1377.

Scheck, M.K., Lehmann, L., Zaucha, M., Schwarzlmueller, P., Huber, K., Pritsch, M., et al. (2022) FluoRNT: A robust, efficient assay for the detection of neutralising

antibodies against yellow fever virus 17D. *PLoS One* **17**: 1–19.

Schmidt, A., Schwerd, T., Hamm, W., Hellmuth, J.C., Cui, S., Wenzel, M., et al. (2009) 5′-triphosphate RNA requires base-paired structures to activate antiviral signaling via RIG-I. *Proc. Natl. Acad. Sci. U. S. A.* **106**: 12067–12072.

Schmiedel, B.J., Rocha, J., Gonzalez-Colin, C., Bhattacharyya, S., Madrigal, A., Ottensmeier, C.H., et al. (2021) COVID-19 genetic risk variants are associated with expression of multiple genes in diverse immune cell types. *Nat. Commun.* **12**: 1–12.

Schneider, W.M., Chevillotte, M.D., and Rice, C.M. (2015) Interferon-Stimulated Genes: A Complex Web of Host Defenses. 513–545.

Schoggins, J.W. and Rice, C.M. (2011) Interferon-stimulated genes and their antiviral effector functions. *Curr. Opin. Virol.* **1**: 519–525.

Schoggins, J.W., Wilson, S.J., Panis, M., Murphy, M.Y., Jones, C.T., Bieniasz, P., and Rice, C.M. (2011) A diverse range of gene products are effectors of the type i interferon antiviral response. *Nature* **472**: 481–485.

Sheng, Q., Vickers, K., Zhao, S., Wang, J., Samuels, D.C., Koues, O., et al. (2017) Multi-perspective quality control of Illumina RNA sequencing data analysis. *Brief. Funct. Genomics* **16**: 194–204.

Sherwood, E.R., Burelbach, K.R., McBride, M.A., Stothers, C.L., Owen, A.M., Hernandez, A., et al. (2022) Innate Immune Memory and the Host Response to Infection. *J. Immunol.* **208**: 785–792.

Sidrauski, C., Tsai, J.C., Kampmann, M., Hearn, B.R., Vedantham, P., Jaishankar, P., et al. (2015) Pharmacological dimerization and activation of the exchange factor eIF2B antagonizes theintegrated stress response. *Elife* **2015**: 1–27.

Sinigaglia, L., Gracias, S., Décembre, E., Fritz, M., Bruni, D., Smith, N., et al. (2018) Immature particles and capsid-free viral RNA produced by Yellow fever virus-infected cells stimulate plasmacytoid dendritic cells to secrete interferons. *Sci. Rep.* **8**: 1–15.

Smyth, G.K., Ritchie, M.E., Law, C.W., Alhamdoosh, M., Su, S., Dong, X., and Tian, L. (2018) RNA-seq analysis is easy as 1-2-3 with limma, Glimma and edgeR. *F1000Research* **5**: 5–6.

Srivastava, S., Savanur, M.A., Sinha, D., Birje, A., Vigneshwaran, R., Saha, P.P., et al. (2017) Regulation of mitochondrial protein import by the nucleotide exchange factors GrpEL1 and GrpEL2 in human cells. *J. Biol. Chem.* **292**: 18075–18090.

Stegle, O., Parts, L., Piipari, M., Winn, J., and Durbin, R. (2012) Using probabilistic estimation of expression residuals (PEER) to obtain increased power and interpretability of gene expression analyses. *Nat. Protoc.* **7**: 500–507.

Steinberg, J., Southam, L., Butterfield, N.C., Roumeliotis, T.I., Fontalis, A., Clark, M.J., et al. (2020) Decoding the genomic basis of osteoarthritis. *bioRxiv* 835850.

Steinberg, J., Southam, L., Roumeliotis, T.I., Clark, M.J., Jayasuriya, R.L., Swift, D., et al. (2021) A molecular quantitative trait locus map for osteoarthritis. *Nat. Commun.* **12**: 1–11.

Stewart, C.A., Gay, C.M., Ramkumar, K., Cargill, K.R., Cardnell, R.J., Monique, B., et al. (2020) SARS-CoV-2 infection induces EMT-like molecular changes, including ZEB1-mediated repression of the viral receptor ACE2, in lung cancer models.

Subramanian, A., Tamayo, P., Mootha, V.K., Mukherjee, S., Ebert, B.L., Gillette, M.A., et al. (2005) Gene set enrichment analysis: A knowledge-based approach for interpreting genome-wide expression profiles. *Proc. Natl. Acad. Sci. U. S. A.* **102**: 15545–15550.

Swertz, M.A., Kumar, V., Li, Y., Toenhake-Dijkstra, H., Joosten, I., Netea-Maier, R.T., et al. (2016) Host and Environmental Factors Influencing Individual Human Cytokine Responses. *Cell* **167**: 1111-1124.e13.

Takahashi, T., Ellingson, M.K., Wong, P., Israelow, B., Lucas, C., Klein, J., et al. (2020) Sex differences in immune responses that underlie COVID-19 disease outcomes. *Nature* **588**: 315–320.

Takeuchi, O. and Akira, S. (2010) Pattern Recognition Receptors and Inflammation. *Cell* **140**: 805–820.

Theiler, M. and Smith, H.H. (1937) The use of yellow fever virus modified by in vitro cultivation for human immunization. *J. Exp. Med.* **65**: 787–800.

Tsang, J.S., Dobaño, C., VanDamme, P., Moncunill, G., Marchant, A., Othman, R. Ben, et al. (2020) Improving Vaccine-Induced Immunity: Can Baseline Predict Outcome? *Trends Immunol.* **41**: 457–465.

Tsang, J.S., Schwartzberg, P.L., Kotliarov, Y., Biancotto, A., Xie, Z., Germain, R.N., et al. (2014) Global analyses of human immune variation reveal baseline predictors of postvaccination responses. *Cell* **157**: 499–513.

Urbut, S.M., Wang, G., Carbonetto, P., and Stephens, M. (2019) Flexible statistical methods for estimating and testing effects in genomic studies with multiple conditions. *Nat. Genet.* **51**: 187–195.

Vaine, C.A. and Soberman, R.J. (2014) The CD200-CD200R1 Inhibitory Signaling Pathway. Immune Regulation and Host-Pathogen Interactions. 1st ed. Elsevier Inc.

Varki, A. and Angata, T. (2006) Siglecs - The major subfamily of I-type lectins. *Glycobiology* **16**: 1–27.

Wang, C., Khatun, M.S., Zhang, Z., Allen, M.J., Chen, Z., Ellsworth, C.R., et al. (2023) COVID-19 and influenza infections mediate distinct pulmonary cellular and transcriptomic changes. *Commun. Biol.* **6**: 1–14.

Westra, H.J. and Franke, L. (2014) From genome to function by studying eQTLs. *Biochim. Biophys. Acta - Mol. Basis Dis.* **1842**: 1896–1902.

Wieten, R.W., Jonker, E.F.F., Van Leeuwen, E.M.M., Remmerswaal, E.B.M., Ten Berge, I.J.M., De Visser, A.W., et al. (2016) A single 17D yellow fever vaccination provides lifelong immunity; characterization of yellow-fever-specific neutralizing antibody and T-cell responses after vaccination. *PLoS One* **11**: 1–18.

Wimmers, F., Donato, M., Kuo, A., Ashuach, T., Gupta, S., Li, C., et al. (2021) The single-cell epigenomic and transcriptional landscape of immunity to influenza vaccination. *Cell* **184**: 3915-3935.e21.

Winheim, E. (2022) Modulation of human dendritic cell phenotype and function in response to yellow fever vaccination and SARS-CoV-2 infection. Dissertation, LMU München

Witte, J.S., Elston, R.C., and Schork, N.J. (1996) Genetic dissection of complex traits. *Nat. Genet.* **12**: 355–356.

Wu, T., Hu, E., Xu, S., Chen, M., Guo, P., Dai, Z., et al. (2021) clusterProfiler 4.0: A universal enrichment tool for interpreting omics data. *Innovation* **2**: 100141.

Yoneyama, M., Kikuchi, M., Matsumoto, K., Imaizumi, T., Miyagishi, M., Taira, K., et al. (2005) Shared and Unique Functions of the DExD/H-Box Helicases RIG-I,

MDA5, and LGP2 in Antiviral Innate Immunity. *J. Immunol.* **175**: 2851–2858.

Yoo, J.S., Sasaki, M., Cho, S.X., Kasuga, Y., Zhu, B., Ouda, R., et al. (2021) SARS-CoV-2 inhibits induction of the MHC class I pathway by targeting the STAT1-IRF1-NLRC5 axis. *Nat. Commun.* **12**:.

Zaucha, M., Winheim, E., Santos-Peral, A., Ahlfeld, J., Schwarzlmüller, P., Dahlström, F., et al. RLR-dependent type I IFN production regulates antigen dose and activation in YF-17D-infected DCs (manuscript in preparation).

Zhang, H., Bernaleau, L., Delacrétaz, M., Hasanovic, E., Drobek, A., Eibel, H., and Rebsamen, M. (2023) SLC15A4 controls endolysosomal TLR7–9 responses by recruiting the innate immune adaptor TASL. *Cell Rep.* **42**:.

Zimmermann, P. and Curtis, N. (2019) Factors That Influence the Immune Response to Vaccination. **31**:.

8. Supplementary Figures
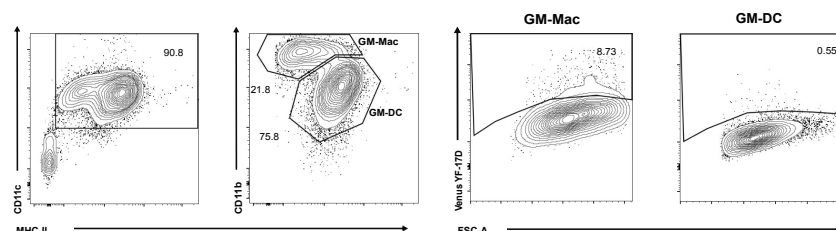
Supplementary Figure 1.Representative flow cytometry plots of the gating strategy for GM-Macrophages and DC subsets

The cells were derived from BM cultures and infected with YF17D-Venus (MOI 5, 48hpi).

A

Sequencing 1

Excluded sample	Mean Quality Score
d7_11	25

Excluded sample	% of alignment
d0_26	15,08%
d7_97	26,18%
d0_210	26,23%
d0_57	29,33%
d0_98	29,5%
d7_87	39,14%

B

Sequencing 2

Excluded sample	Mean Quality Score
d7_167	27
d0_26	28

Excluded sample	% of alignment
d0_210	26,9%
d0_57	27,2%
d0_98	28,7%
d7_87	36,9%
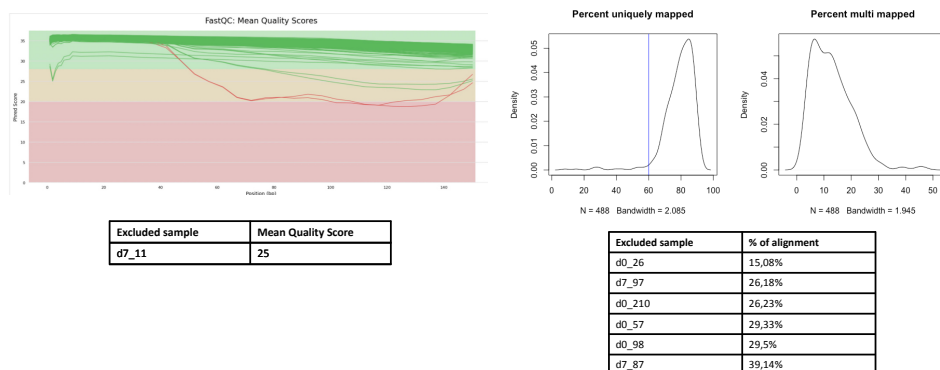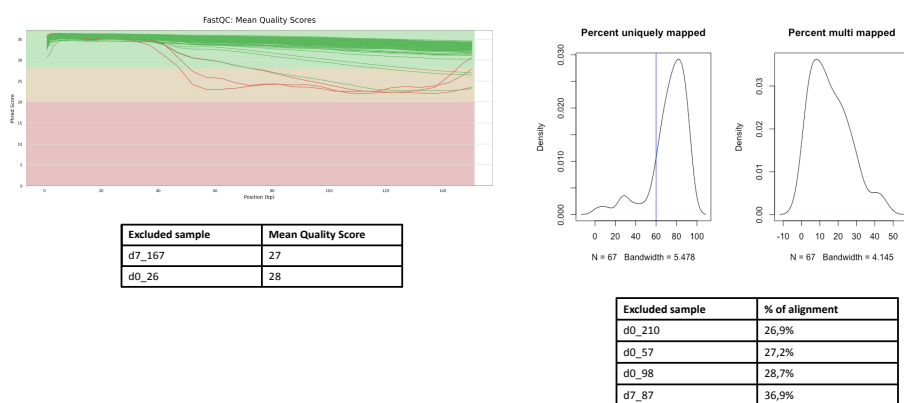
Supplementary Figure 2.Quality control of raw sequencing reads after Illumina sequencing.

A) Mean quality score and percent of uniquely mapped and multi-mapped reads for sequencing run 1; B) Mean quality score and percent of uniquely mapped and multi-mapped reads for sequencing run 2. The tables show the excluded individuals at each of the described steps.

9. Supplementary Tables

	GENENAME	adj.P.Val	logFC
1	IFI44L	1.68500171937963e-175	4.00434212411396
2	SIGLEC1	2.23837727553183e-169	3.7995471822911
3	XAF1	1.37355722787737e-159	2.29007173336326
4	OAS2	5.3509781588292e-157	2.29586023703983
5	EPSTI1	1.98911401891045e-154	2.62206861169335
6	USP18	4.7972401275416e-153	4.19077165341644
7	MX2	2.21441990420791e-152	1.9405482400454
8	RSAD2	4.59620270728511e-152	4.03244317777147

9	LY6E	1.08567467506912e-151	2.63532740821597
10	IFI44	1.62846718120628e-151	2.38170362220621
11	EIF2AK2	2.52764724072513e-151	1.96473034413059
12	MX1	3.29902930867799e-151	2.78139938578361
13	IFIT3	7.96569131081723e-151	3.52451744456068
14	SPATS2L	1.31975022413993e-148	2.75431882287428
15	IFI6	6.82112290185914e-148	2.96795080552559
16	IFIT1	1.30405855649361e-147	3.71144883490572
17	IRF7	5.83939327655217e-147	2.07591727311777
18	OAS3	2.48465867068023e-144	2.45122658799049
19	PARP9	5.53890017057167e-143	1.97822148311934
20	SAMD9	2.34829040182543e-141	1.94968716034878
21	OASL	2.46765159174787e-140	2.64427076871523
22	LGALS3BP	1.48560683731611e-137	2.92596869964396
23	CMPK2	2.04314167056664e-137	2.75821030291579
24	IFITM1	3.40830142599957e-135	4.12117407560418
25	TRIM22	3.58768977083969e-134	1.57296004243767
26	IFIT2	1.35688419662389e-133	2.78817116308483
27	IFI27	2.36557892626158e-133	6.56151532785414
28	GMPR	8.31818238228718e-133	3.07925049645841
29	CXCR2P1	1.18854767527245e-132	2.94142775335198
30	DDX60	1.62478234542053e-132	2.05650081440433
31	DHX58	4.59859621771208e-131	1.83755174919086
32	NEXN	9.26075404048439e-131	2.53411371122519
33	HERC5	1.58249051633559e-130	2.49501315689958
34	SAMD9L	1.21503618194907e-129	2.21978978453365
35	OAS1	1.69341041167597e-128	2.03767124591769
36	C19orf66	4.13707438352139e-124	1.01770122417992
37	SERPING1	7.03255259310051e-124	3.23469484400558
38	IFI35	5.50810638768395e-123	1.56078865193616
39	HSH2D	8.94577820174242e-122	1.44052520426191
40	ZBP1	2.99953540352218e-121	2.72910311176669
41	ISG15	1.54025652908825e-118	2.83421296326058
42	EIF4B	2.33141210121348e-116	-1.29611692129625
43	DANCR	1.00776366264537e-115	-2.10299344633292
44	DDX58	1.69673202956989e-115	2.10211794109085
45	OTOF	5.26665700098403e-115	5.8954121448579
46	SHISA5	8.69382320399908e-114	0.878548717842391
47	EIF3L	3.56344251657499e-113	-1.07095215125453
48	STAT2	1.80745540128804e-111	1.19035534642212
49	ITGAE	1.46559669771866e-108	-1.53401395197332
50	TMEM123	2.06442653299594e-108	1.07983438076307
51	STAT1	6.46750304833484e-108	1.48994390533893

52	SP110	7.1585142855525e-108	1.17916805825982
53	TRIM69	6.77730017918973e-107	1.41478021963806
54	IFITM3	8.8588951309543e-106	2.69444478631682
55	LAP3	1.85982841637597e-105	1.42143209756558
56	PPM1K	2.64563007762613e-105	1.78248423066208
57	CUL1	4.44353430748665e-105	1.34646380405545
58	HESX1	2.98871291379138e-105	3.74784572044279
59	ETV7	6.60484835100731e-105	3.04901592232764
60	IFIH1	9.24547678909697e-105	1.58976336558409
61	PARP14	3.14506488881548e-104	1.25224228820626
62	RP11-273G15.2	1.42161228364415e-104	3.05276630656698
63	HERC6	1.47701668338726e-103	1.85665053807354
64	PML	1.58520589029775e-102	1.38339296084838
65	DTX3L	1.48549689291726e-101	1.39742996809384
66	IRF9	5.51432154134111e-101	0.883378811483279
67	PLAC8	2.94727177228728e-100	1.81725752953946
68	IFIT5	2.29088444297999e-99	1.58737311775088
69	PHF11	1.56521731096435e-98	0.881620255666462
70	TNFSF10	2.15103894052271e-98	1.89842035985961
71	AXL	2.20143563015094e-97	3.3229136600093
72	GBP1	6.82265535213571e-97	2.09832429466768
73	TOR1B	5.25650350830061e-96	1.16684360632444
74	TRIM5	1.69525754154896e-95	1.28918670667431
75	TAP1	2.03309696968106e-95	1.17887011596237
76	NMI	2.84651327461963e-95	1.0789948913863
77	BATF2	3.00422118567184e-95	2.46562075866501
78	NCOA7	2.78706496651241e-94	1.88661577822697
79	UBE2L6	4.76490383735536e-94	1.22789883287084
80	APOBEC3A	5.3737671080283e-94	2.00231005582291

Supplementary Table 1.The list of 80 DEGs

		Marker	Titer	Clone
	ICS			
Violet 405 nm	V450	IFNg	80	B27
	Brilliant Violet™ 510	CD45RA	160	HI100
	Brilliant Violet™ 605	CD27	80	O323
	Brilliant Violet™ 650	CD8	320	SK1
	Brilliant Violet™ 711	IL2	80	MQ1-17H12
	Brilliant Violet™ 785	CCR7	80	G043H7
Blue 488 nm	FITC	CD40L	50	24-31
	PerCP	CD3	80	SK7
Yellow/green 561nm	PE	IL21	40	3A3-N2
	PE/Dazzle 594	CD107a	200	H4A3
	PE/Cyanine7	CXCR5	80	J252D4
Red 633 nm	APC	TNFa	80	MAb11
	Alexa Fluor® 700	CD4	320	OKT4
	APC Cy7	Viability	3000	

Supplementary Table 2. ICS panel for ex vivo restimulation assay

		Marker	Titer	Clone
T cells			1:	
UV 355 nm	BUV395	**CD45RA**	100	HI100
	Zombie UV	**Viability**	500	
	BUV496	**CD16**	100	3G8
	BUV563	**CD127**	100	HIL76M21
	BUV661	**CCR6**	100	11A9
	BUV737	**PD1**	100	EH12.1
	BUV805	**ICOS**	100	DX29
Violet 405 nm	Brilliant Violet™ 421	**Tetramer**	100	
	Pacific Blue™	**CD57**	400	HNK-1
	Brilliant Violet™ 480	**CD56**	200	NCAM16.2
	Brilliant Violet™ 510	**CD4**	200	SK3
	Brilliant Violet™ 570			
	Brilliant Violet™ 605	**CXCR3**	200	G025H7
	Brilliant Violet™ 650	**Ki67**	100	B56
	Brilliant Violet™ 711	**KLRG1**	100	2F1
	Brilliant Violet™ 750	**CXCR5**	100	J252D4
	Brilliant Violet™ 785	**CCR7**	80	G043H7
Blue 488 nm				
	FITC	**Tbet**	200	4B10
	Spark Blue™ 550	**CD3**	200	SK7
	BB700	**CD25**	100	BC96
Yellow/green 561nm	PE	**TCF1**	200	7F11A10
	PE/Dazzle 594	**FoxP3**	200	206D
	PE/Cyanine5.5	**EOMES**	400	WD1928
	PE/Cyanine7	**CCR4**	400	L291H4
Red 633 nm	APC	**Tetramer**		
	PE Fire 810	**HLADR***	100	L243
	Alexa Fluor® 700	**CD8**	400	HIT8a
	APC/Fire™ 750	**CD95**	400	DX2
	APC Fire 810	**CD38**	100	HB-7

Supplementary Table 3.Flow Cytometry T-cell panel

Cell Type	Gated population
CD4	CD4
CD4	CD4 Ki67
CD4	CD4 CCR4
CD4	CD4 CCR4 Ki67
CD4	CD4 CCR6
CD4	CD4 CCR6 Ki67
CD4	CD4 CD38
CD4	CD4 CD38 Ki67
CD4	CD4 CD45RA$^+$CCR7$^+$
CD4	CD4 CD45RA$^+$CCR7$^+$CD95$^-$ (Naïve)
CD4	CD4 Naive Ki67
CD4	CD4 CD45RA$^+$CCR7$^+$CD95$^+$ (Tscm)
CD4	CD4 Tscm Ki67
CD4	CD4 CD57$^+$CD127$^-$ senescent
CD4	CD4 CD57$^+$CD127$^-$ senescent Ki67
CD4	CD4 CD127$^+$CD57$^-$ Long-term
CD4	CD4 CD127$^+$CD57$^-$ Long-term Ki67
CD4	CD4 CD45RA$^-$CCR7$^+$ (CM)
CD4	CD4 CM Ki67
CD4	CD4 CXCR5$^+$ (ctfh)
CD4	CD4 ctfh CCR4
CD4	CD4 ctfh CCR4 Ki67
CD4	CD4 ctfh CCR6
CD4	CD4 ctfh CCR6 Ki67
CD4	CD4 ctfh CD38
CD4	CD4 ctfh CD38 Ki67
CD4	CD4 ctfh CXCR3
CD4	CD4 ctfh CXCR3 Ki67
CD4	CD4 ctfh CXCR3$^-$CCR6$^-$
CD4	CD4 ctfh ICOS CD38
CD4	CD4 ctfh ICOS CD38 Ki67
CD4	CD4 ctfh Ki67
CD4	CD4 ctfh PD1 CD38
CD4	CD4 ctfh PD1 CD38 Ki67
CD4	CD4 ctfh PD1$^+$ICOS$^-$
CD4	CD4 ctfh PD1$^+$ICOS$^-$ Ki67
CD4	CD4 ctfh PD1$^+$ICOS$^+$
CD4	CD4 ctfh PD1$^+$ICOS$^+$ Ki67
CD4	CD4 ctfh PD1$^-$ICOS$^+$
CD4	CD4 ctfh PD1$^-$ICOS$^+$ Ki67
CD4	CD4 ctfh PD1$^-$ICOS$^-$
CD4	CD4 ctfh Th1
CD4	CD4 ctfh Th1 CD38
CD4	CD4 ctfh Th1CD38 Ki67
CD4	CD4 ctfh Th1 Ki67
CD4	CD4 ctfh Th17
CD4	CD4 ctfh Th17 CD38
CD4	CD4 ctfh Th17 CD38 Ki67
CD4	CD4 ctfh Th17 Ki67
CD4	CD4 ctfh Th1 17
CD4	CD4 ctfh Th1 17 CD38
CD4	CD4 ctfh Th1 17 CD38 Ki67
CD4	CD4 ctfh Th1 17 Ki67
CD4	CD4 CXCR3
CD4	CD4 CXCR3 Ki67
CD4	CD4 CXCR3$^-$CCR6$^-$
CD4	CD4 CXCR3$^-$CCR6$^-$CCR4$^+$ (Th2)
CD4	CD4 Th2 Ki67
CD4	CD4 CD45RA$^-$CCR7$^-$ (EM)
CD4	CD4 EM Ki67
CD4	CD4 CD45RA$^+$CCR7$^-$ (EMRA)
CD4	CD4 EMRA Ki67
CD4	CD4 CD127$^+$CD57$^+$
CD4	CD4 CD127$^+$CD57$^+$ Ki67
CD4	CD4 CD127$^-$CD57$^-$
CD4	CD4 PD1$^-$TCF1$^+$
CD4	CD4 PD1$^-$TCF1$^+$ Ki67
CD4	CD4 PD1$^+$TCF1$^+$
CD4	CD4 PD1$^+$TCF1$^+$ Ki67
CD4	CD4 PD1$^+$TCF1$^-$
CD4	CD4 PD1$^-$TCF1$^-$
CD4	CD4 Tbet Eomes
CD4	CD4 Tbet Eomes Ki67
CD4	CD4 Tbet High
CD4	CD4 Tbet High Ki67
CD4	CD4 Tbet High Eomes$^-$
CD4	CD4 Tbet High Eomes$^+$
CD4	CD4 Tbet High Eomes$^+$ Ki67
CD4	CD4 Tbet Low Eomes$^+$
CD4	CD4 Tbet Low Eomes$^+$ Ki67
CD4	CD4 CXCR3$^+$CCR6$^-$ (Th1)
CD4	CD4 Th1 Ki67
CD4	CD4 CXCR3$^-$CCR6$^+$ (Th17)
CD4	CD4 Th17 Ki67
CD4	CD4 CXCR3$^+$CCR6$^+$ (Th1 17)
CD4	CD4 Th1 17 Ki67
CD4	CD4 Fosp3$^+$CD127$^-$CD25$^+$ (Treg)
CD4	CD4 Treg CCR4
CD4	CD4 Treg CCR4 Ki67
CD4	CD4 Treg CXCR3$^-$CCR6$^-$
CD4	CD4 Treg Ki67
CD4	CD4 Treg Th1
CD4	CD4 Treg Th1 Ki67
CD4	CD4 Treg Th17
CD4	CD4 Treg Th17 Ki67
CD4	CD4 Treg Th1 17
CD4	CD4 Treg Th1 17 Ki67
CD8	CD8
CD8	CD8 CD38
CD8	CD8 CD38 Ki67
CD8	CD8 CD45RA$^+$CCR7$^+$
CD8	CD8 CD45RA$^+$CCR7$^+$ Ki67
CD8	CD8 CD45RA$^+$CCR7$^+$ CD95$^-$ (Naive)
CD8	CD8 Naive Ki67
CD8	CD8 CD45RA$^+$CCR7$^+$ CD95$^+$ (Tscm)

CD8	CD8 Tscm Ki67
CD8	CD8 CD57+CD56+
CD8	CD8 CD57+CD56+ Ki67
CD8	CD8 CD57+CD56-
CD8	CD8 Ki67
CD8	CD8 CD57+PD1+
CD8	CD8 CD57+PD1+ Ki67
CD8	CD8 CD57+PD1-
CD8	CD8 CD57-CD56+
CD8	CD8 CD57-CD56+ Ki67
CD8	CD8 CD57-PD1+
CD8	CD8 CD57-PD1+ Ki67
CD8	CD8 CD57-CD56-
CD8	CD8 CD57-PD1-
CD8	CD8 CD57+CD127- Senescent
CD8	CD8 CD57+CD127- Senescent Ki67
CD8	CD8 CD127+CD57- Longterm
CD8	CD8 CD127+CD57- Longterm Ki67
CD8	CD8 CM
CD8	CD8 CM Ki67
CD8	CD8 EM
CD8	CD8 EM Ki67
CD8	CD8 EMRA
CD8	CD8 EMRA Ki67
CD8	CD8 PD1+TCF1- Exhausted
CD8	CD8 PD1+TCF1+
CD8	CD8 PD1+TCF1+ Ki67
CD8	CD8 PD1+CD56+
CD8	CD8 PD1+CD56+ Ki67
CD8	CD8 PD1+CD56-
CD8	CD8 PD1-TCF1+
CD8	CD8 PD1-TCF1+ Ki67
CD8	CD8 PD1-TCF1-
CD8	CD8 PD1-CD56+
CD8	CD8 PD1-CD56+ Ki67
CD8	CD8 PD1-CD56-
CD8	CD8 CD127+CD57+
CD8	CD8 CD127+CD57+ Ki67
CD8	CD8 CD127-CD57-
CD8	CD8 Tbet Eomes
CD8	CD8 Tbet Eomes Ki67
CD8	CD8 Tbet High CD56
CD8	CD8 Tbet High CD56 Ki67
CD8	CD8 Tbet High
CD8	CD8 Tbet High Ki67
CD8	CD8 Tbet High Eomes-
CD8	CD8 Tbet High Eomes+
CD8	CD8 Tbet High Eomes+ Ki67
CD8	CD8 Tbet Low Eomes+
CD8	CD8 Tbet Low Eomes+ Ki67
CD8	CD8 Tbet+TCF1-
CD8	CD8 TCF1-CD57+
CD8	CD8 TCF1-CD57+ Ki67
CD8	CD8 TCF1-Tbet-
CD8	CD8 TCF1+
CD8	CD8 TCF1+ Ki67
CD8	CD8 TCF1+Tbet-

CD4	CD4 ctfh HLADRCD38
CD4	CD4 ctfh Th1 HLADRCD38
CD4	CD4 HLADR CD38
CD8	CD8 HLADR CD38

Supplementary Table 4.Immune populations identified in spectral flow cytometry.

Acknowledgments

Affidavit

LMU LUDWIG-MAXIMILIANS-UNIVERSITÄT MÜNCHEN	Promotionsbüro Medizinische Fakultät	MMRS	

Affidavit

Zaucha Magdalena

_____
Surname, first name

_____
Street

_____
Zip code, town, country

I hereby declare, that the submitted thesis entitled:

'Interindividual variability and the interplay of innate and adaptive immunity in the yellow fever vaccination model'

is my own work. I have only used the sources indicated and have not made unauthorised use of services of a third party. Where the work of others has been quoted or reproduced, the source is always given.
I further declare that the dissertation presented here has not been submitted in the same or similar form to any other institution for the purpose of obtaining an academic degree.

___Munich, 23.12.24____   **Magdalena Zaucha**
place, date   Signature doctoral candidate

Confirmation of congruency

	LUDWIG-MAXIMILIANS-UNIVERSITÄT MÜNCHEN	Promotionsbüro Medizinische Fakultät	MMRS	

Confirmation of congruency between printed and electronic version of the doctoral thesis

Magdalena Zaucha

_____
Surname, first name

_____
Street

_____
Zip code, town, country

I hereby declare, that the submitted thesis entitled:

'Interindividual variability and the interplay of innate and adaptive immunity in the yellow fever vaccination model'

is congruent with the printed version both in content and format.

__Munich, 23.12.24___
place, date

Magdalena Zaucha

Signature doctoral candidate